Supplementary Information for

Microwave-powered liquid metal depolymerization for plastic upcycling

Jianye Gao[1]†, Jun Zhao[2,4]†, Zerong Xing[3], Minghui Guo[3], Haijiao Xie[6], Wangjing Ma[2]*, Jing Liu[1,3,5]*

[1] School of Biomedical Engineering, Tsinghua University, Beijing 100084, China.

[2] Key Laboratory of Photochemical Conversion and Optoelectronic Materials & HKU-CAS Joint Laboratory on New Materials, Technical Institute of Physics and Chemistry, Chinese Academy of Sciences, Beijing 100190, China.

[3] Key Lab of Cryogenic Science and Technology, Technical Institute of Physics and Chemistry, Chinese Academy of Sciences, Beijing 100190, China.

[4] School of Chemical Sciences, University of Chinese Academy of Sciences, Beijing 100049, China.

[5] School of Future Technology, University of Chinese Academy of Sciences, Beijing 100049, China.

[6] Hangzhou Yanqu Information Technology Co., Ltd., Hangzhou 310003, China.

* Corresponding author. Email: wjma@mail.ipc.ac.cn; jliubme@tsinghua.edu.cn

† These authors contributed equally to this work.

Table of Contents

Supplementary Discussion

Supplementary Table 1

The bond energy of different C-C bonds within n-hexane molecule under vacuum and EGaIn cluster environment.

Bond	Bond energy, E_{bond} (kcal/mol)		ΔE_{bond} (kcal/mol)
	Vacuum (Without EGaIn)	**With EGaIn**	
CH_3–C_5H_{11}	95.21	**19.54**	-75.67
C_2H_5–C_4H_9	91.57	**7.99**	-83.58
C_3H_7–C_3H_7	91.55	**7.84**	-83.71

Supplementary Table 2

Depolymerization of PP-based disposable lunch boxes using microwave-powered liquid metal EGaIn under different microwave power.

Microwave power *P* (W)	Evolved gas composition (Vol. %)									Gas yield (wt%)	Oil yield (wt%)	Solid yield (wt%)	Mass balance (%)
	CH_4	C_2H_4	C_2H_6	C_3H_6	C_3H_8	$C_4^=$	C_4^O	C_{5+}	H_2				
120	12.1	20.7	3.5	27.6	0.8	10.6	2.8	10	11.9	70.6	14.4	14.8	99.8
240	15.1	22.0	4.0	26.3	0.7	9.0	3.0	7.8	12.1	55.1	32.8	11.7	99.6
360	14.9	20.8	4.2	26.8	0.7	8.8	2.7	9.4	11.7	53.4	40.4	6.0	99.8
480	19.3	21.6	3.6	22.3	0.7	6.7	2.9	6.5	16.4	53.0	40.5	6.1	99.6
600	**18.3**	**18.9**	**4.4**	**24.4**	**0.8**	**6.6**	**2.3**	**6.8**	**17.5**	**51.5**	**43.2**	**5.2**	**99.9**
720	19.1	17.4	4.1	24.1	0.9	5.5	2.1	6	20.8	35.9	50.9	13.3	100.1

$C_4^=$: Olefin product with 4 carbons; **C_4^O:** Paraffin products with 4 carbons; **C_{5+}:** Hydrocarbon products with 5 or more carbons. **Reaction condition: Mass ratio of plastic to liquid metal, $\omega_{(PP:\ EGaIn)}$ = 1: 1.**

Supplementary Table 3

Depolymerization of PP-based disposable lunch boxes using microwave-powered liquid metal EGaIn under different mass ratios.

$\omega_{(PP:\ EGaIn)}$	Evolved gas composition (Vol. %)									Gas yield (wt%)	Oil yield (wt%)	Solid yield (wt%)	Mass balance (%)
	CH_4	C_2H_4	C_2H_6	C_3H_6	C_3H_8	$C_4^=$	C_4^O	C_{5+}	H_2				
1: 1	18.3	18.9	4.4	24.4	0.8	6.6	2.3	6.8	17.5	51.5	43.2	5.0	99.7
5: 1	10.9	10.3	6.0	38.6	1.7	7.3	1.9	13.4	9.9	27.5	71.0	1.4	99.9
10: 1	12.9	11.1	6.3	38.1	1.8	6.9	1.5	12.4	9.0	22.4	76.1	1.3	99.8
12.5: 1	10.9	11.3	5.8	41.7	1.5	7.8	1.8	12.4	6.8	21.3	78.1	0.8	100.2
15: 1	**8.2**	**7.2**	**7.2**	**43.5**	**2.3**	**7.7**	**1.5**	**17.2**	**5.2**	**19.2**	**80.2**	**0.4**	**99.8**
17.5: 1	11.0	9.9	5.3	37.8	1.6	7.3	1.7	16.9	8.5	27.7	72.2	0.2	100.1

$C_4^=$: Olefin product with 4 carbons; **C_4^O:** Paraffin products with 4 carbons; **C_{5+}:** Hydrocarbon products with 5 or more carbons. **Reaction condition: Microwave power, P = 600 W.**

Supplementary Table 4

Time-dependent yields of three depolymerization cycles for LDPE-based plastic wraps using microwave-powered liquid metal EGaIn.

EGaIn@LDPE	Cycle-1 Yield (wt%)			Cycle-2 Yield (wt%)			Cycle-3 Yield (wt%)		
	Gas	Oil	Solid	Gas	Oil	Solid	Gas	Oil	Solid
5 min	2.98	5.40	91.63	2.25	1.00	96.75	2.26	2.26	94.01
10 min	7.11	22.56	70.32	8.82	14.58	76.60	4.67	4.67	86.07
15 min	10.18	39.67	50.15	13.54	45.50	40.96	9.05	9.05	64.59
20 min	13.94	61.17	24.88	17.41	66.09	16.50	14.98	14.98	15.95
25 min	17.95	81.73	0.32	21.38	78.26	0.36	17.42	17.42	6.38

Reaction condition: P = 600 W, $\omega_{(\text{LDPE: EGaIn})}$ = 15: 1.

Supplementary Table 5

The ratios of H_{Olefin}/H_{Total} and branching within oil products at different depolymerization times of LDPE-based wraps using microwave-powered liquid metal EGaIn.

EGaIn@LDPE	Cycle-1 ^{1}H NMR		Cycle-2 ^{1}H NMR		Cycle-3 ^{1}H NMR	
	H_{Olefin}/H_{Total}	Branching (%)	H_{Olefin}/H_{Total}	Branching (%)	H_{Olefin}/H_{Total}	Branching (%)
5 min	0.052	6.3	0.057	6.9	0.056	6.7
10 min	0.068	8.6	0.072	8.8	0.07	8.9
15 min	0.063	8.8	0.06	8.8	0.058	9
20 min	0.06	9.4	0.059	9.4	0.057	9.2
25 min	0.061	9.8	0.061	9.8	0.062	9.7

Reaction condition: P = 600 W, $\omega_{(LDPE:\ EGaIn)}$ = 15: 1.

Branching is the branches per 100 C, calculated by the following formula:

$$\text{Branching} = \frac{(\text{Integral of } CH_3)/3}{(\text{Integral of } CH\ +\ \text{Integral of } CH_2\ +\ \text{Integral of } CH_3)/2} \times 100\%$$

Supplementary Table 6

Composition of gas products at different depolymerization times of LDPE-based plastic wraps using microwave-powered liquid metal EGaIn.

EGaIn@LDPE	Evolved gas composition (Vol. %)								
	CH_4	C_2H_4	C_2H_6	C_3H_6	C_3H_8	$C_4^=$	C_4^O	C_{5+}	H_2
5 min	11.48	32.96	8.40	12.30	6.60	5.08	6.70	4.78	11.69
10 min	11.31	32.05	9.89	13.27	7.78	5.70	7.28	4.92	7.80
15 min	12.10	31.53	9.91	13.39	7.56	5.61	7.24	4.90	7.76
20 min	12.02	28.95	9.96	13.75	7.89	5.93	7.86	5.88	7.75
25 min	12.63	28.28	9.73	13.64	7.20	5.85	7.77	6.21	8.69

$C_4^=$: Olefin product with 4 carbons; **C_4^O:** Paraffin products with 4 carbons; **C_{5+}:** Hydrocarbon products with 5 or more carbons. **Reaction condition: P = 600 W, $\omega_{(LDPE:\ EGaIn)}$ = 15: 1.**

Supplementary Table 7

Thirty successive depolymerization cycles for LDPE-based plastic wrap using microwave-powered liquid metal EGaIn.

EGaIn@LDPE	Evolved gas composition (Vol. %)									Yield (wt%)			Mass
	CH_4	C_2H_4	C_2H_6	C_3H_6	C_3H_8	$C_4^=$	C_4^O	C_{5+}	H_2	Gas	Oil	Solid	balance (%)
Cycle 1	10.1	30.2	6.4	13.6	4.5	6.8	8.8	12	7.6	12.3	86.7	0.8	99.8
Cycle 2	12.0	29.7	6.4	12.3	4.5	6.1	8.0	9.7	11.3	13.1	86.1	0.9	100.1
Cycle 3	10.7	33.2	6.3	13.6	5.2	6.5	9.1	10.5	4.9	16.2	82.8	1.3	100.3
Cycle 4	9.4	27.5	8.2	14.5	7.3	7.2	9.4	9.4	7.1	13.2	86.5	0.1	99.8
Cycle 5	10.0	28.5	7.3	14.0	5.7	7.5	9.2	10.6	7.2	15.9	83.6	0.2	99.7
Cycle 6	10.3	29.5	8.8	15.0	6.9	6.8	8.6	7.8	6.3	16.7	82.5	0.9	100.1
Cycle 7	8.7	27.0	7.4	14.3	6.5	7.6	9.9	13.5	5.1	17.1	82.5	0.2	99.8
Cycle 8	9.5	24.9	8.9	14.7	8.5	7.1	9.4	8.3	8.7	11.4	88.0	0.3	99.7
Cycle 9	9.9	28.5	8.2	14.6	7.0	6.8	8.9	8.4	7.7	14.5	85.1	0.3	99.9
Cycle 10	9.5	29.4	7.4	13.9	6.1	6.8	8.8	10.3	7.8	16.6	82.7	0.8	100.1
Cycle 11	9.9	27.1	8.7	14.8	7.3	6.8	8.7	9.2	7.5	18.7	80.9	0.2	99.8
Cycle 12	9.9	27.9	8.7	15.1	7.1	7.0	8.9	8.9	6.5	13.3	86.4	0.5	100.2
Cycle 13	9.8	23.8	8.2	14.4	6.2	7.3	9.5	12.8	8.0	14.2	85.6	0.3	100.1
Cycle 14	10.5	28.2	8.4	15.2	6.7	6.4	7.9	6.9	9.8	12.0	87.5	0.2	99.7
Cycle 15	10.0	27.5	8.8	15.4	7.5	7.2	9.4	7.1	7.1	12.5	87.0	0.4	99.9
Cycle 16	11.3	25.9	9.3	15.5	6.9	6.7	8.9	6.6	8.9	12.6	87.1	0.4	100.1
Cycle 17	9.8	26.8	9.7	15.8	8.5	7.1	9.2	7	6.1	12.5	87.2	0.1	99.8
Cycle 18	10.5	29.2	9.3	15.4	7.3	6.6	8.6	7.1	6.0	13.7	86.0	0.1	99.8
Cycle 19	9.8	26.6	10.0	15.8	8.6	7.2	9.5	7.2	5.3	13.1	86.7	0.3	100.1
Cycle 20	9.1	24.8	9.5	15.3	8.3	7.7	10.0	10.7	4.6	15.4	84.2	0.5	100.1
Cycle 21	9.7	25.3	10.6	16.0	9.2	7.2	9.1	8.1	4.8	13.4	86.1	0.3	99.8
Cycle 22	9.4	22.9	10.3	15.8	9.3	7.9	9.9	9.5	5.0	15.2	84.1	0.5	99.8
Cycle 23	10.2	28.0	9.7	15.3	7.9	6.7	8.7	7.7	5.8	14.5	85.3	0.4	100.2
Cycle 24	9.5	24.2	10.4	15.5	9.2	7.2	9.5	9	5.5	14.6	84.9	0.6	100.1
Cycle 25	10.1	24.8	9.5	15.4	7.9	6.9	9.1	9.6	6.7	14.3	85.5	0.3	100.1
Cycle 26	10.5	27.2	9.0	14.9	6.9	6.9	8.7	9.3	6.6	16.7	82.6	0.3	99.6
Cycle 27	10.1	24.7	10.9	16.0	9.2	7.3	9.1	7.7	5.0	11.8	87.9	0.4	100.1
Cycle 28	10.1	24.2	11.1	16.1	9.5	7.5	9.2	7.3	5.0	11.6	88.2	0.3	100.1
Cycle 29	10.1	25.8	9.5	15.5	8.3	7.2	9.3	7.8	6.5	16.7	83.1	0.1	99.9
Cycle 30	9.7	24.2	10.4	15.3	9.4	7.1	9.3	8.2	6.4	13.4	86.3	0.1	99.8

$C_4^=$: Olefin product with 4 carbons; **C_4^O:** Paraffin products with 4 carbons; **C_{5+}:** Hydrocarbon products with 5 or more carbons. **Reaction condition: P = 600 W, $\omega_{(LDPE:\ EGaIn)}$ = 15:1.**

Supplementary Table 8

EXAFS fitting parameters at the Ga K-edge for various samples.

Sample	Shell	*CN*[a]	*R*(Å)[b]	σ^2(Å^2)[c]	ΔE_0(eV)[d]	*R* factor
EGaIn Bef.	Ga-O	0.7	1.84	0.0062	-1.02	0.0103
	Ga-Ga	2.1	2.72	0.0131	4.67	
EGaIn Aft.	Ga-O	2.4	1.88	0.0097	3.18	0.0076
	Ga-Ga	0.8	2.65	0.0085	-3.92	
	Ga-Ga	0.5	3.28	0.0020	-10.26	
Ga_2O_3	Ga-O	6*	1.88	0.0101	0.54	0.0119
	Ga-Ga1	12*	3.10	0.0069	7.05	
	Ga-Ga2	12*	3.22	0.0062	-9.93	
Ga foil	Ga-Ga	12.2	2.76	0.0195	6.47	0.0136

[a]*CN*, coordination number; [b]*R*, the distance between absorber and backscatter atoms; [c]σ^2, Debye-Waller factor to account for both thermal and structural disorders; [d]ΔE_0, inner potential correction; *R* factor indicates the goodness of the fit. S_0^2 was fixed to 0.735. A reasonable range of EXAFS fitting parameters: $0.600 < S_0^2 < 1.000$; $CN > 0$; $\sigma^2 > 0$ Å^2; $|\Delta E_0| < 15$ eV; *R* factor < 0.02.

Supplementary Table 9

Comparison of microwave-powered liquid metal depolymerization with other methods.

Plastic	Catalyst	Depolymerization methods	Time (min)	Gas yield (wt.%)	Oil yield (wt.%)	Cycle number	PUC($g_{Plastic}$ /$g_{Catalyst}$/h)	Ref.
LDPE	SiC-MgO	Microwave pyrolysis (2.45 GHz, 350~550 ℃, 1 bar) &*ex-situ* catalysis (350~550 ℃, 1 bar)	~25	＞56.6	24.2~38.5	1	0.072	Ref. 1
LDPE	(SiC & NiO)-HY	Microwave catalytic pyrolysis (2.45 GHz, 450~600 ℃, 1 bar) & *ex-situ* catalysis (350~500 ℃, 1 bar)	~30	47.77~50.46	48.08~51.23	1	0.06	Ref. 2
HDPE	$FeAlO_x$	Microwave-initiated catalytic deconstruction	5	62.7	2.1	10	12	Ref. 3
HDPE	SiC-ZSM-5	Microwave catalytic pyrolysis (2.45 GHz, 500 °C, 1 bar) & *ex-situ* catalysis (400 ℃, 1 bar)	-	17.6	73.7	1	0.333	Ref. 4
HDPE	Activated carbon	Microwave catalysis (2.45 GHz, 520 ℃, 1 bar)	110	15.0	85.0	1	0.545	Ref. 5
LDPE	ZSM-5	Microwave catalysis (2.45 GHz, 300 ℃, 1 bar)	~44	91.8	3.8	5	1.364	Ref. 6
LDPE	Ru/ZSM-5	Microwave catalysis (2.45 GHz, 300 ℃, 1 bar)	~44	88.0	2.0	7	1.364	Ref. 7
HDPE	2.4 nm $mSiO_2$/Pt/SiO_2	Hydrogenolysis (300 ℃, 17.2 bar)	1440	21.5	76.6(C_{16}-centred)	1	2.805	Ref. 8
LDPE	Ru/C	Hydrogenolysis (200 ℃, 20 bar)	960	55	45(C_8-C_{35})	3	1.688	Ref. 9
LDPE	Ru/WZr	Hydrogenolysis (250 ℃, 50 bar)	120	10-20	40-70	1	20	Ref. 10
LDPE	$mSiO_2$/Pt-1.7/SiO_2	Hydrogenolysis (300 ℃, 8.9 bar)	900	12.4	73.6(C_{23}-centred)	1	8.087	Ref. 11
LDPE	L-ZrO_2 @$mSiO_2$	Hydrogenolysis (300 ℃, 9.92 bar)	1200	14	86(C_{18}-centred)	1	27.25	Ref. 12
HDPE	Ru/HZSM-5(300)	Hydrogenolysis (280 ℃, 20 bar)	1440	11.6	58.0	3	0.417	Ref. 13
HDPE	LSP-Z100	Hydrogenolysis (240 ℃, 1 bar)	1470	3.0	87.2	1	0.204	Ref. 14
Low-molecular-weight PE	Pt/γ-Al_2O_3	Tandem hydrogenolysis /aromatization (280 ℃, 1 bar)	1440	9	70	3	0.025	Ref. 15
LDPE				6	69			
HDPE				6	55			
PE	-	Temperature-gradient thermolysis (Fragmentation 360 ℃, 1 bar)	480~960	14/21/45 N_2/10%O_2/Air	86/79/55 N_2/10%O_2/Air	-	-	Ref. 16
PP				10/15/13 N_2/10%O_2/Air	90/85/87 N_2/10%O_2/Air			
PP&*i*C_5	[C_4Py]Cl-$AlCl_3$ ionic liquids	Tandem cracking-alkylation (70~100 ℃, 1 bar)	360	-	90~95	5	0.011[a]	Ref. 17
LDPE&*i*C_5			2880	-	80		0.001[a]	
HDPE&*i*C_5			2880	-	70		0.001[a]	
LDPE	**GaIn**	**Microwave catalysis (2.45 GHz, 400 ℃, 1 bar)**	**~25**	**14.3**	**85.3**(C_{21}-centred)	**30**	**36 (or 226.8 $g_{plastic}$/$mL_{catalyst}$/h)**	**This work**
HDPE				**13.3**	**85.9**(C_{21}-centred)			
PP				**15.4**	**81.0**			

PUC: Plastic upcycling capability of different depolymerization methods. **[a]:** Unit is $g_{plastic}/mL_{catalyst}/h$.

Supplementary Table 10

Comparison of experimental results between microwave-powered liquid metal depolymerization and other methods.

Plastic	Agents	$\omega_{(Plastic:Agent)}$	Depolymerization methods	Time (min)	Evolved gas composition (Vol. %)					Yield (wt%)			Energy consum. (kWh)
					CH_4	$C_{2-4}^{=}$	C_{2-4}^{O}	C_{5+}	H_2	Gas	Oil	Solid	
PP	-	-	Thermal, 450 ℃	480	2.2	20.9	4.5	55.1	17.3	12.4	19.6	68	3.226
PP	-	-	Thermal, 600 ℃	30	6.6	49.3	11.6	30.2	2.3	13.3	84.3	2.4	1.194
PP	EGaIn	15: 1	Thermal, 600 ℃	30	6	48.1	11.2	31.6	3.2	13.3	86.0	0.7	1.194
PP	EGaIn	15: 1	Microwave, 600 W	25	10.7	58.7	9.0	11.4	10.2	18.6	80.3	0.8	0.425
PP	50nmFe	5: 1	Microwave, 600 W	30	13.1	32.8	8.7	5.7	39.6	42.7	46.3	11.0	0.51
PP	50nmCo	5: 1	Microwave, 600 W	30	10	38.9	8.5	8.3	34.4	17.4	78.4	4.3	0.51
LDPE	-	-	Thermal, 450 ℃	360	2.9	12.3	24.2	52	8.6	3.3	4.0	92.7	2.506
LDPE	EGaIn	15: 1	Thermal, 600 ℃	30	12.8	37.6	26.4	13.7	9.6	10.2	83.1	6.7	1.194
LDPE	SiC	15: 1	Microwave, 600 W	25	21.3	50.8	8.5	7.0	12.4	32.2	41.9	25.9	0.425
LDPE	AC	15: 1	Microwave, 600 W	25	17.9	39.7	13.2	5.0	24.3	39.7	47.2	13.1	0.425
LDPE	EGaIn	15: 1	Microwave, 600 W	25	10.1	50.6	19.7	12.0	7.6	12.3	86.7	0.8	0.425

$C_{2-4}^{=}$: Olefin product with 2~4 carbons; **C_{2-4}^{O}:** Paraffin products with 2~4 carbons; **C_{5+}:** Hydrocarbon products with 5 or more carbons.

Supplementary Table 11

Ten successive depolymerization cycles for HDPE-based drug bottles using microwave-powered liquid metal EGaIn.

EGaIn@HDPE	Evolved gas composition (Vol. %)									Gas yield (wt%)	Oil yield (wt%)	Solid yield (wt%)	Mass balance (%)
	CH_4	C_2H_4	C_2H_6	C_3H_6	C_3H_8	$C_4^=$	C_4^O	C_{5+}	H_2				
Cycle 1	9.3	35.4	6.3	14.9	6.2	5.5	8.6	7	6.8	16.4	82.5	0.9	99.8
Cycle 2	9.7	34.1	6.9	15.8	6.8	5.3	8.5	5.8	7.1	12.7	86.8	0.6	100.1
Cycle 3	9.2	32.9	6.8	15.6	7.2	5.6	9.0	6.9	6.8	13.3	85.5	0.8	99.6
Cycle 4	9.2	30.7	7.5	16.2	8.0	5.7	9.0	6.7	7.0	12.0	87.6	0.3	99.9
Cycle 5	9.8	31.8	7.8	16.3	8.0	5.3	8.3	5.8	6.9	12.5	86.6	0.7	99.8
Cycle 6	10.2	30.1	7.9	16.3	7.0	6.0	9.0	6.8	6.7	14.0	84.9	1.3	100.2
Cycle 7	9.5	30.7	8.1	16.2	7.5	6.6	9.1	6.6	5.7	13.2	85.9	0.8	99.9
Cycle 8	9.3	27.3	8.5	16.2	8.2	6.9	10.2	7.9	5.5	12.8	86.5	0.5	99.8
Cycle 9	9.8	29.3	8.6	16.3	7.6	6.7	9.6	7	5.1	13.5	85.9	0.7	100.1
Cycle 10	9.4	28.7	8.7	16.4	8.4	7.1	9.5	6.7	5.1	12.3	87.5	0.4	100.2

$C_4^=$: Olefin product with 4 carbons; **C_4^O:** Paraffin products with 4 carbons; **C_{5+}:** Hydrocarbon products with 5 or more carbons. **Reaction condition: P = 600 W, $\omega_{(HDPE:\ EGaIn)}$ = 15: 1.**

Supplementary Table 12

Ten successive depolymerization cycles for PP-based disposable lunch boxes using microwave-powered liquid metal EGaIn.

EGaIn@PP	Evolved gas composition (Vol. %)									Gas yield (wt%)	Oil yield (wt%)	Solid yield (wt%)	Mass balance (%)
	CH_4	C_2H_4	C_2H_6	C_3H_6	C_3H_8	$C_4^=$	C_4^O	C_{5+}	H_2				
Cycle 1	10.7	12.2	5.7	40.9	1.7	5.6	1.6	11.4	10.2	18.6	80.3	0.8	99.7
Cycle 2	10.7	10.5	7.7	43.0	2.2	7.2	1.8	10.3	6.6	23.6	75.9	0.9	100.4
Cycle 3	10.0	10.3	7.8	43.2	2.2	7.7	1.9	11.6	5.3	20.1	79.0	1.1	100.2
Cycle 4	8.4	7.5	8.8	47.4	2.6	7.8	1.6	12.3	3.6	17.2	81.9	0.8	99.9
Cycle 5	10.6	9.8	7.8	43.3	2.3	8.5	1.6	11.2	4.9	18.0	81.0	0.7	99.7
Cycle 6	8.0	6.5	8.9	48.7	2.8	8.0	1.4	12.2	3.5	15.4	84.0	0.9	100.3
Cycle 7	8.6	8.4	8.6	47.4	2.5	8.1	1.6	10.9	3.9	17.5	82.1	0.2	99.8
Cycle 8	8.4	8.0	8.8	47.3	2.6	8.7	1.7	10.9	3.6	18.9	80.7	0.3	99.9
Cycle 9	8.0	6.0	9.7	50.2	2.7	8.1	1.3	11.2	2.8	16.5	83.2	0.1	99.8
Cycle 10	7.7	6.0	9.3	48.7	2.8	8.4	1.4	12.5	3.2	17.5	82.3	0.5	100.3

$C_4^=$: Olefin product with 4 carbons; **C_4^O:** Paraffin products with 4 carbons; **C_{5+}:** Hydrocarbon products with 5 or more carbons. **Reaction condition: P = 600 W, $\omega_{(PP:\ EGaIn)}$ = 15: 1.**

Supplementary Table 13

Ten successive depolymerization cycles for LDPE-based plastic wrap using microwave-powered liquid metal EGaInSn.

EGaInSn @LDPE	Evolved gas composition (Vol. %)									Gas yield (wt%)	Oil yield (wt%)	Solid yield (wt%)	Mass balance (%)
	CH_4	C_2H_4	C_2H_6	C_3H_6	C_3H_8	$C_4^=$	C_4^O	C_{5+}	H_2				
Cycle 1	11.5	35.2	5.6	12.1	3.7	5.5	6.6	7.4	12.4	22.6	72.9	4.4	99.9
Cycle 2	9.8	32.6	7.4	14.0	6.0	7.1	8.4	7.7	7.0	15.2	84.5	0.6	100.3
Cycle 3	9.8	28.6	7.7	14.2	6.4	6.6	8.9	9.3	8.5	15.5	84.1	0.5	100.1
Cycle 4	9.5	29.5	8.1	14.6	6.5	6.6	8.8	9.3	7.1	16.7	82.8	0.8	100.3
Cycle 5	9.6	28.9	8.2	14.6	6.8	6.7	8.9	9.2	7.1	15.3	83.9	0.7	99.9
Cycle 6	9.9	30.8	7.6	14.2	6.3	6.3	8.5	8.7	7.7	15.8	83.5	0.9	100.2
Cycle 7	10.5	29.5	8.7	15.0	6.6	6.7	8.3	7.6	7.1	16.1	83.4	0.2	99.7
Cycle 8	9.6	28.3	8.8	14.8	7.3	6.9	8.8	9.1	6.4	16.9	82.1	0.6	99.6
Cycle 9	10.0	31.3	7.1	14.1	5.4	6.6	8.5	9.7	7.3	18.6	80.8	0.4	99.8
Cycle 10	11.5	31.3	8.8	15.6	6.4	6.4	8.0	5.5	6.5	15.5	83.4	1.3	100.2

$C_4^=$: Olefin product with 4 carbons; **C_4^O:** Paraffin products with 4 carbons; **C_{5+}:** Hydrocarbon products with 5 or more carbons. **Reaction condition: P = 600 W, $\omega_{(LDPE:\ EGaInSn)}$ = 15: 1.**

Supplementary Table 14

Ten successive depolymerization cycles of PP-based disposable lunch boxes using microwave-powered liquid metal EGaInSn.

EGaInSn@PP	Evolved gas composition (Vol. %)									Gas yield (wt%)	Oil yield (wt%)	Solid yield (wt%)	Mass balance (%)
	CH_4	C_2H_4	C_2H_6	C_3H_6	C_3H_8	$C_4^=$	C_4^O	C_{5+}	H_2				
Cycle 1	10.1	9.4	6.9	45.1	2.1	6.4	1.1	10.3	8.6	15.1	84.2	0.5	99.8
Cycle 2	9.3	8.0	8.7	48.6	2.6	7.3	1.6	7.9	6.0	16.2	83.2	0.3	99.7
Cycle 3	9.2	7.7	9.3	49.0	2.8	7.9	1.5	7.6	5.0	16.9	83.0	0.5	100.4
Cycle 4	8.2	6.8	9.4	49.5	2.8	8.2	1.5	9.4	4.2	19.2	80.5	0.8	100.5
Cycle 5	7.9	6.3	9.4	50.0	2.7	8.8	1.5	9.4	4.0	14.7	84.2	0.7	99.6
Cycle 6	8.2	6.8	9.4	49.4	2.8	8.4	1.4	9.4	4.2	15.3	84.0	0.9	100.2
Cycle 7	8.4	8.0	8.4	46.6	2.5	9.1	1.7	11.2	4.1	18.1	81.3	0.2	99.6
Cycle 8	9.2	6.9	10.3	51.9	2.8	7.5	1.1	5.7	4.6	13.4	86.3	0.6	100.3
Cycle 9	8.5	7.3	9.8	50.2	2.8	8.7	1.4	7.5	3.8	16.2	83.1	0.4	99.7
Cycle 10	7.6	4.8	10.9	54.4	3.3	7.9	1.1	6.9	3.1	14.0	85.3	1.3	100.6

$C_4^=$: Olefin product with 4 carbons; **C_4^O:** Paraffin products with 4 carbons; **C_{5+}:** Hydrocarbon products with 5 or more carbons. **Reaction condition: P = 600 W, $\omega_{(PP:\ EGaIn)}$ = 15: 1.**

Supplementary Discussion 1

Lab-scale polyolefin depolymerization

The structure of polyolefin plastics and raw materials was determined using an X-ray diffractometer (XRD, D8 focus, Bruker, Germany), as illustrated in **Supplementary Figure 1**. The polyolefin plastics utilized in our experiments exhibited a nearly identical structure to that of the raw materials.

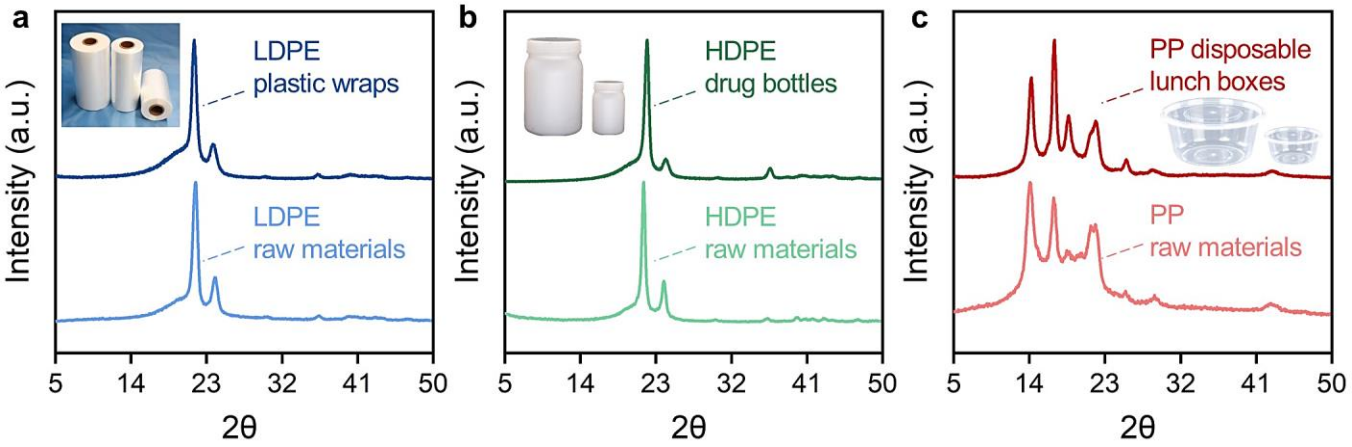

Supplementary Figure 1. XRD spectra depicting the composition of polyolefin plastics and raw materials. From left to right: (a) LDPE-based plastic wraps and LDPE raw materials; (b) HDPE-based drug bottles and HDPE raw materials; (c) PP-based disposable lunch boxes and PP raw materials.

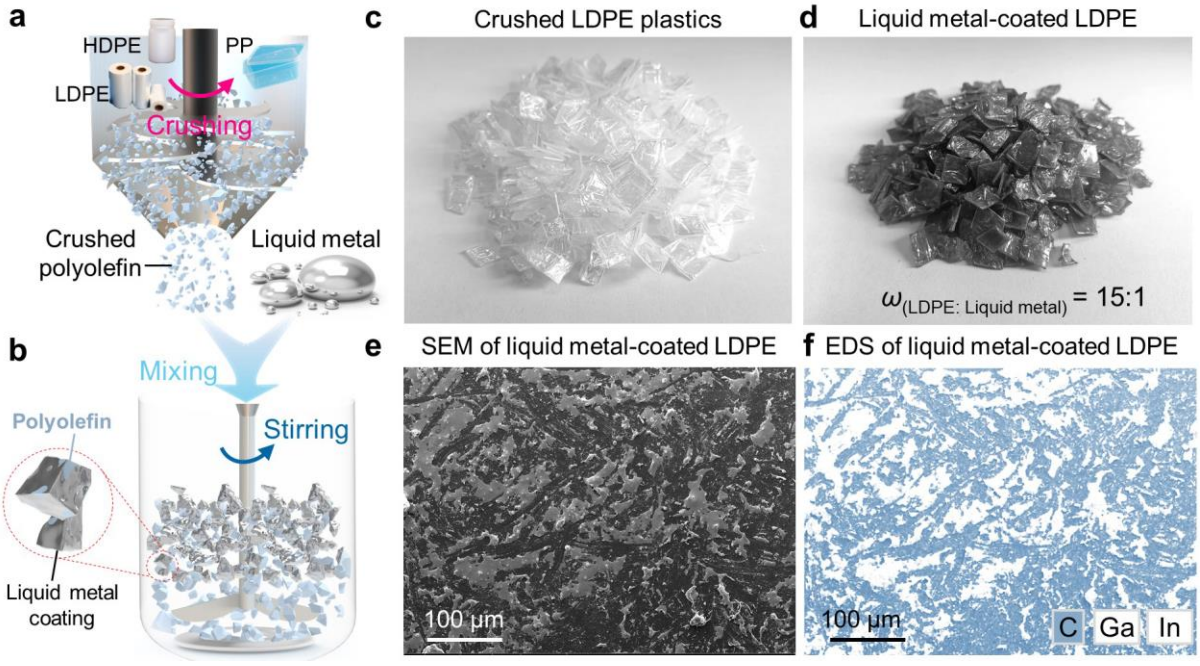

Supplementary Figure 2. Preparation of liquid metal-coated polyolefins. (a) Schematic depicting the mechanical crushing of polyolefins. (b) Schematic illustrating the mechanical stirring to prepare liquid metal-coated polyolefins. The partial zoom reveals polyolefins coated with liquid metal. (c) Photograph of the crushed LDPE plastics. (d-e) Photograph (d), SEM image (e), and EDS image (f) of the liquid metal-coated LDPE plastics. The mass ratio between LDPE and liquid metal is 15: 1. The color change in (d) was mainly attributed to the liquid metal coatings.

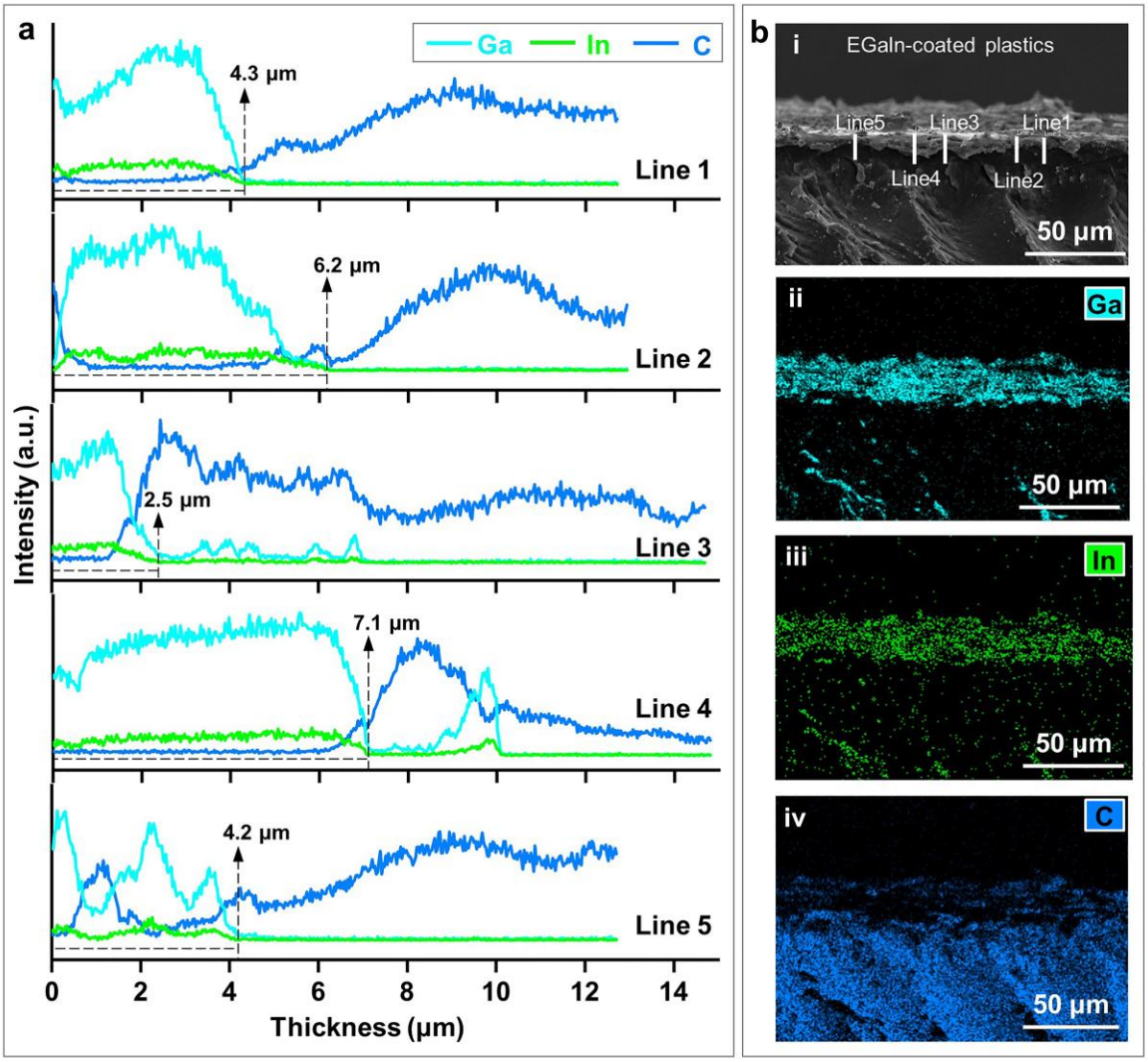

Supplementary Figure 3. The thickness of the liquid metal coating on the crushed LDPE. (a) The elementary composition on lines 1 to 5 in image (b) i using quantitative EDS analysis. (b) ESEM image and EDS mappings of the cross-sectional view of EGaIn-coated LDPE. The thickness of the EGaIn layer remains at a micron level (2.5~7.1μm) when the mass ratio between LDPE and EGaIn is set at 15: 1.

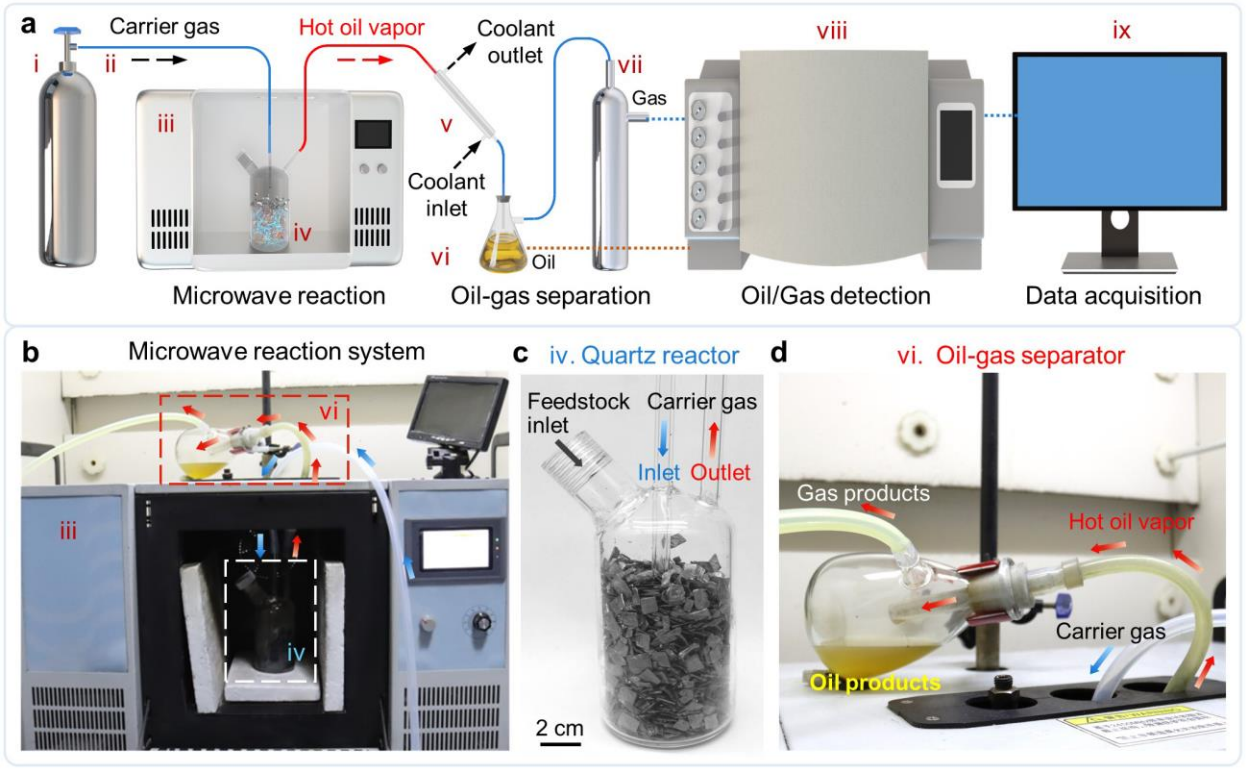

Supplementary Figure 4. Lab-scale depolymerization of polyolefin plastics via microwave-powered liquid metals. (a) Schematic illustrating the equipment and experimental system. From left to right: i) carrier gas storage cylinder, ii) duct, iii) microwave reaction equipment, iv) quartz reactor, v) condenser, vi) oil-gas separator, vii) gas product storage cylinder, viii) oil or gas detection equipment, and ix) data acquisition equipment. (b) Photograph of iii) microwave reaction instrument, iv) customized quartz reactor and vi) oil-gas separator. (c) Photograph of the customized quartz reactor packed with liquid metal-coated LPDE. The left inlet was used to load the feedstock, which was sealed with a Teflon screw plug after loading. The middle inlet served as the carrier gas inlet. To completely purge the oxygen in the quartz reactor, the carrier gas was introduced into the reactor bottom and then passed through the feedstock. The right outlet was utilized to exhaust both carrier gas and depolymerization products. (d) Enlarged view of the oil-gas separator. The oil products were successfully separated from the depolymerization products.

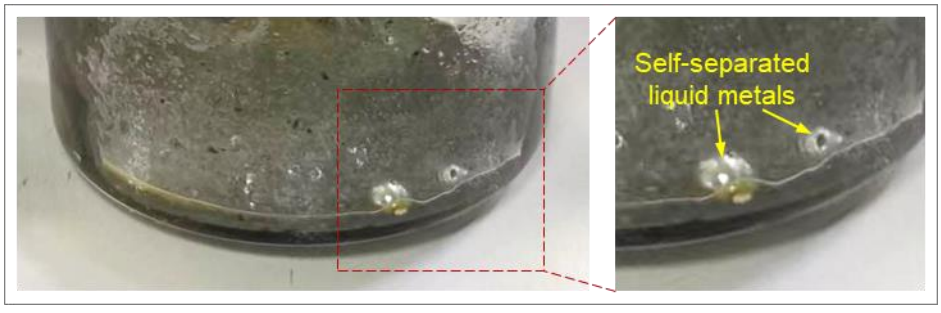

Supplementary Figure 5. Photographs depicting the settling of self-separated liquid metals at the bottom of a quartz reactor bottle after depolymerization.

Supplementary Discussion 2

Pulsed plasma phenomena

The plasma ignited by microwave-powered liquid metals was captured using a Canon camera and a high-speed camera (Phantom C320, York Technologies Ltd., USA), respectively. Interestingly, the arc discharge plasma appeared around the polyolefins and gradually transformed into localized plasma hotspots (see **Supplementary Video 1** and **Supplementary Figure 6**). We successfully captured the formation of these localized plasma hotspots during the microwave-powered liquid metal depolymerization utilizing the high-speed camera. As shown in **Supplementary Video 2 and Supplementary Figure 7**, the arc discharge plasma exhibited a pulsed feature with an interval of approximately 5 ms. The above change in plasma behavior might be attributed to alterations in the gaseous atmosphere from pure Ar gas to a mixture within the quartz reactor, caused by the generation of depolymerization products. Some of these depolymerization products could transform into plasma, which also participated in the subsequent depolymerization process. As the depolymerization progresses, the depolymerization products gradually increase within the reaction vessel. Simultaneously, the temperature of the packed bed continued to rise, leading to the gradual softening of the plastic and reduction in its tips, thereby diminishing the arc discharge phenomena while accentuating local plasma hotspots. Eventually, under the actuation of local plasma hotspots, polyolefin depolymerization persisted until the polyolefin was completely depolymerized.

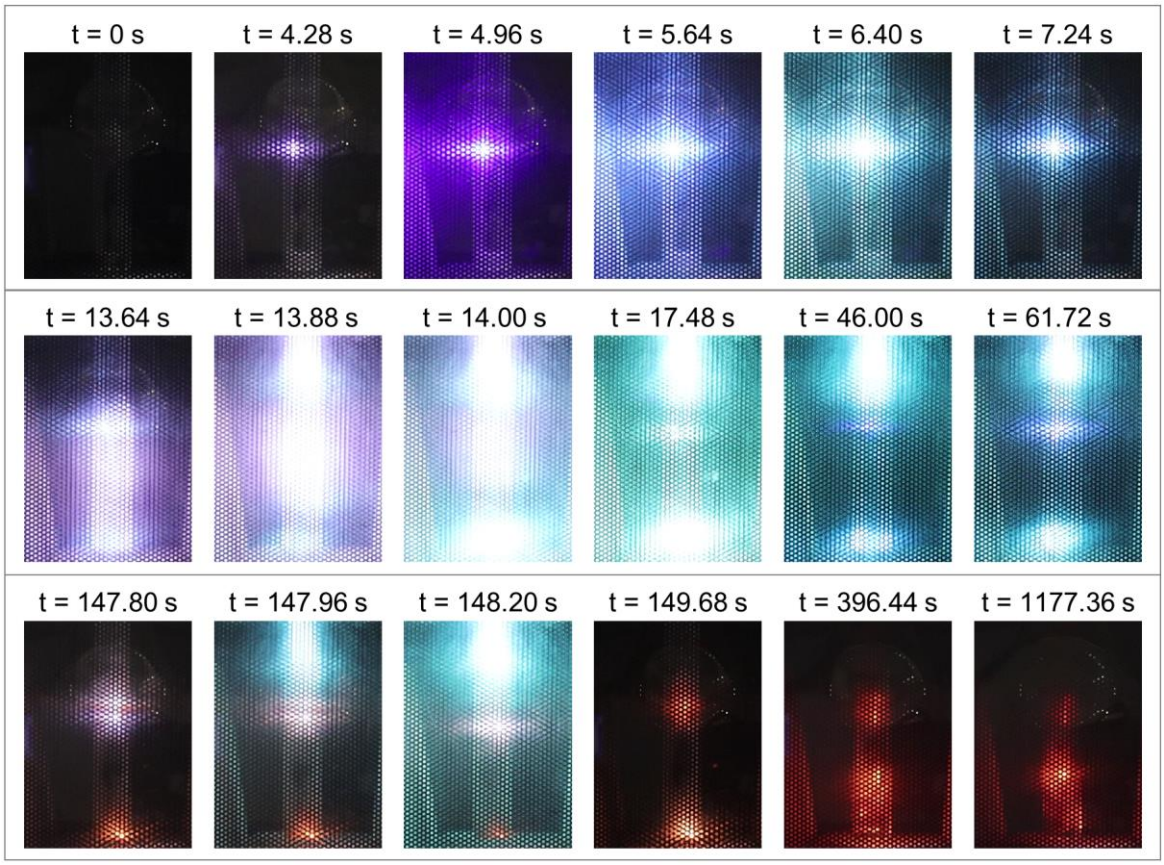

Supplementary Figure 6. Plasma phenomena were captured using a Canon camera at 50 fps during the microwave-powered liquid metal depolymerization.

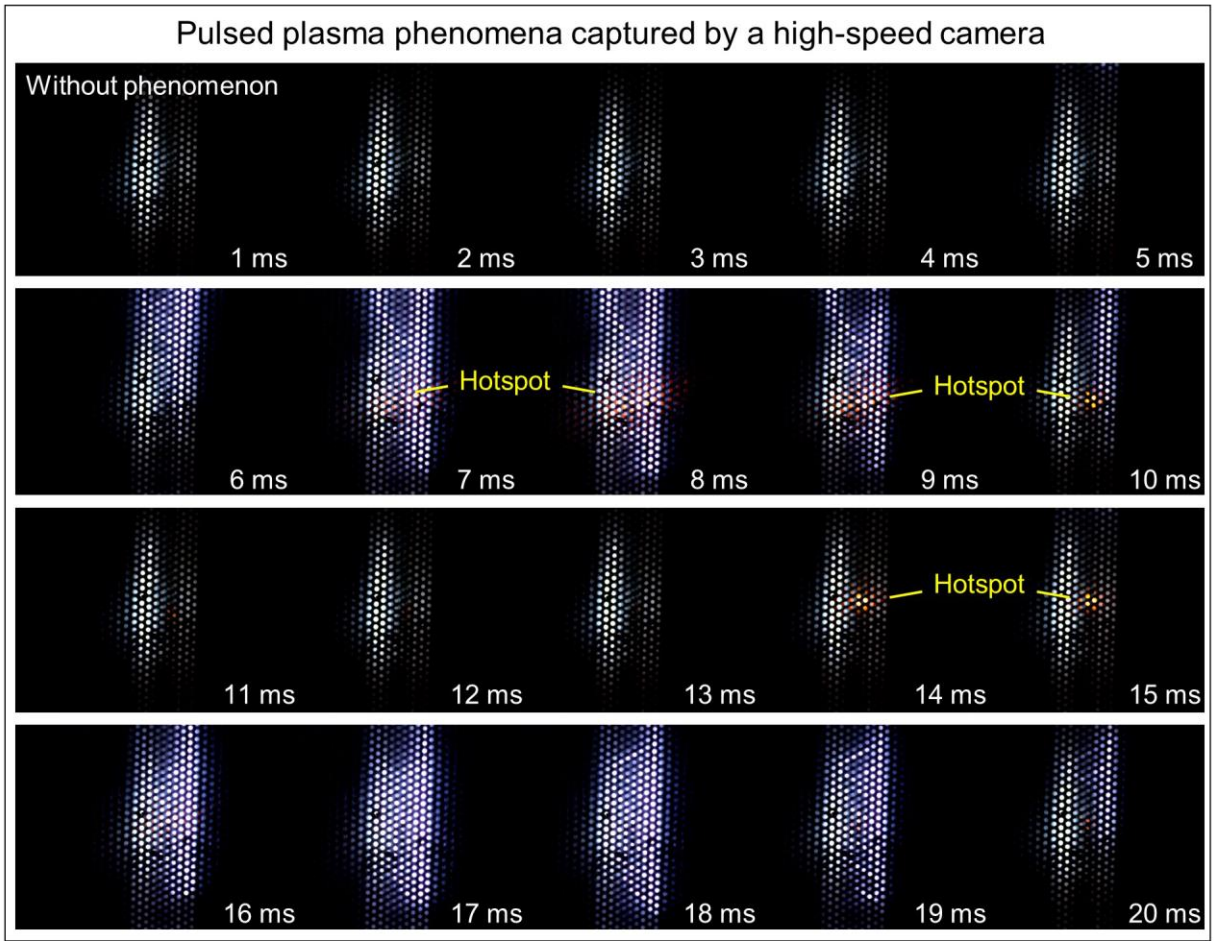

Supplementary Figure 7. Pulsed plasma phenomena were captured using a high-speed camera at 1000 fps during the microwave-powered liquid metal depolymerization.

To further substantiate the pivotal role of plasma, we performed 10 intermittent microwave irradiation experiments, with each irradiation lasting for 10 seconds. It was found that the plasma participated in the plastic depolymerization and could depolymerize plastic into gas products, while the reactor temperature slightly increased from 21 ℃ to 33 ℃ after 10 irradiation cycles (**Supplementary Figure 8**). The temperature was far below the thermal decomposition temperatures of plastics (410 ℃ for LDPE, 367 ℃ for PP, see **Supplementary Figure 9**), indicating that the plastic indeed underwent depolymerization under the action of plasma.

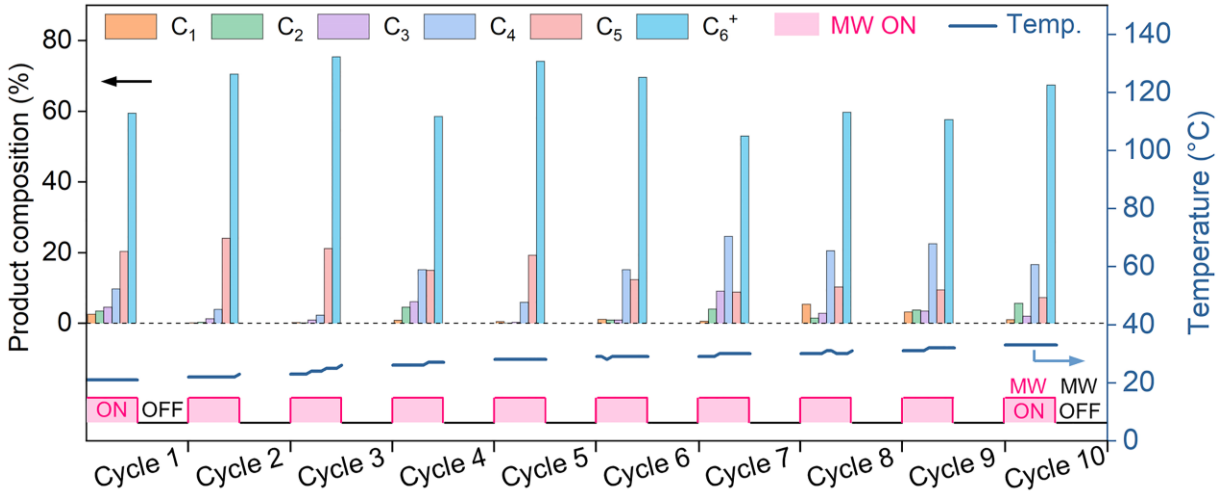

Supplementary Figure 8. Gas product composition and reactor temperature variation during 10 intermittent microwave irradiation cycles, with a constant microwave power of 600 W and an on-time of 10 s.

Thermogravimetric analysis (TGA, STA449C, NETZSCH, Germany) was utilized to characterize the depolymerization temperature of plastics, which were heated from room temperature to 1000 ℃ with a ramping rate of 10 ℃ min^{-1} in a nitrogen atmosphere. The temperature of the packed bed was directly obtained using the infrared temperature monitoring module of the microwave oven (Microwave Scientific Instruments, Qingdao Microwave Creative Technology Co., Ltd., China). As illustrated in **Supplementary Figures 9a and 9b**, the LDPE-based plastics displayed apparent weight loss at 410 ℃, while PP-based plastics showed apparent weight loss at 367 ℃, suggesting that the volatile species start forming at such temperatures. Compared to the pure plastic group (pure LDPE and PP), the addition of liquid metal EGaIn could significantly increase the temperature of the packed bed under a microwave field, which was sufficient to initiate the depolymerization process, as depicted in **Supplementary Figures 9c and 9d**. However, the addition of Ga_2O_3 could only slightly increase the temperature of LDPE, which was insufficient to initiate its depolymerization process (**Supplementary Figure 9c**).

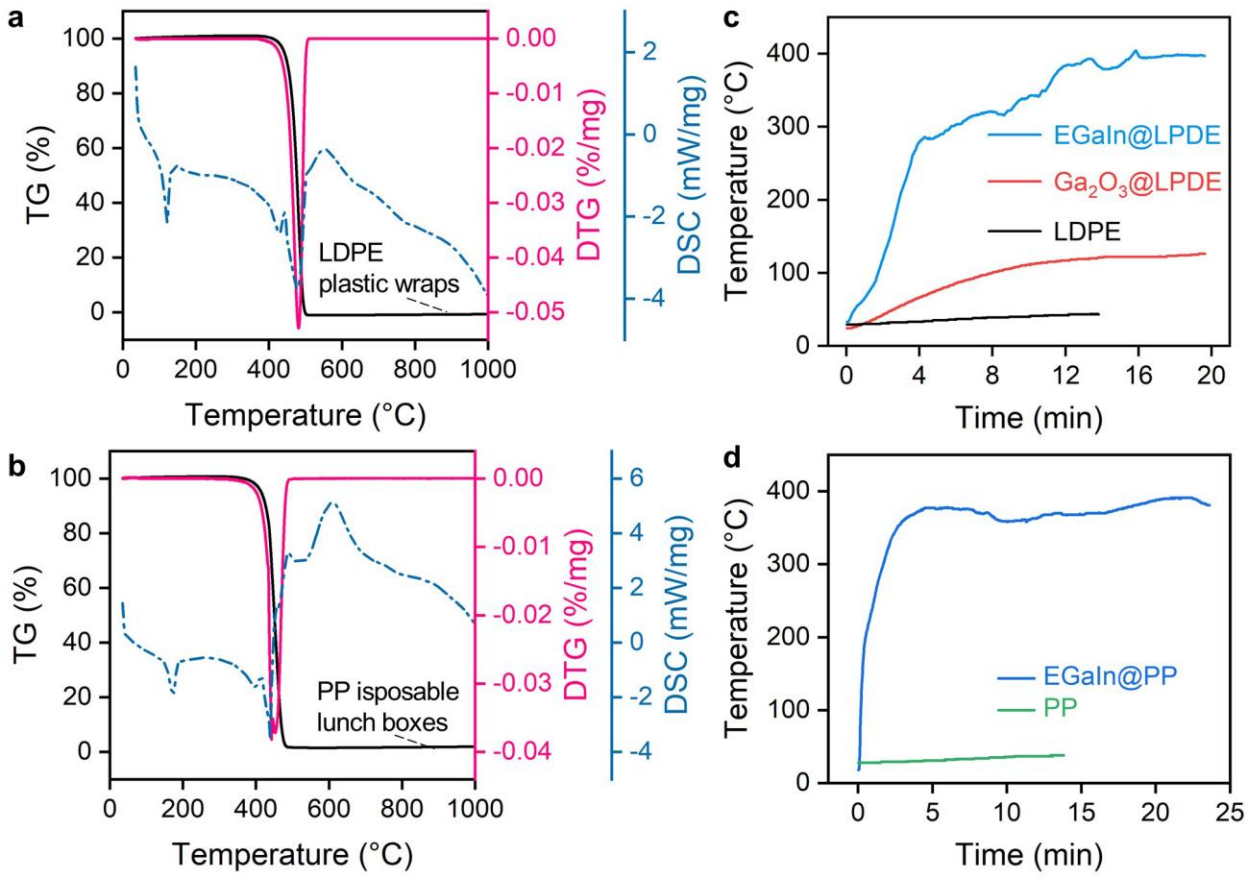

Supplementary Figure 9. Thermodynamic analysis of plastic depolymerization. (a-b) Thermogravimetric analysis of LDPE-based plastic wraps (a) and PP-based disposable lunch boxes (b). (c) The temperature of the quartz reactor versus time when packed with LDPE-based plastics, EGaIn-coated LDPE plastics, and Ga_2O_3-coated LDPE plastics respectively. $\omega_{(LDPE:\ EGaIn)}$=15: 1; $\omega_{(LDPE:\ Ga2O3)}$=15: 1; P=600 W. (d) The temperature of the quartz reactor versus with time when packed with PP-based disposable lunch boxes and EGaIn-coated disposable lunch boxes, respectively. $\omega_{(PP:\ EGaIn)}$=15: 1, P=600 W.

Supplementary Discussion 3

First-principles calculations

Coordinates from ORCA-job CH_3

C	1.06089819003967	-0.76424908750281	-0.21840564394356
H	1.56855413791658	-1.66166655657030	0.09245399952742
H	1.56856247047546	-0.04633167624790	-0.84015577149446
H	0.04559320156828	-0.58474593967899	0.09245590591061

Coordinates from ORCA-job C_2H_5

C	-1.67712277217237	0.11609693222624	-0.01286549617020
C	-0.22332008853089	0.36261438188238	-0.00902780801300
H	-2.20975865564515	-0.06104096610351	-0.93530900683753
H	-2.22106128991700	-0.02281112877068	0.90953239812903
H	0.35655887118483	-0.57214296223980	0.01443868106819
H	0.10383456797824	0.89725403046072	-0.90162436116515
H	0.09278669710235	0.93472222254465	0.86412550298866

Coordinates from ORCA-job C_3H_7

C	-1.91324102954831	0.42089233618534	-0.00012565439057
C	-0.44007277063532	0.53105110158909	0.00032556741455
H	-2.45995507464975	0.28939252993067	-0.92291187053198
H	-2.46043998968940	0.28834248842080	0.92222237078942
C	0.26471443734002	-0.83588804521470	-0.00025376885093
H	-0.10394307490555	1.09187291711353	-0.87524651914900
H	-0.10440561889418	1.09088778743342	0.87670514580639
H	1.34844627380959	-0.71328597782872	0.00009204013996
H	-0.00947983022895	-1.41738383970498	0.87883910696653
H	-0.00903209259814	-1.41641107792446	-0.88012841819437

Coordinates from ORCA-job C_4H_9

C	-1.56148942300906	-0.80413680824020	0.00071060160667
C	-0.08671615554014	-0.74408143432201	0.00187337848962
H	-2.11263111955636	-0.91336709550954	-0.92224457685083
H	-2.11396821837755	-0.91610029312741	0.92253649914899
C	0.58462283783627	-2.13169915134644	0.00021450651324
H	0.27186008643792	-0.19512132296584	-0.87340894944199
H	0.27059030752697	-0.19784059986718	0.87937104511055
C	2.10143022839096	-2.04687809213415	0.00150410048811
H	0.24059861674715	-2.69189366484167	0.87181037039081
H	0.24191068491995	-2.68917270521881	-0.87363855375144
H	2.55503814352617	-3.03748787977741	0.00038732344409
H	2.46810056644723	-1.51436794840785	-0.87653511616737
H	2.46673344465049	-1.51696975424148	0.88168436101954

Coordinates from ORCA-job C_5H_{11}

C	-0.21402239983014	-0.11751364109682	0.00135655995895
C	1.26192693584464	-0.09817105950255	0.00313810028088
H	-0.76726286565118	-0.21216240784133	-0.92196182736954
H	-0.76941897563590	-0.21696495756842	0.92287150730601
C	1.89192123039295	-1.50434707760391	0.00002407148926
H	1.63557495979269	0.44147846965598	-0.87144454199991
H	1.63351974338526	0.43665582846697	0.88154642503468
C	3.41263728692314	-1.47449613086243	0.00195428027873
H	1.53310786288701	-2.05749160476810	0.87125416287605
H	1.53522582073962	-2.05269909496099	-0.87509209283279
H	3.76161722317841	-0.91293875642248	-0.86866180027920
H	3.75948543828190	-0.91751275171081	0.87635089798088
C	4.03704551293778	-2.85936909217424	-0.00091621134779
H	3.73586267575971	-3.42740474270464	-0.88157949355983
H	5.12549492546670	-2.80685985598718	0.00045261481729
H	3.73388567552739	-3.43193905491903	0.87612710736635

Coordinates from ORCA-job C_6H_{14}

C	-2.57546601549669	-2.67194415028033	-1.47345286016761
C	-2.95684847159561	-3.90206162254138	-0.66490438854583
H	-1.77512140139244	-2.13341665847206	-0.95596486410431
H	-2.15026263923680	-2.99460437807049	-2.42657269769039
C	-1.79762327204740	-4.85830227640145	-0.44201871881452
H	-3.36186095701213	-3.58640609332099	0.30038355164074
H	-3.77089193281836	-4.42691337625892	-1.17251590380688
H	-2.10011207953757	-5.72673127356786	0.14258910120220
H	-1.39816634222314	-5.22195334894848	-1.38943912148803
H	-0.98016729289364	-4.37097478815911	0.09054704240641
C	-3.73943480829338	-1.72345844218631	-1.71835652882275
C	-3.36572333233484	-0.42430099940174	-2.42262042614395
H	-4.20507720656622	-1.48232004468338	-0.75880993578111
H	-4.50760555983991	-2.24085454772718	-2.30162043716998
C	-2.83099887815431	-0.60619077564351	-3.83388268189603
H	-4.24642397713188	0.22147016356877	-2.45549854009993
H	-2.62625566347040	0.10979065542453	-1.81934000038356
H	-1.88644160317864	-1.14785097196290	-3.84581955208865
H	-3.53671509590752	-1.16387365171420	-4.45155510973513
H	-2.65890347086911	0.35479658034698	-4.31784792851071

Coordinates from ORCA-job GaIn CH_3-C_5H_{11}

Ga	0.75843247903768	-1.67810079428865	0.70892814884154
Ga	1.87780253506681	0.71211780137303	1.63001133346258
Ga	-1.02815222613792	0.15448900681009	1.06383402329031
Ga	-0.70688401120219	1.78077377924321	-0.72862438265341
Ga	0.88318465107740	-0.26212621951065	-1.52165837639543
Ga	0.02735187867532	1.66638096547946	2.98966375808592
Ga	2.95327579582660	-0.77690953143971	-3.40833817009259
Ga	3.17036208233046	-1.04982376861259	0.22235964846596
Ga	-0.26549578978167	3.42113108893811	1.21676798671646
Ga	3.37284799097427	0.78779906668925	-1.53771532542141
In	2.93404814912256	-3.14214827259979	-1.44428902670902
In	1.92250490637216	2.66890391090952	-0.33319317152280
C	-0.42005857053073	-4.47547366016586	-0.68121146244271
C	-1.38090172269657	-5.21075424355762	-1.59919326042372
H	0.44780567188874	-5.11465101666392	-0.48570681256320
H	-0.03789706129890	-3.59741729121534	-1.21188451147063
C	-0.73131036480449	-5.65459963740352	-2.89853810835308
H	-1.77929684968141	-6.08137302102023	-1.07210037482390
H	-2.23732868677786	-4.56789189398799	-1.81507264904326
H	-1.44015871138090	-6.17281174483264	-3.54286850845794
H	-0.33901347716692	-4.80493846322492	-3.45806857564024
H	0.09875698226582	-6.33609390825949	-2.70923447389744
C	-1.01736945508780	-4.03066288154759	0.64268346458563
C	-0.01525475502808	-3.33759377243759	1.55646186024525
H	-1.43254012904631	-4.90611352570731	1.15360443068693
H	-1.86566616479682	-3.36827027293413	0.44999235118285
C	-0.50502430439686	-1.18133210175211	-2.69715499019853
H	-0.47790320700999	-3.05138218074894	2.49951972655965
H	0.81804167265093	-4.00165375651499	1.78985115611503
H	-0.10982854103200	-2.02129290397499	-3.26376247816634
H	-1.32388276926288	-1.52440318375692	-2.06870606054915
H	-0.89279928816847	-0.43667743328483	-3.39043807941318

Coordinates from ORCA-job GaIn C_2H_5-C_4H_9

Ga	1.25620472290051	-2.03710843251218	0.09909903271914
Ga	1.30630118058393	0.24559325957556	2.03475220533799
Ga	-0.69351328235973	-0.36876859532786	0.41164159575089
Ga	0.10442479707212	1.55394701060846	-1.05515248093232
Ga	1.17717381068947	-0.57935556131826	-1.96693668318665
Ga	-1.16582417181354	0.75198113948685	2.71033218143802
Ga	3.53661338033799	0.57563414802558	-3.10429115298176
Ga	3.04669822073953	-0.22370976087963	0.15429420020407
Ga	-1.63993776479226	2.17809496907346	0.63024433000770
Ga	2.65381678850914	1.87918790780820	-1.18254172596281
In	4.04375758237990	-2.14426733901919	-1.51942370813927
In	1.07694328914325	2.89024715334962	1.33311312697115
C	-1.31364780100453	-4.14761284874582	-0.41237076379525
C	-2.80344393167122	-4.42658268429775	-0.33346715681246
H	-0.82844978184149	-4.87945090300878	-1.06390027520913
H	-1.15723931257844	-3.17571961433617	-0.89537172116697
H	-3.00007757750767	-5.40148603448568	0.11358108146177
H	-3.30761067317560	-3.67739547112565	0.27758451888230
C	-0.62412586400114	-4.14812216908542	0.94169181431076
C	0.86250388736812	-3.84181616510471	0.86698896112576
H	-0.77814295027813	-5.12425523300986	1.41495331277674
H	-1.11608808168777	-3.41990303573305	1.59296367526580
C	0.22362557992566	-1.46739552836956	-3.51089709067991
H	1.32192149464043	-3.86297475046576	1.85660910196743
H	1.38526783753780	-4.58336303823884	0.26001952413331
H	-0.81178821438152	-1.59200640811019	-3.19327154845174
H	0.22049835731811	-0.75847008784865	-4.33871769311571
C	0.84395096753428	-2.78960655962305	-3.91600691134119
H	0.31167694344879	-3.25002205484028	-4.75210554262743
H	1.88305796393635	-2.66723403788851	-4.22466476839312
H	0.83582452571626	-3.50596017450622	-3.09384384346340
H	-3.26717404268863	-4.41591415004637	-1.31902594609358

Coordinates from ORCA-job GaIn C_3H_7-C_3H_7

Ga	1.10522684166631	-1.95804413242729	0.22853477703597
Ga	1.66086648425166	0.32559435321912	2.06838529414811
Ga	-0.56935765528703	-0.04737072420808	0.69747098879116
Ga	0.30694241515488	1.73024005430011	-0.91465227998698
Ga	1.00246938916145	-0.53435031925346	-1.87020541767983
Ga	-0.62376978266232	1.17165924840308	3.00575225151034
Ga	3.32419373957653	0.29234858714638	-3.29162960715494
Ga	3.12049401792965	-0.41951449900092	0.03415669032805
Ga	-1.14052751057174	2.60159992033028	0.93408942911015
Ga	2.85663633070070	1.70861796100665	-1.30165311282159
In	3.65183597616549	-2.46336852206006	-1.69580486968238
In	1.70631150654582	2.95668399272797	1.30917846355726
C	-1.72370160322345	-3.80221273894929	0.00332220765740
H	-1.40053973947440	-4.57145073156345	-0.69887127051433
H	-1.61051057027132	-2.83751350868838	-0.49737610099174
C	-0.91640001270211	-3.85087172360763	1.28784750961905
C	0.58045066466440	-3.69586009054731	1.06628285991607
H	-1.11056935192158	-4.79965569890350	1.79838325008190
H	-1.26753635820062	-3.06897444545680	1.96577517582268
C	-0.23994036505629	-1.35930936040407	-3.23068394223362
H	1.12628739252219	-3.75272904724925	2.00990168995934
H	0.96364015191521	-4.49758499637511	0.43185950969069
H	-1.23134219091593	-1.35861321398722	-2.77503992942572
H	-0.28388557720589	-0.69227997400241	-4.09252473447244
C	0.17062385480147	-2.76056421661826	-3.64236807730882
H	1.16620328134759	-2.73253531051750	-4.09431001282647
H	0.26957012858106	-3.39150632303285	-2.75454884276894
C	-0.80451674893671	-3.41226766411555	-4.61278154517020
H	-0.89702192028254	-2.82697327833254	-5.52771228008594
H	-0.48131259214466	-4.41623145977234	-4.89028616010457
H	-1.79822819200336	-3.49248406148507	-4.17159252423521
H	-2.78710864412449	-3.94643711657496	0.18964104023570

Supplementary Discussion 4

Optimization of operating parameters and plastic upcycling capability

Optimization of microwave irradiation power

The optimization was initially performed for the microwave irradiation power, which dominated the depolymerization product distribution. Here, the microwave irradiation power ranged from 120 W to 720 W. As shown in **Supplementary Table 2** and **Supplementary Figure 10a**, the oil yield exhibited a positive correlation with the increment of microwave power, while the gas yield presented an opposite trend. For instance, the oil yield increased from 14.4 wt% to 50.9 wt%, the gas yield decreased from 70.6 wt% to 35.9 wt% when the microwave power ranged from 120 W to 720 W. As a result, the conversion of plastic into oil and gas peaked at a microwave power of 600W (94.8 wt%). Note that, although increasing microwave power could lead to higher oil yield, it also implied higher energy consumption. Moreover, excessive irradiation might cause elevated reaction temperatures, resulting in secondary cracking and coking of products. For example, when the microwave power increased from 600 W to 720 W, the solid products increased from 5.2 wt% to 13.2 wt%, while the selectivity of methane rose from 8.6% to 9.6% (**Supplementary Figure 10b**). Based on this, there exists an optimal microwave irradiation power (600 W), which can not only achieve the maximum conversion for oil and gas products but also attain a higher selectivity of olefin monomers (64.5 %) in the gaseous products.

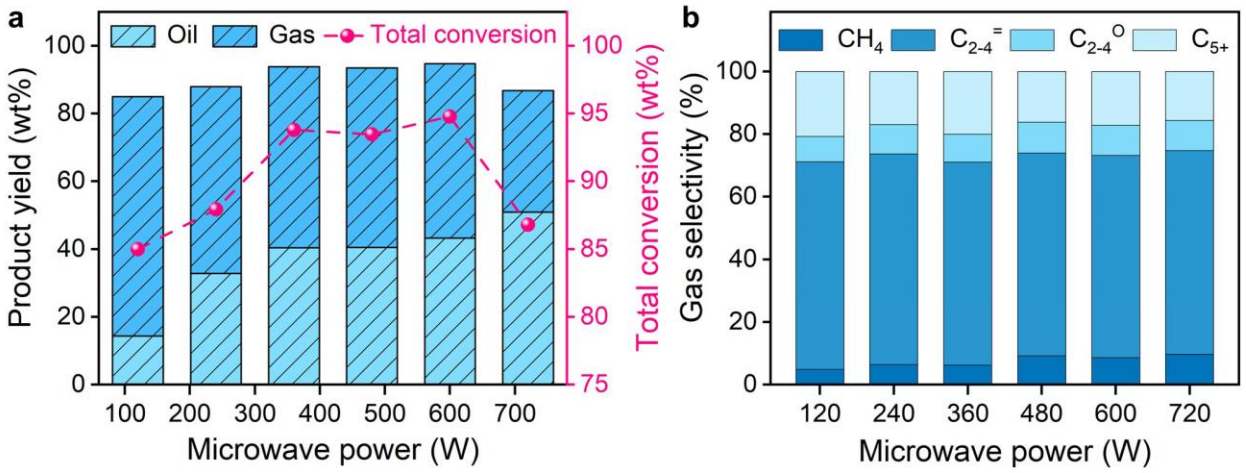

Supplementary Figure 10. Effect of microwave power on the product distribution of depolymerization. (a) Product yield and total conversion of gas and oil vary with microwave power. (b) Gas selectivity varies with microwave power. Plastic: PP-based disposable lunch boxes; Liquid metal: EGaIn; $\omega_{(PP:\ EGaIn)}$ = 1: 1.

Optimization of mass ratio between plastic and liquid metal

To investigate the maximum plastic upcycling capacity of microwave-powered liquid metals, we optimized the mass ratio between plastic (PP) and liquid metal (EGaIn), using oil yield as the optimization criterion. The mass ratio was set from 1: 1 to 17.5: 1. It was observed that the mass ratio significantly influenced the oil yield. As shown in **Supplementary Table 3** and **Supplementary Figure 11 a**, the oil yield reached the maximum value (about 80.2 wt.%) at the mass ratio of 15: 1. Additionally, increasing this ratio could slightly improve the oil production per unit mass of liquid metal (e.g., from 12.0 g/g_{EGaIn} to 12.6 g/g_{EGaIn} when the ratio increased from 15: 1 to17.5: 1). However, it also led to an increase in low-value alkane production (e.g., alkane yield increased from 1.2 g/g_{EGaIn} to 2.1 g/g_{EGaIn}) (**Supplementary Figure 11 b**). Therefore, setting the mass ratio at 15:1 was reasonable, which could also ensure the effective contact between liquid metal and plastic.

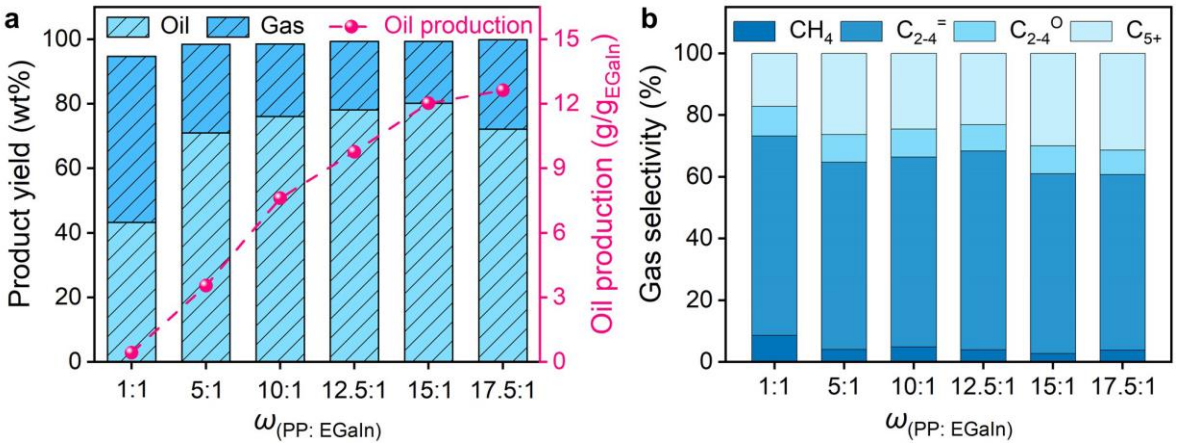

Supplementary Figure 11. Effect of mass ratio between plastic and liquid metal on the product distribution of depolymerization. (a) Product yield and oil production vary with the mass ratio. (b) Gas selectivity varies with the mass ratio. Plastic: PP-based disposable lunch boxes; Liquid metal: EGaIn; P = 600 W.

Supplementary Discussion 5

Time-dependent study of LDPE depolymerization

The results of time-dependent yield for three depolymerization cycles of LDPE-based plastic wrap using microwave-powered EGaIn were presented in **Supplementary Table 6**. The ^{1}H NMR spectrum and GC-MS trace of the oil products at different depolymerization times were illustrated in **Supplementary Figures 12 to 16** and **Supplementary Figures 18 and 22**, respectively.

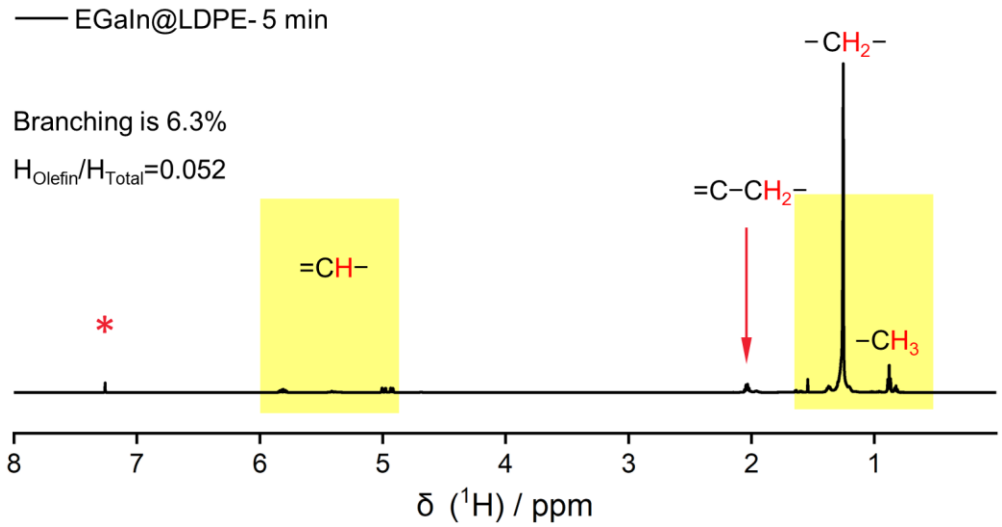

Supplementary Figure 12. 1H NMR spectrum of the oil products at 5min.

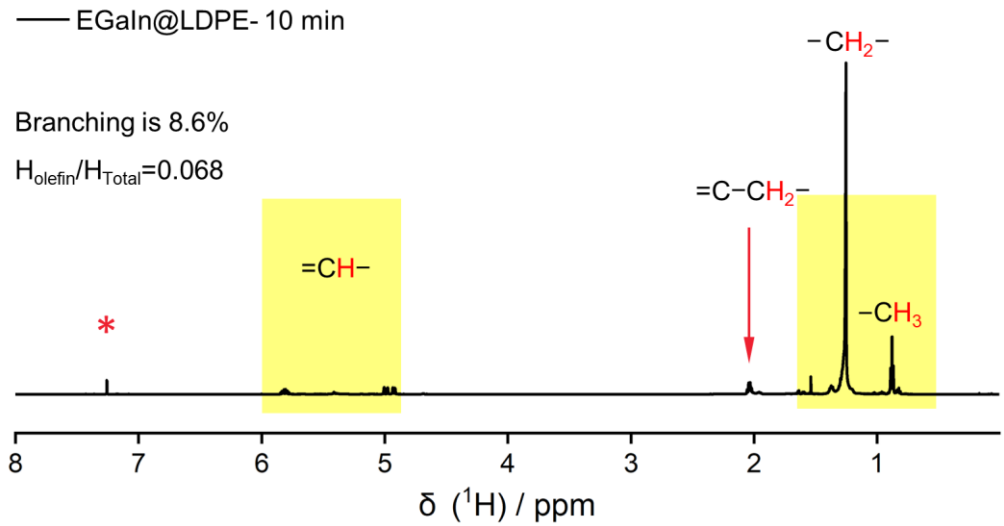

Supplementary Figure 13. 1H NMR spectrum of the oil products at 10 min.

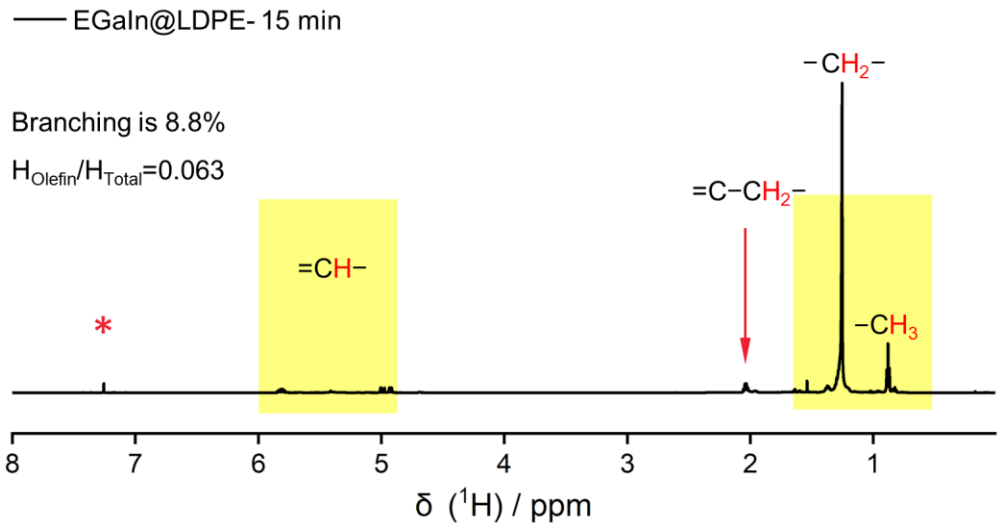

Supplementary Figure 14. ^{1}H NMR spectrum of the oil products at 15 min.

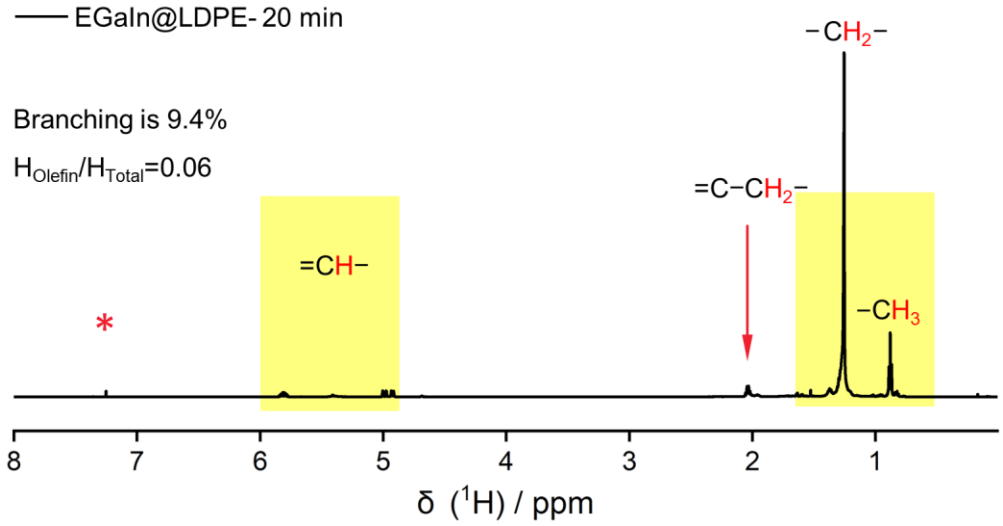

Supplementary Figure 15. ^{1}H NMR spectrum of the oil products at 20 min.

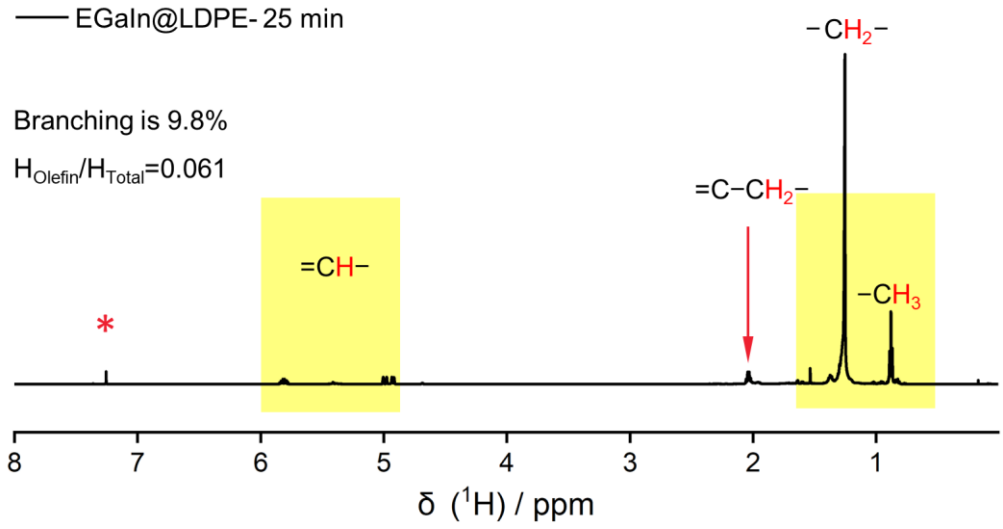

Supplementary Figure 16. ^{1}H NMR spectrum of the oil products at 30 min.

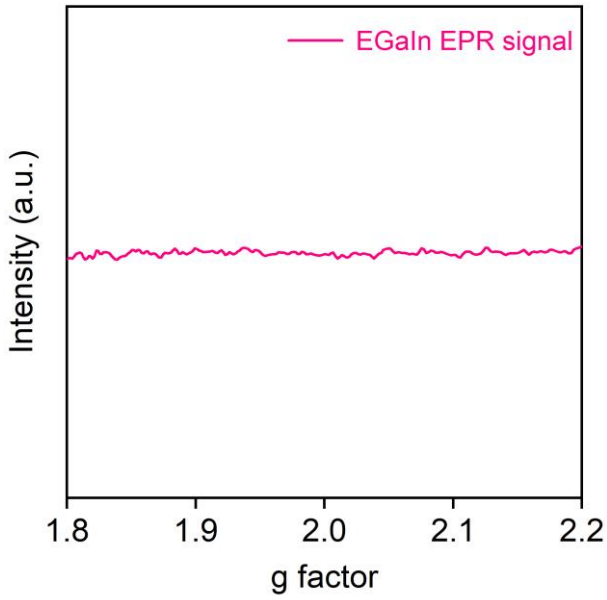

Supplementary Figure 17. Electron paramagnetic resonance signal of liquid metal EGaIn at 90 K.

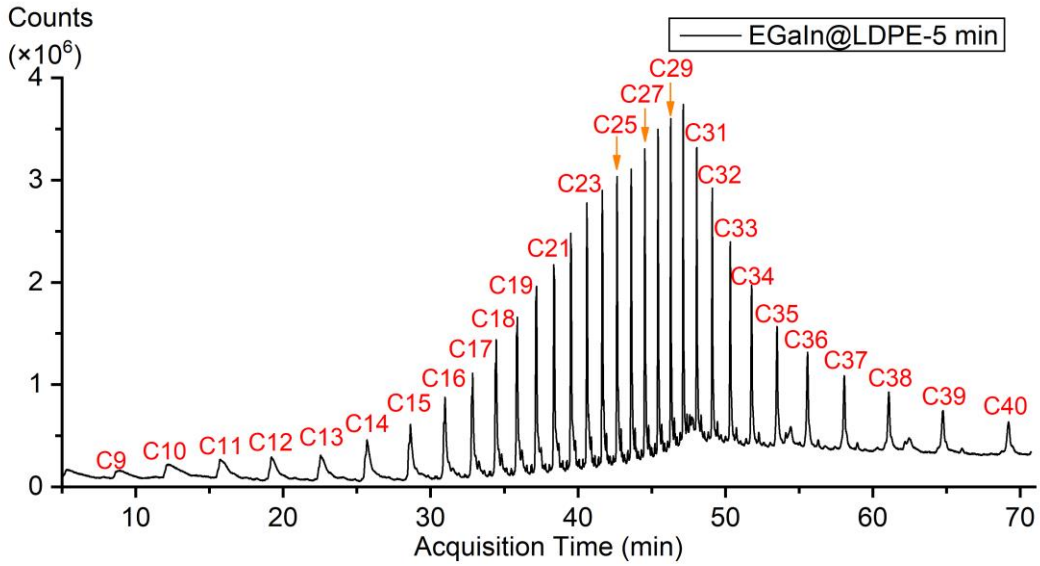

Supplementary Figure 18. GC-MS trace of the oil products at 5 min.

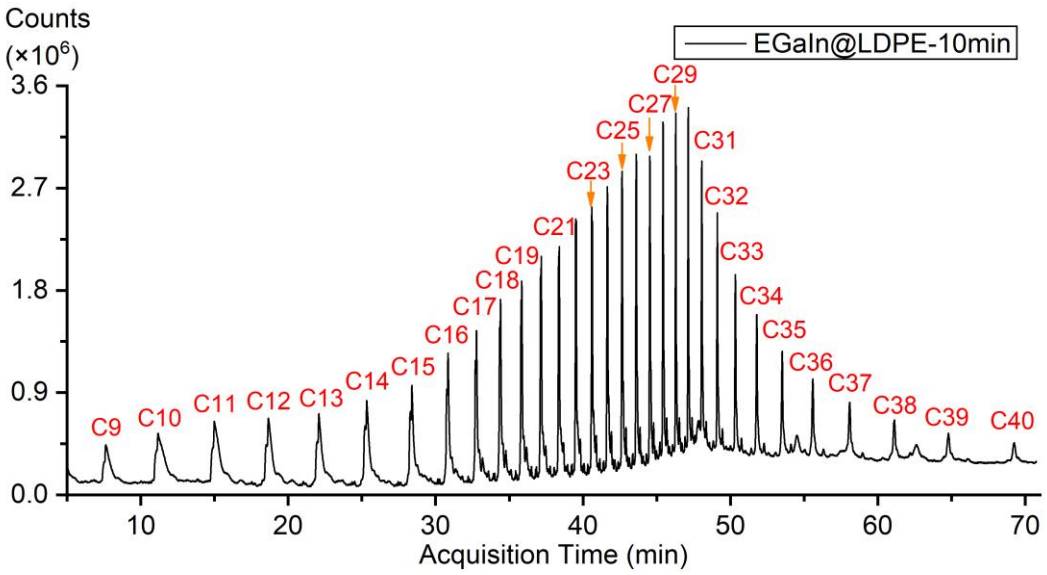

Supplementary Figure 19. GC-MS trace of the oil products at 10 min.

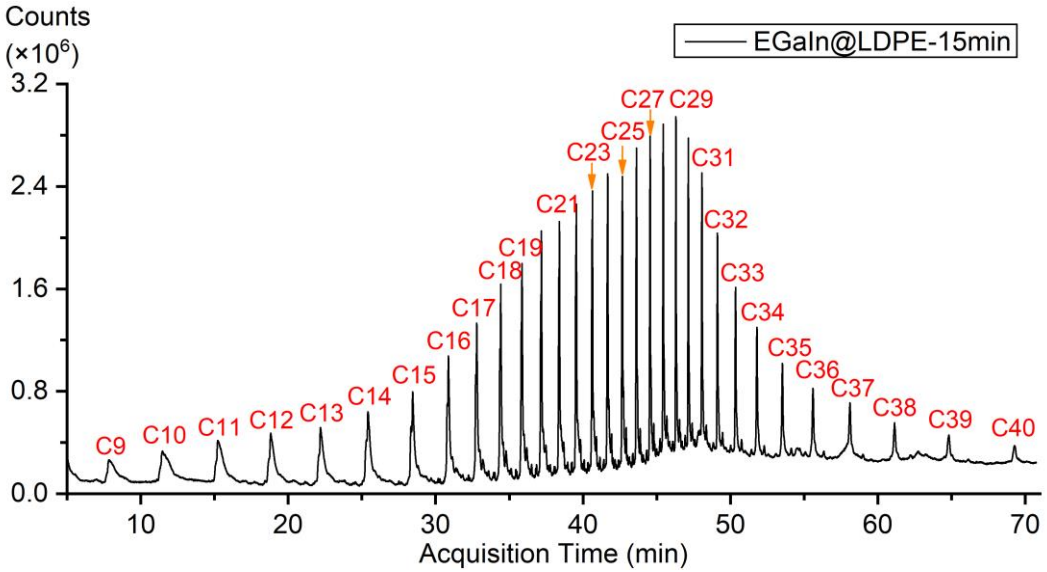

Supplementary Figure 20. GC-MS trace of the oil products at 15 min.

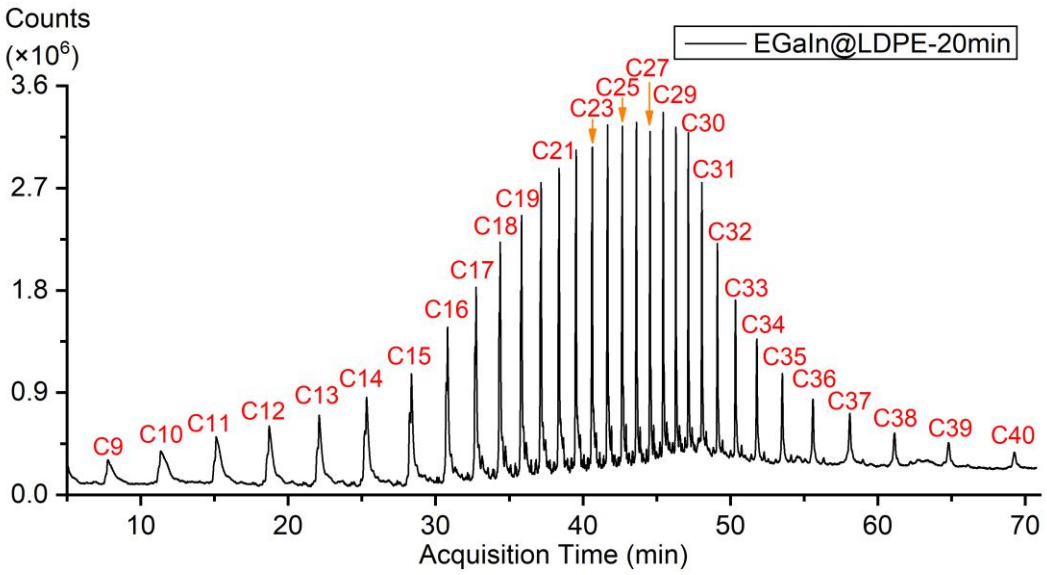

Supplementary Figure 21. GC-MS trace of the oil products at 20 min.

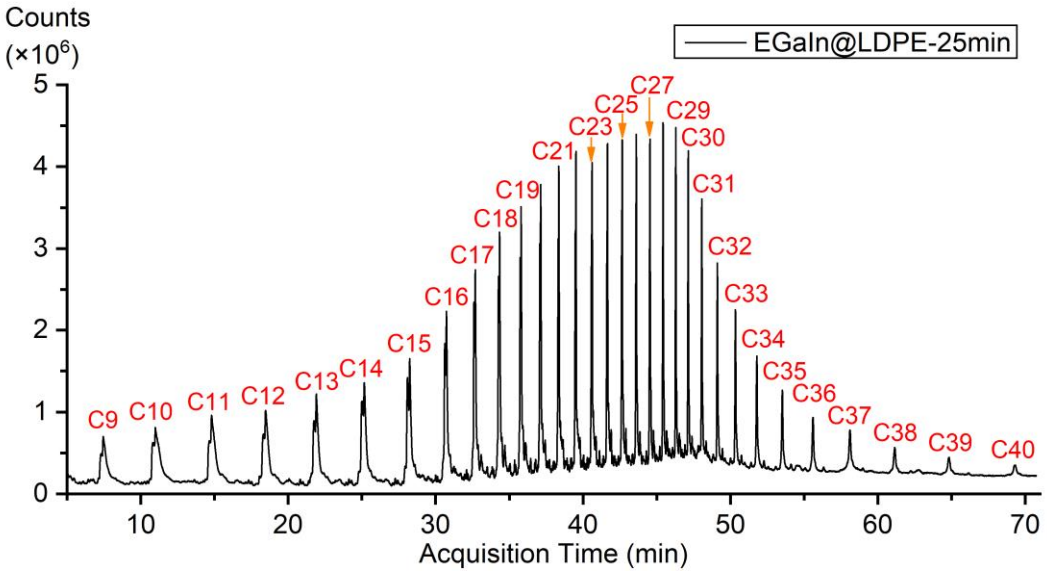

Supplementary Figure 22. GC-MS trace of the oil products at 25 min.

Supplementary Discussion 6

Depolymerization of LDPE by microwave-powered EGaIn

Experimental results for 30 successive depolymerization cycles of LDPE-based plastic wraps via microwave-powered EGaIn were presented in **Supplementary Table 7.** GC-FID trace of the volatile products of representative depolymerization cycles was shown in **Supplementary Figures 22 to 27**; GC-MS trace of the oil products was shown in **Supplementary Figures 28 to 33**; ^{1}H NMR spectrum and ^{13}C NMR spectrum of the oil products were shown in **Supplementary Figures 34 to 39** and **Supplementary Figures 40 to 45**, respectively.

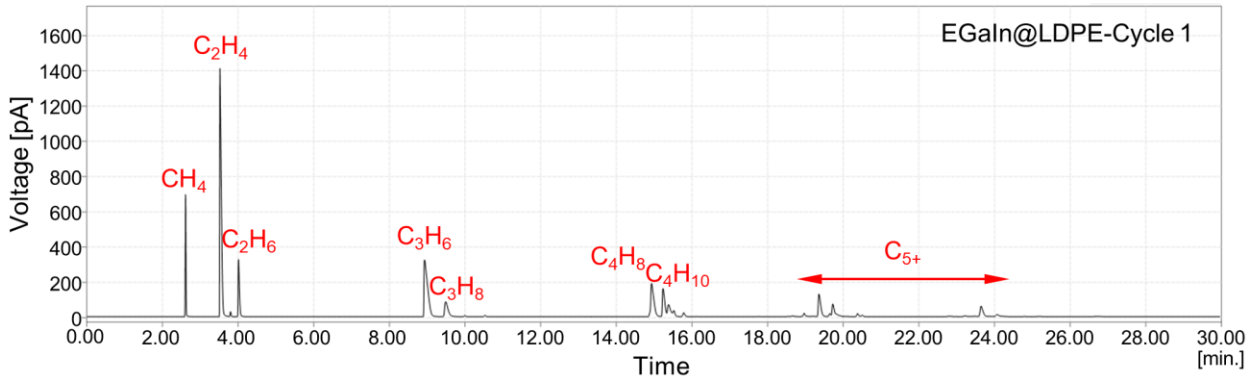

Supplementary Figure 23. GC-FID trace of the volatile products from the first depolymerization cycle of LDPE-based plastic wraps via microwave-powered EGaIn.

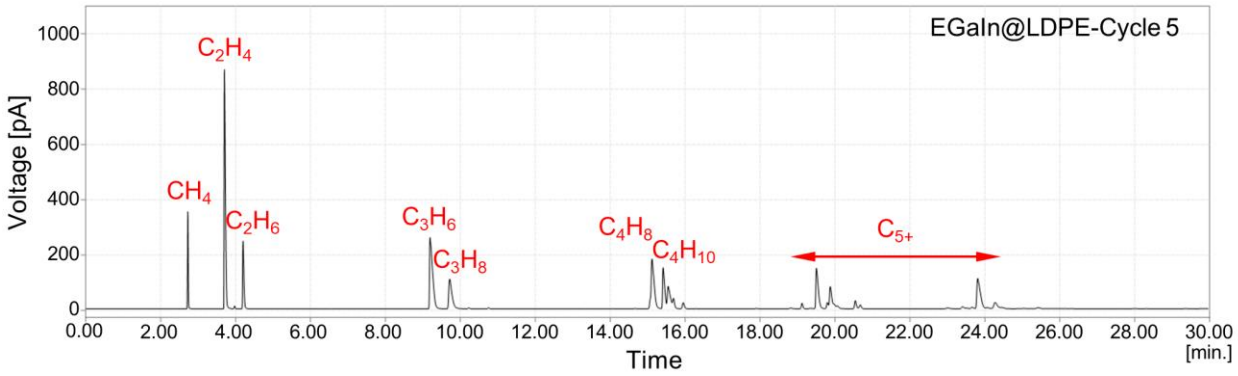

Supplementary Figure 24. GC-FID trace of the volatile products from the fifth depolymerization cycle of LDPE-based plastic wraps via microwave-powered EGaIn.

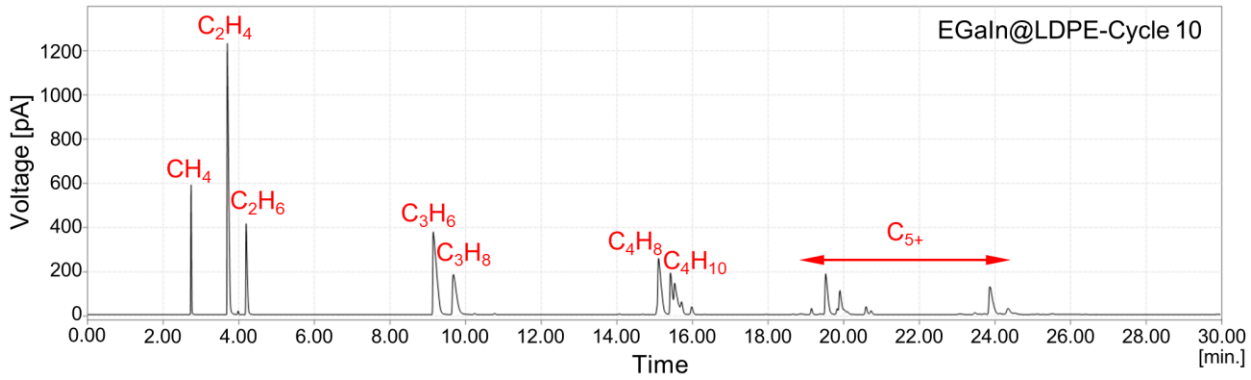

Supplementary Figure 25. GC-FID trace of the volatile products from the tenth depolymerization cycle of LDPE-based plastic wraps via microwave-powered EGaIn.

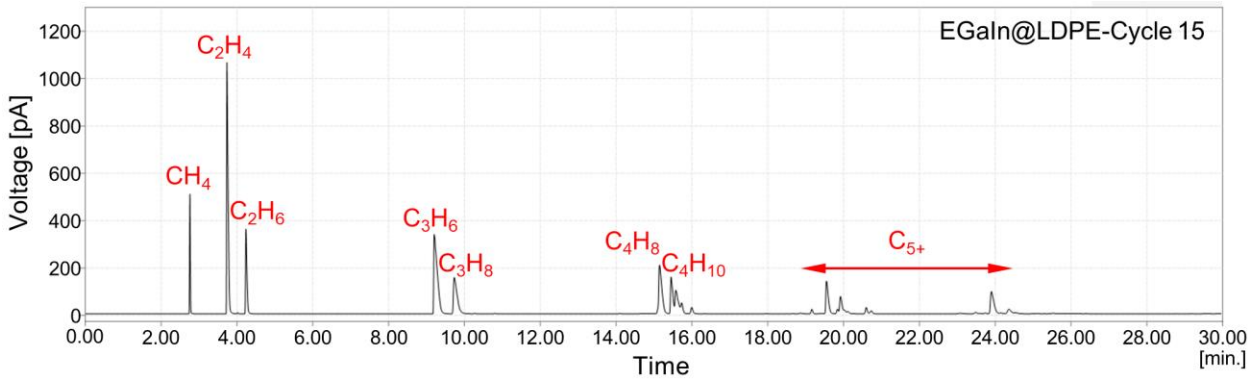

Supplementary Figure 26. GC-FID trace of the volatile products from the fifteenth depolymerization cycle of LDPE-based plastic wraps via microwave-powered EGaIn.

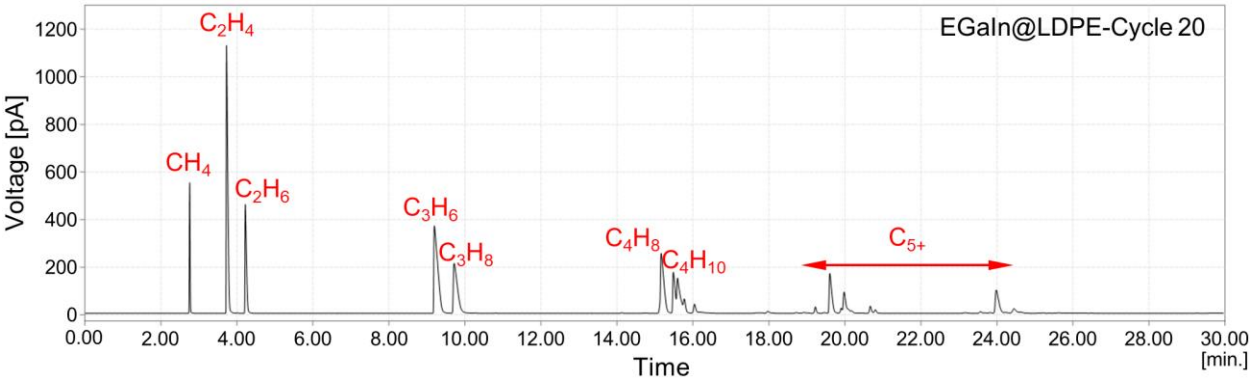

Supplementary Figure 27. GC-FID trace of the volatile products from the twentieth depolymerization cycle of LDPE-based plastic wraps via microwave-powered EGaIn.

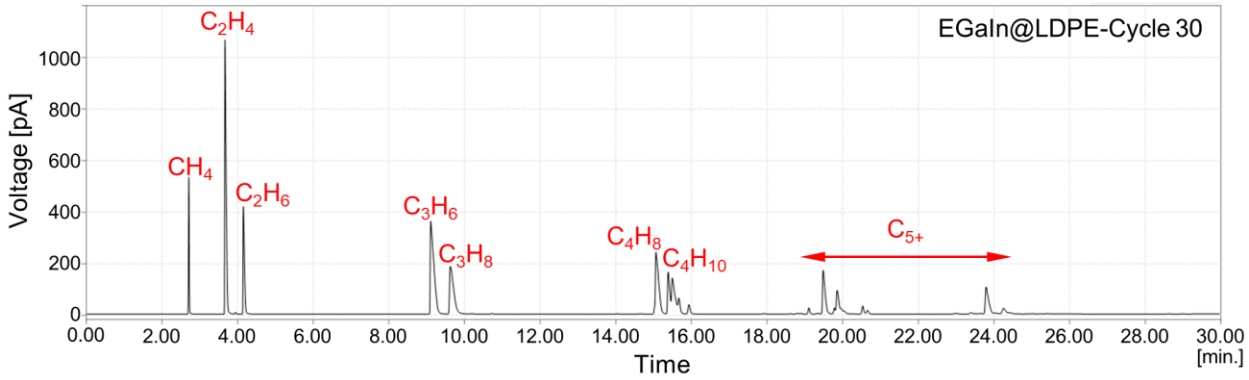

Supplementary Figure 28. GC-FID trace of the volatile products from the thirtieth depolymerization cycle of LDPE-based plastic wraps via microwave-powered EGaIn.

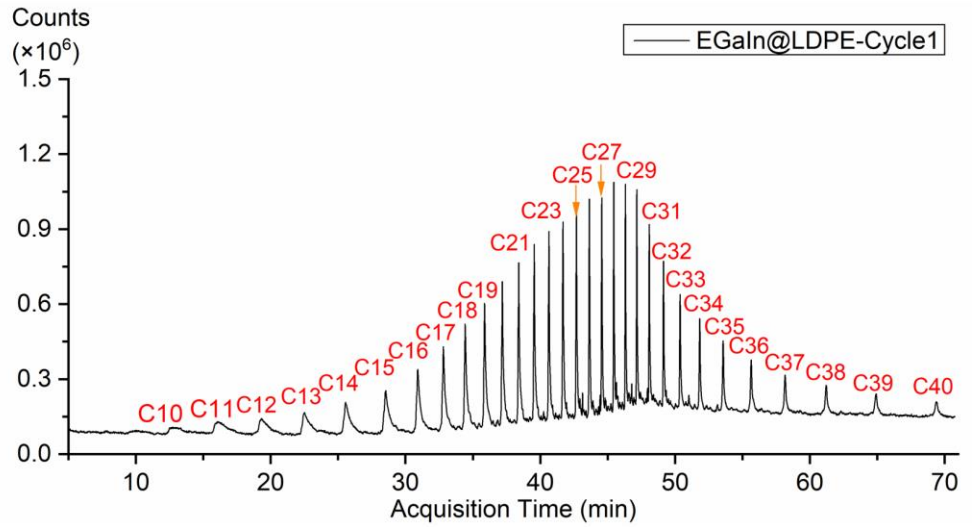

Supplementary Figure 29. GC-MS trace of the oil products from the first depolymerization cycle of LDPE-based plastic wraps via microwave-powered EGaIn.

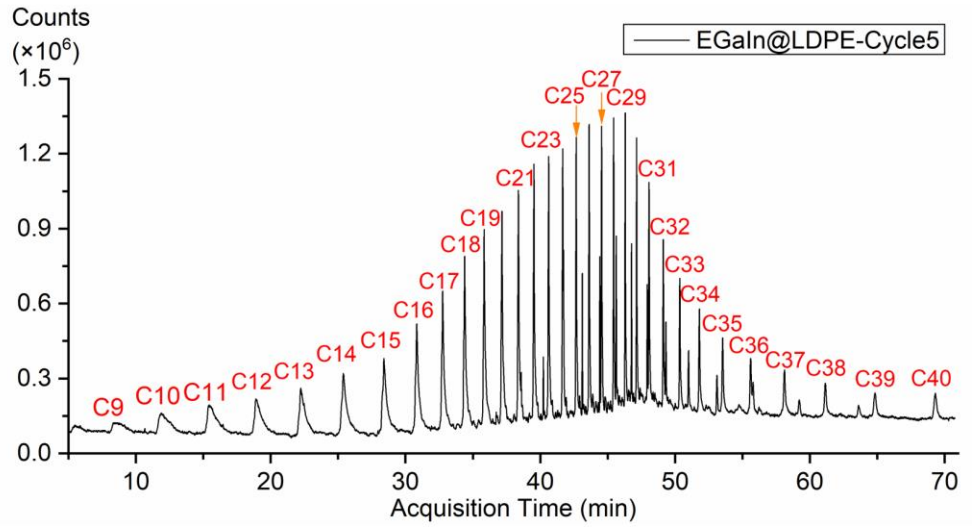

Supplementary Figure 30. GC-MS trace of the oil products from the fifth depolymerization cycle of LDPE-based plastic wraps via microwave-powered EGaIn.

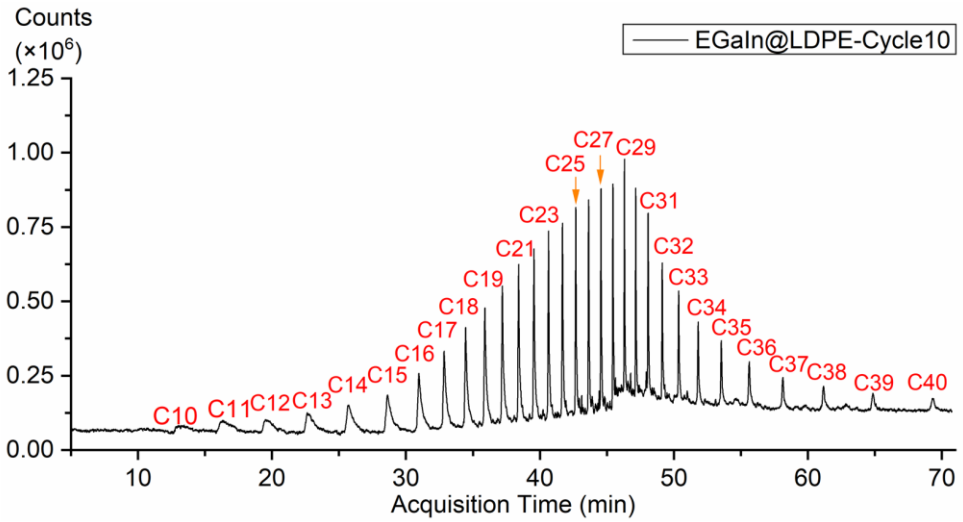

Supplementary Figure 31. GC-MS trace of the oil products from the tenth depolymerization cycle of LDPE-based plastic wraps via microwave-powered EGaIn.

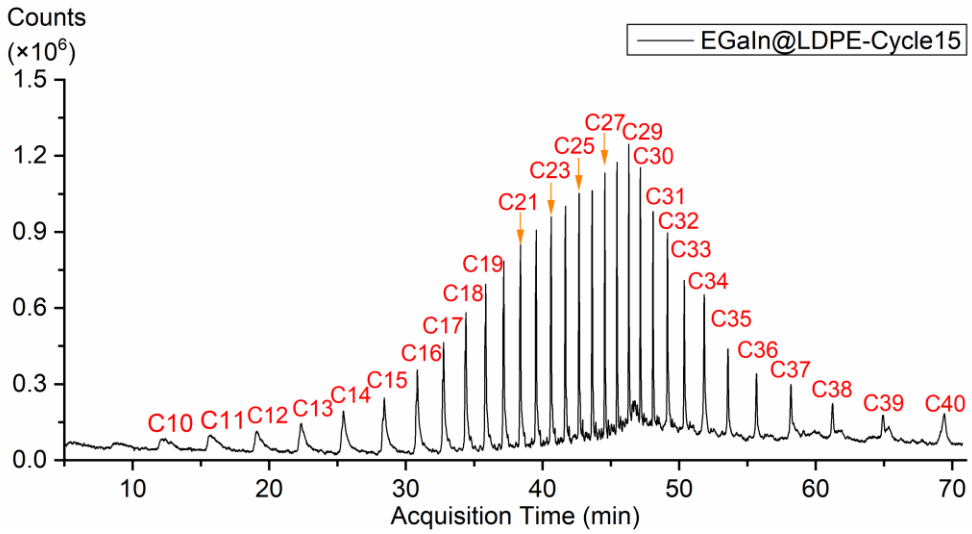

Supplementary Figure 32. GC-MS trace of the oil products from the fifteenth depolymerization cycle of LDPE-based plastic wraps via microwave-powered EGaIn.

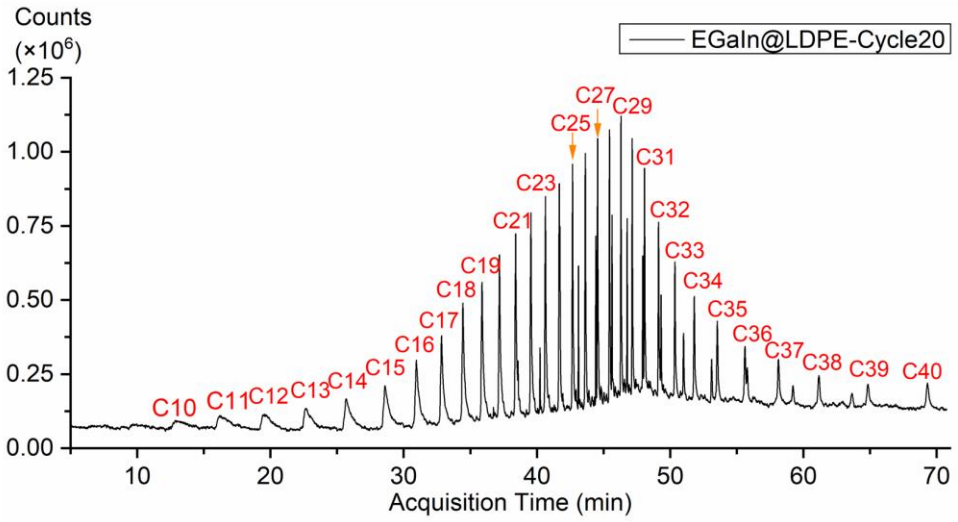

Supplementary Figure 33. GC-MS trace of the oil products from the twentieth depolymerization cycle of LDPE-based plastic wraps via microwave-powered EGaIn.

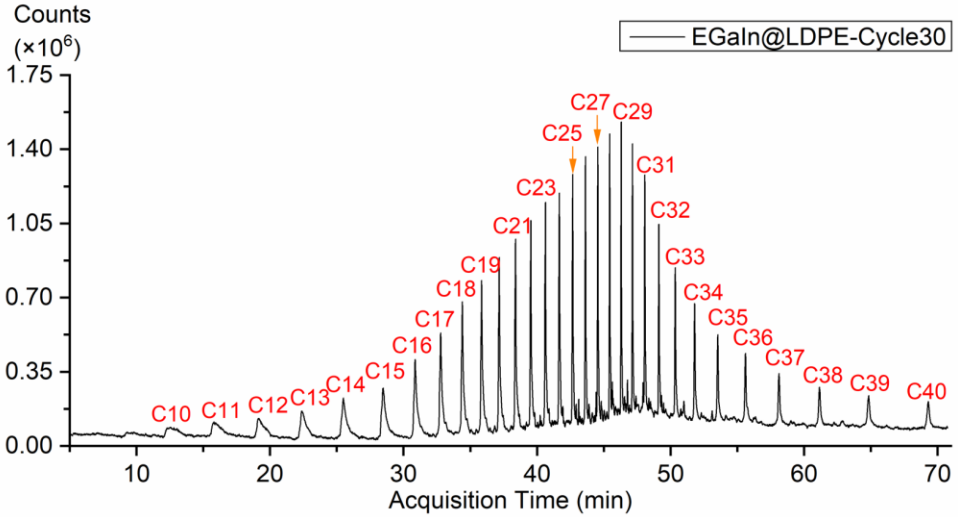

Supplementary Figure 34. GC-MS trace of the oil products from the thirtieth depolymerization cycle of LDPE-based plastic wraps via microwave-powered EGaIn.

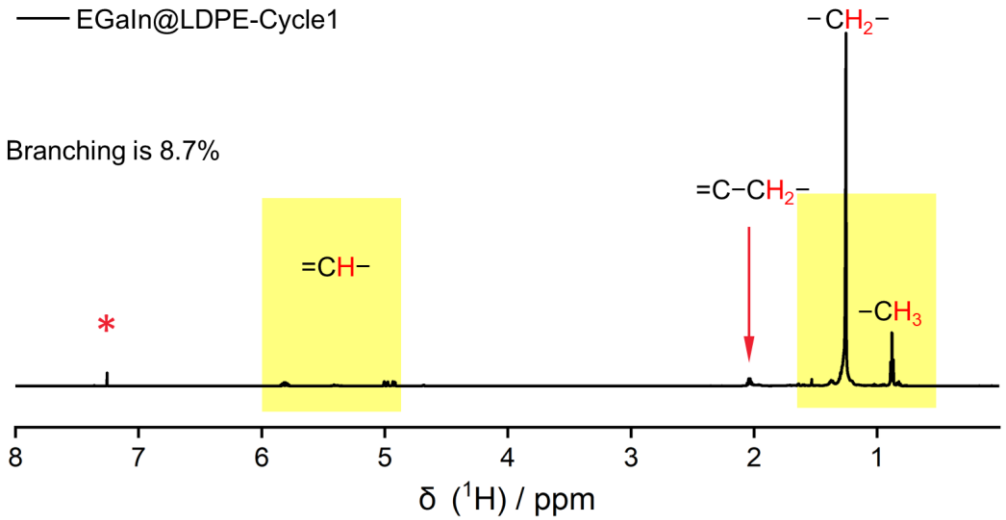

Supplementary Figure 35. ^{1}H NMR spectrum of the oil products from the first depolymerization cycle of LDPE-based plastic wraps via microwave-powered EGaIn.

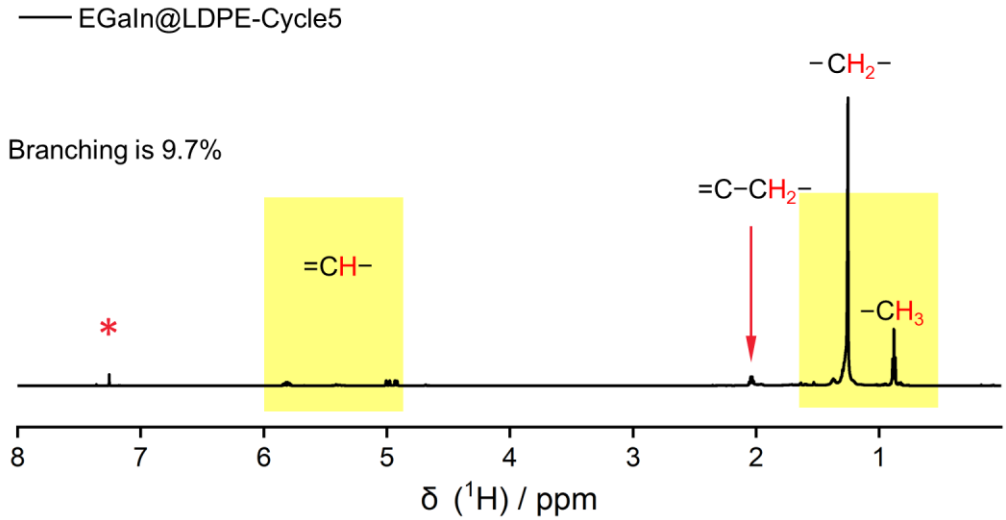

Supplementary Figure 36. 1H NMR spectrum of the oil products from the fifth depolymerization cycle of LDPE-based plastic wraps via microwave-powered EGaIn.

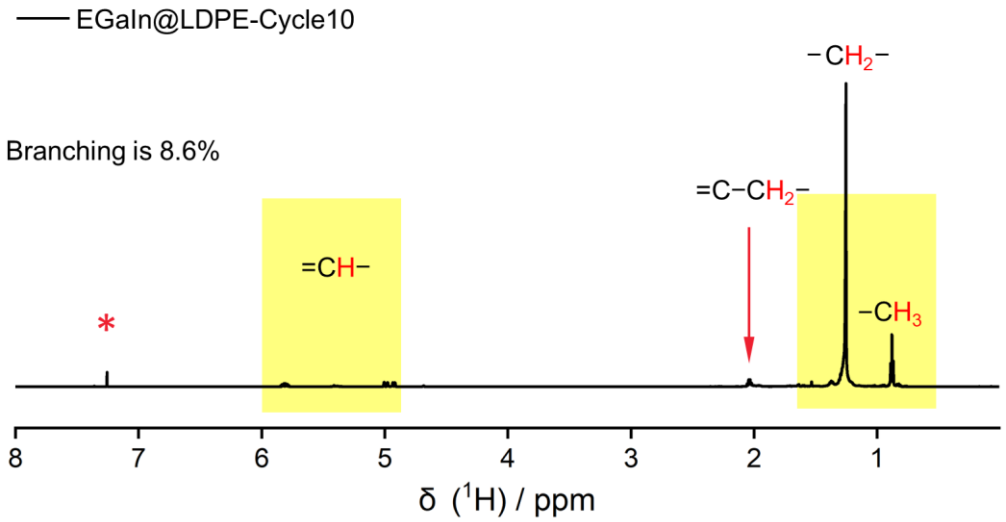

Supplementary Figure 37. 1H NMR spectrum of the oil products from the tenth depolymerization cycle of LDPE-based plastic wraps via microwave-powered EGaIn.

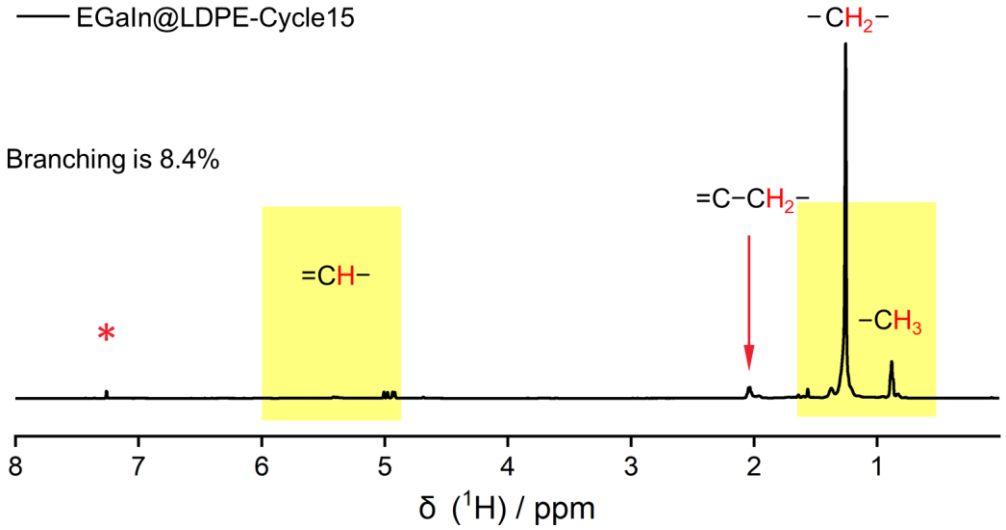

Supplementary Figure 38. 1H NMR spectrum of the oil products from the fifteenth depolymerization cycle of LDPE-based plastic wraps via microwave-powered EGaIn.

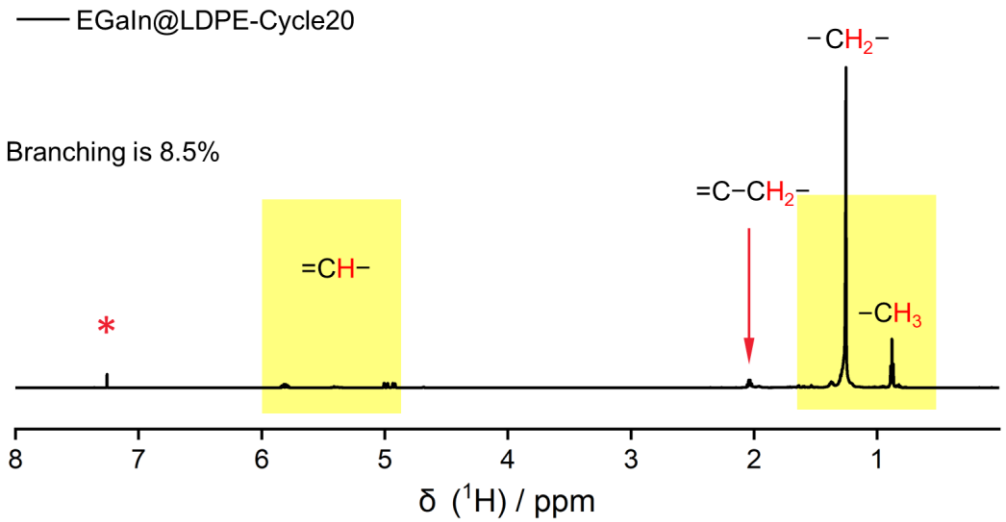

Supplementary Figure 39. 1H NMR spectrum of the oil products from the twentieth depolymerization cycle of LDPE-based plastic wraps via microwave-powered EGaIn.

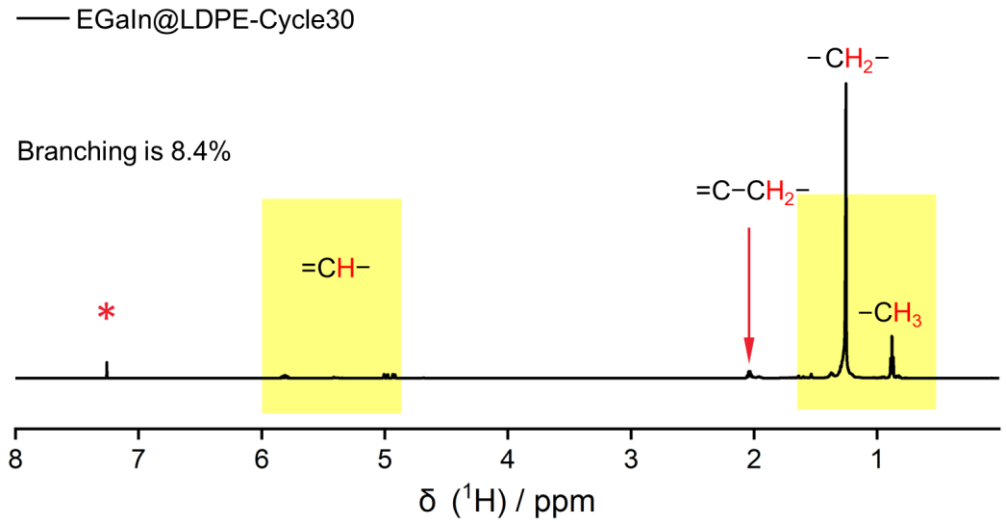

Supplementary Figure 40. 1H NMR spectrum of the oil products from the thirtieth depolymerization cycle of LDPE-based plastic wraps via microwave-powered EGaIn.

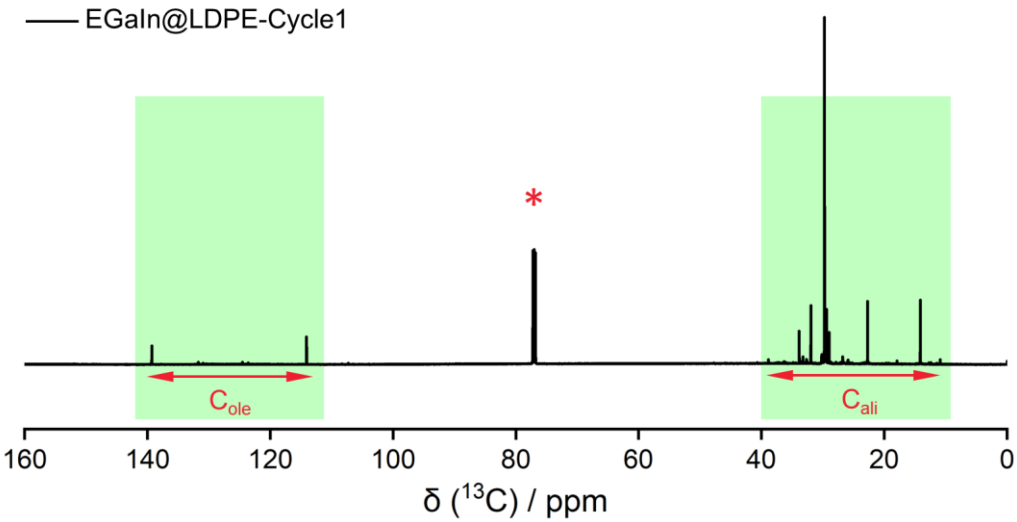

Supplementary Figure 41. 13C NMR spectrum of the oil products from the first depolymerization cycle of LDPE-based plastic wraps via microwave-powered EGaIn.

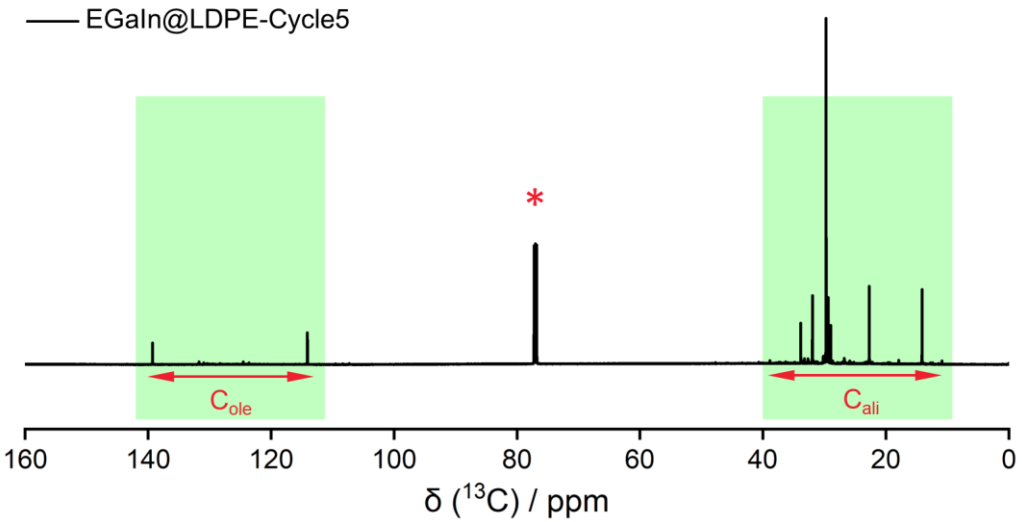

Supplementary Figure 42. 13C NMR spectrum of the oil products from the fifth depolymerization cycle of LDPE-based plastic wraps via microwave-powered EGaIn.

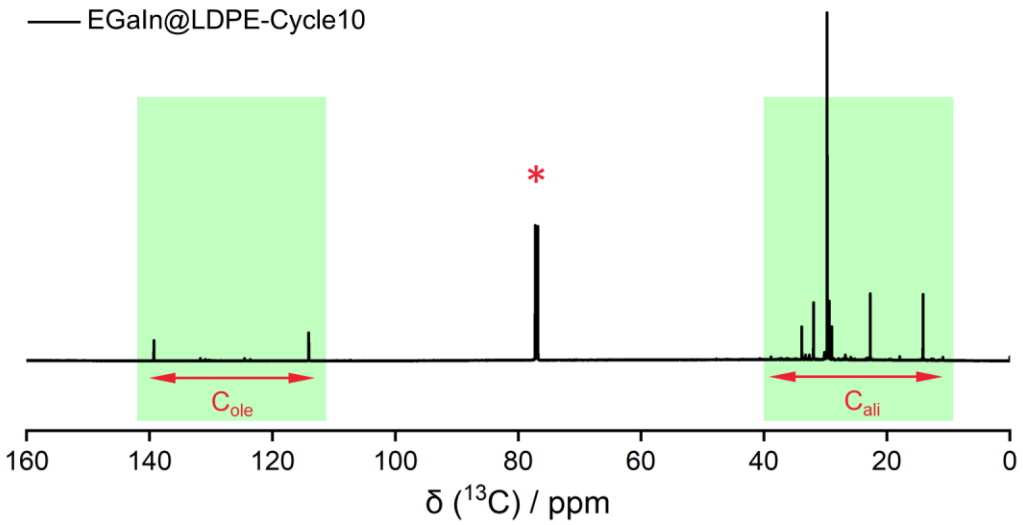

Supplementary Figure 43. 13C NMR spectrum of the oil products from the tenth depolymerization cycle of LDPE-based plastic wraps via microwave-powered EGaIn.

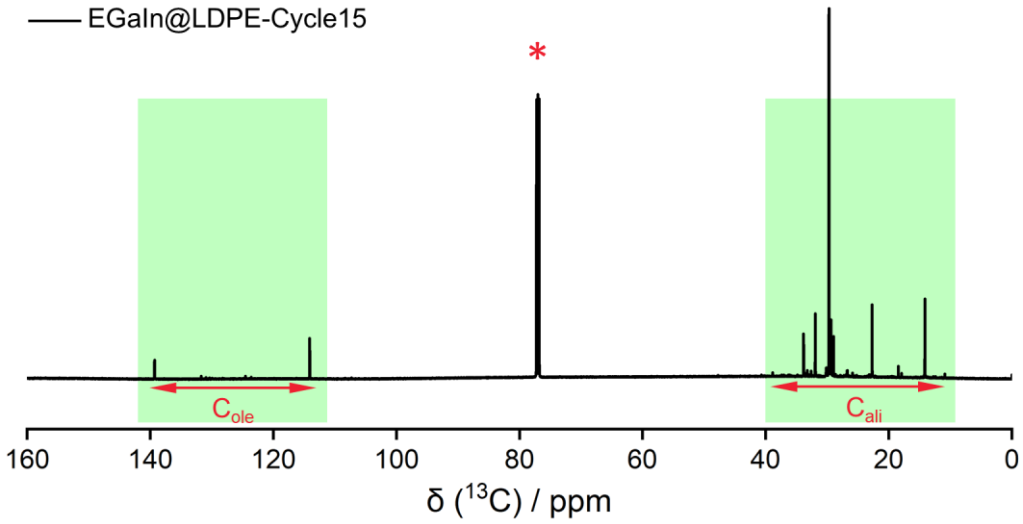

Supplementary Figure 44. 13C NMR spectrum of the oil products from the fifteenth depolymerization cycle of LDPE-based plastic wraps via microwave-powered EGaIn.

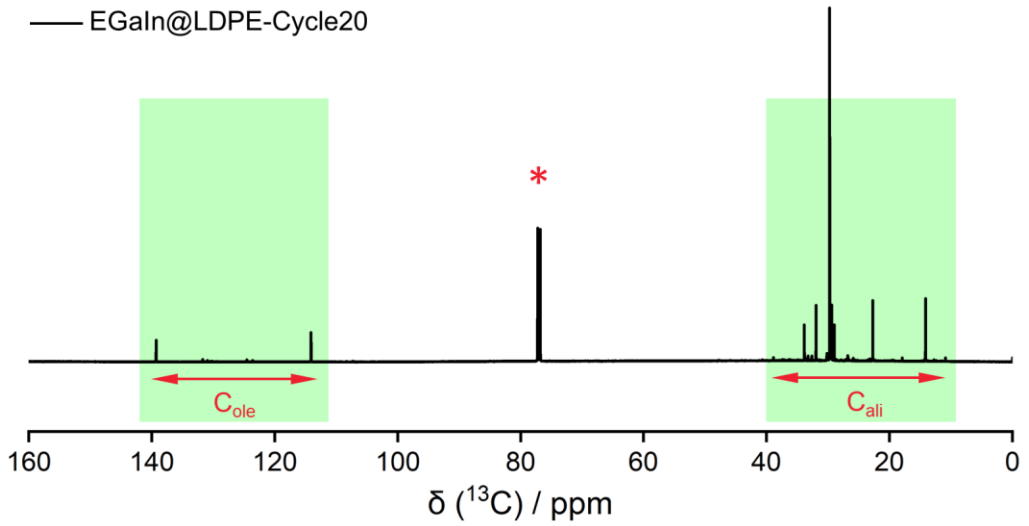

Supplementary Figure 45. 13C NMR spectrum of the oil products from the twentieth depolymerization cycle of LDPE-based plastic wraps via microwave-powered EGaIn.

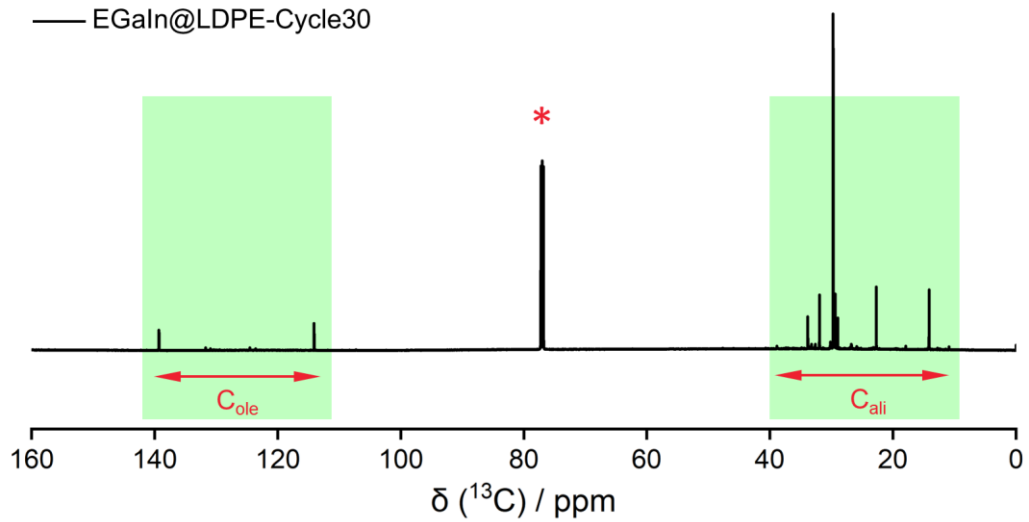

Supplementary Figure 46. 13C NMR spectrum of the oil products from the thirtieth depolymerization cycle of LDPE-based plastic wraps via microwave-powered EGaIn.

The simulated distillation gas chromatography (SD-GC) was carried out to illustrate the boiling point distribution of oil products at different depolymerization cycles, as shown in **Supplementary Figure 47**. SD-GC disclosed that the boiling points of oil products of LDPE-based plastic wraps were mainly concentrated in the range of 80-600 ℃. Moreover, the boiling point distribution of oil products showed high consistency in different depolymerization cycles, suggesting the stability of microwave-powered liquid metal depolymerization.

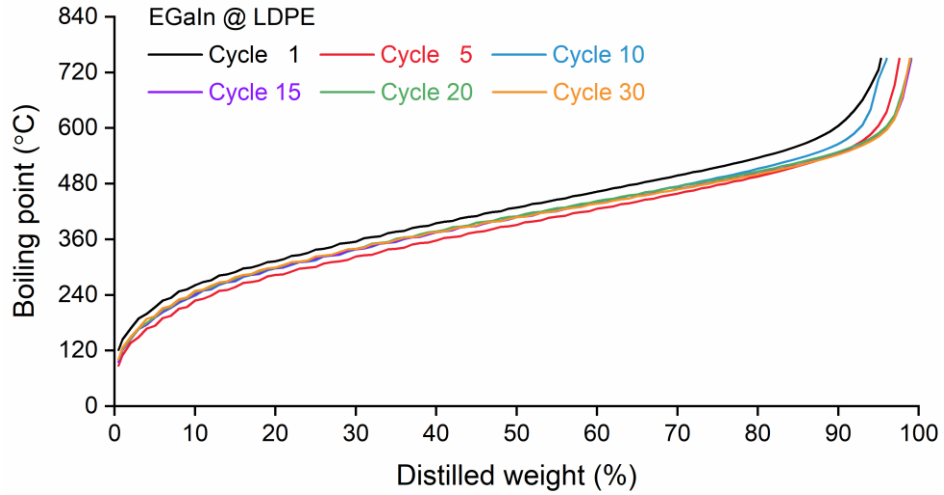

Supplementary Figure 47. Boiling point distribution of oil products after different depolymerization cycles. Plastic: LDPE-based plastic wraps; Liquid metal: EGaIn; Microwave power: P = 600 W.

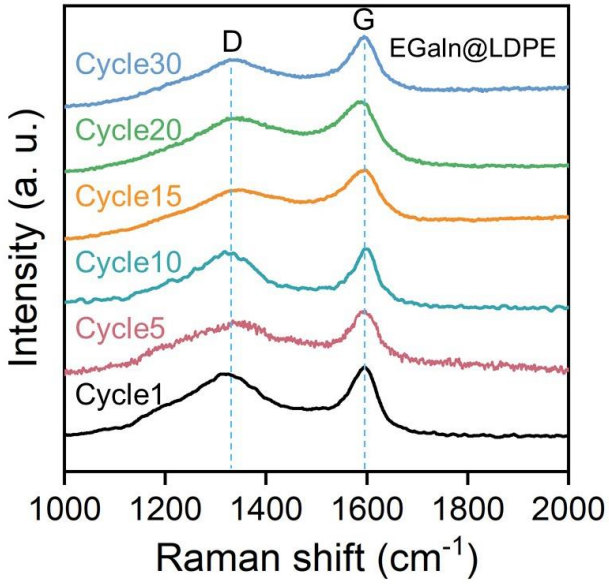

Supplementary Figure 48. Raman spectra of carbon residues obtained from 30 successive depolymerization cycles of LDPE-based plastic wraps using microwave-powered EGaIn. The Raman spectroscopy illustrated characteristic D-band and G-band of graphite at around 1350 cm^{-1} and 1590 cm^{-1}, respectively [18,19].

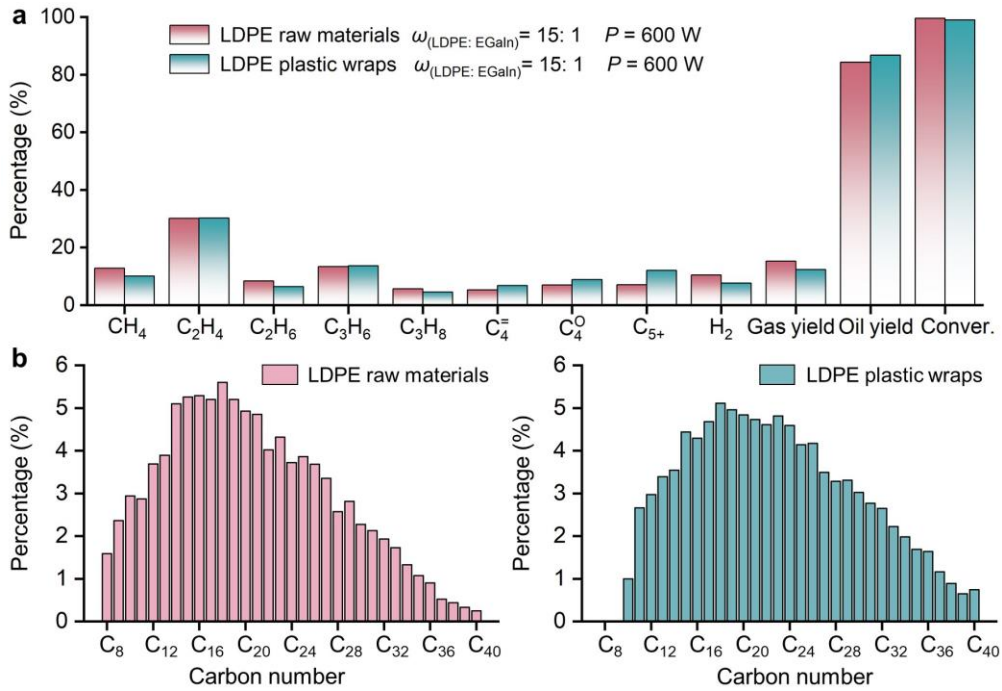

Supplementary Figure 49. Comparison of product distribution of LDPE-based plastic wraps and LDPE raw materials under the same depolymerization condition. (a) Comparison of gas distribution, product yield, and total conversion. (b) Comparison of carbon number distribution of oil products. Plastic: LDPE-based plastic wraps and raw materials; Liquid metal: EGaIn; $\omega_{(Plastic: Liquid\ metal)}$=15: 1; P = 600 W.

Supplementary Discussion 7

Characterizations of the liquid metal EGaIn

The morphology and microstructure of the liquid metal EGaIn were captured using transmission electron microscopy (TEM) after 10 and 30 consecutive depolymerization cycles (**Supplementary Figure 50**). Via scanning TEM-energy dispersive X-ray spectroscopy (STEM–EDX), we also revealed the element distribution on the LMs. Combined with the dark-field STEM (DF-STEM) and selected area electron diffraction pattern (SAED) image that appeared in an obvious amorphous phase diffraction ring, we further confirmed that the spherical particles within the depolymerization residues were liquid metal GaIn. Importantly, even after 30 consecutive depolymerization cycles, the liquid metal still appeared in spherical morphology due to its high surface tension. The inherent tendency of shrinking shape into spherical endowed liquid metal favorable ability to self-separate from the carbon residues or impurities during the depolymerization of LDPE-based plastic wraps.

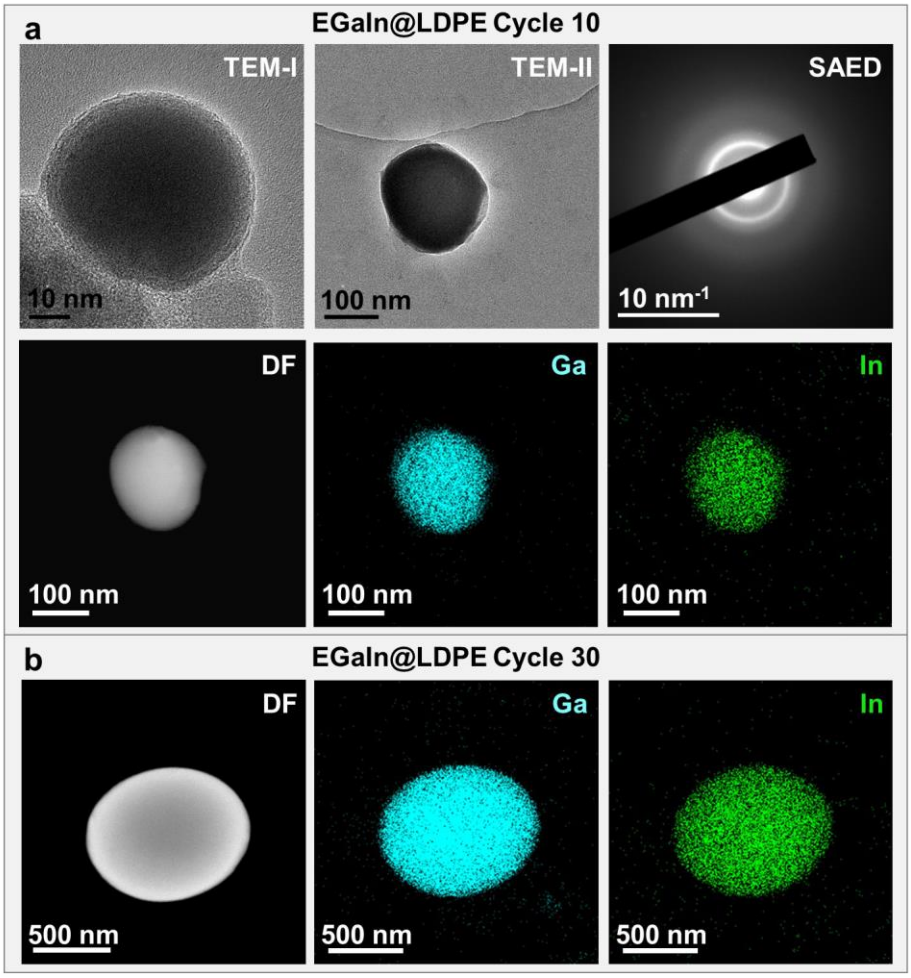

Supplementary Figure 50. Characterizations of the liquid metal EGaIn after 10 and 30 consecutive depolymerization cycles. (a) TEM images (TEM-I and TEM-II) of depolymerization residues from cycle 10. The SAED pattern, DF image, and EDX elemental mappings correspond to TEM-II. (b) DF image (left) and corresponding EDX elemental mappings (right) of depolymerization residues from cycle 30.

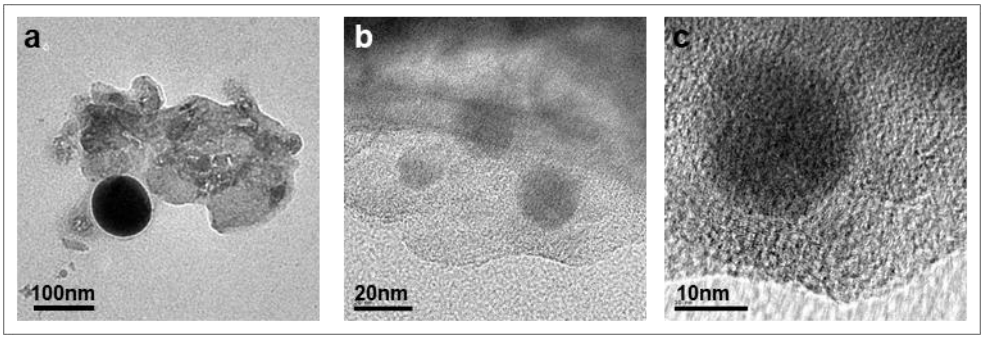

Supplementary Figure 51. The morphology and microstructure of carbon products. (a) TEM image and (b-c) high-resolution TEM micrographs.

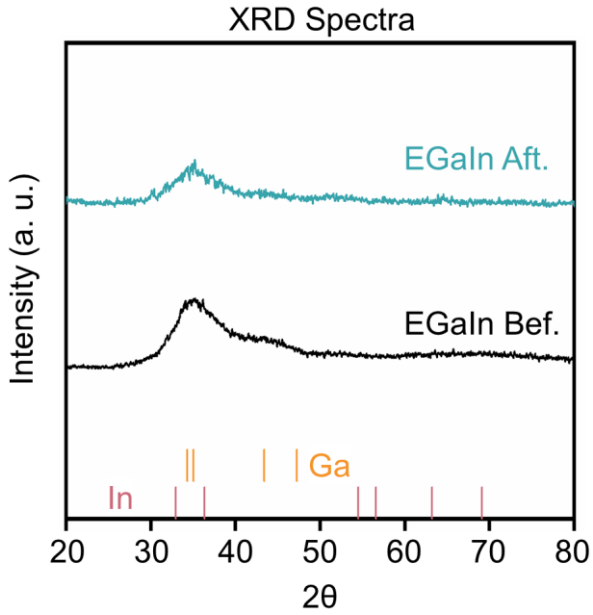

Supplementary Figure 52. XRD spectra describing the crystal composition of the EGaIn before and after catalyzing the plastics upcycling. There was no obvious crystal peak just as in the initial state.

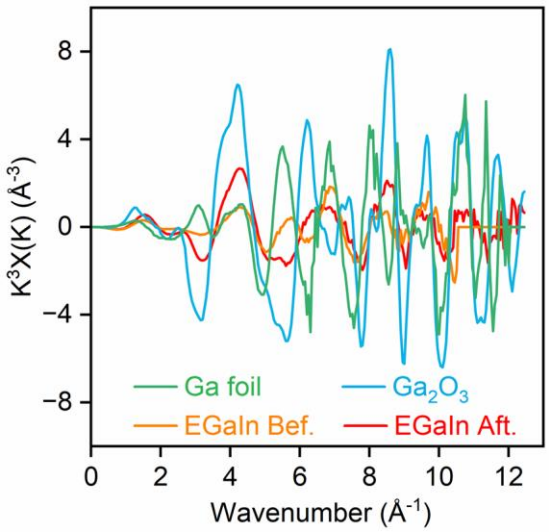

Supplementary Figure 53. The Fourier transform spectra of Ga K-edge spectra in standard samples of Ga foil and Ga_2O_3, and EGaIn before and after catalyzing the plastics upcycling.

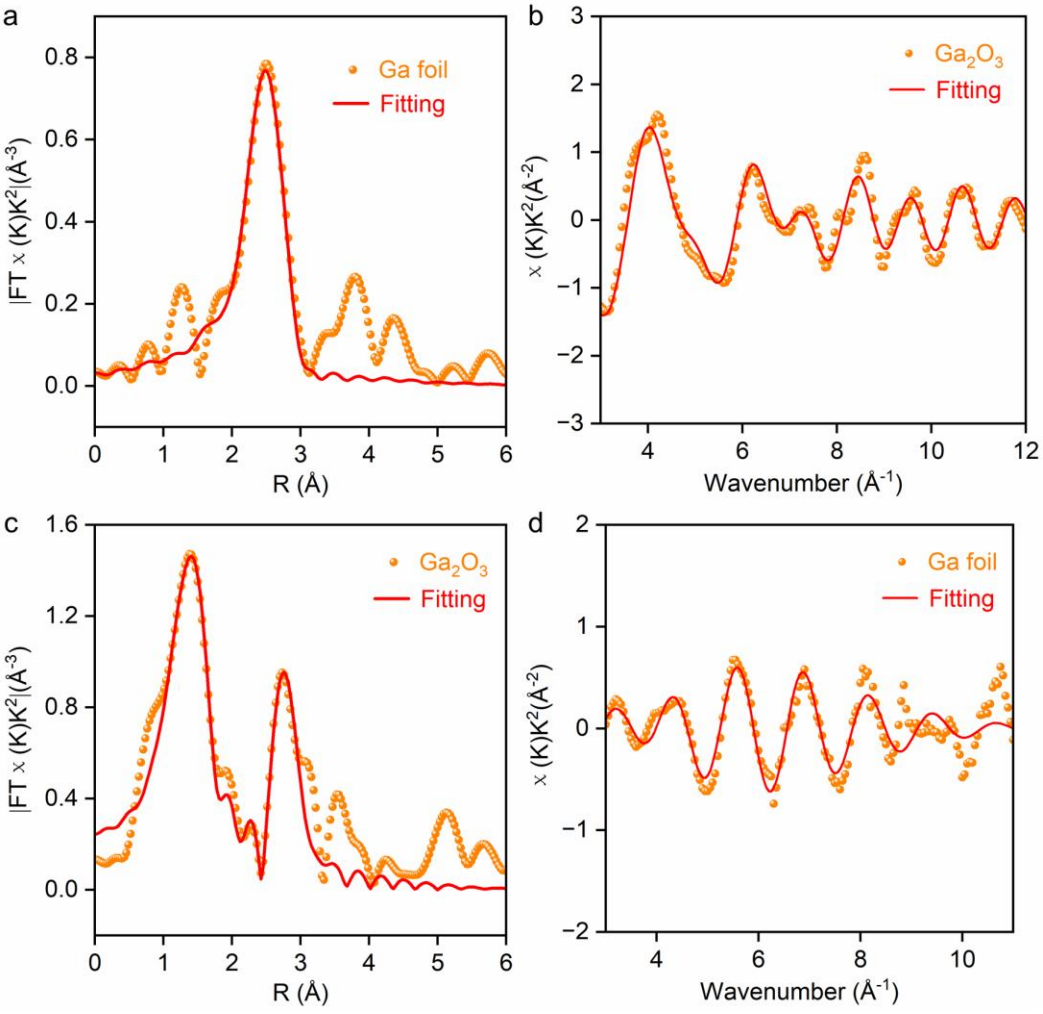

Supplementary Figure 54. EXAFS R-space and K-space fitting curves of Ga foil and Ga_2O_3 standard sample.

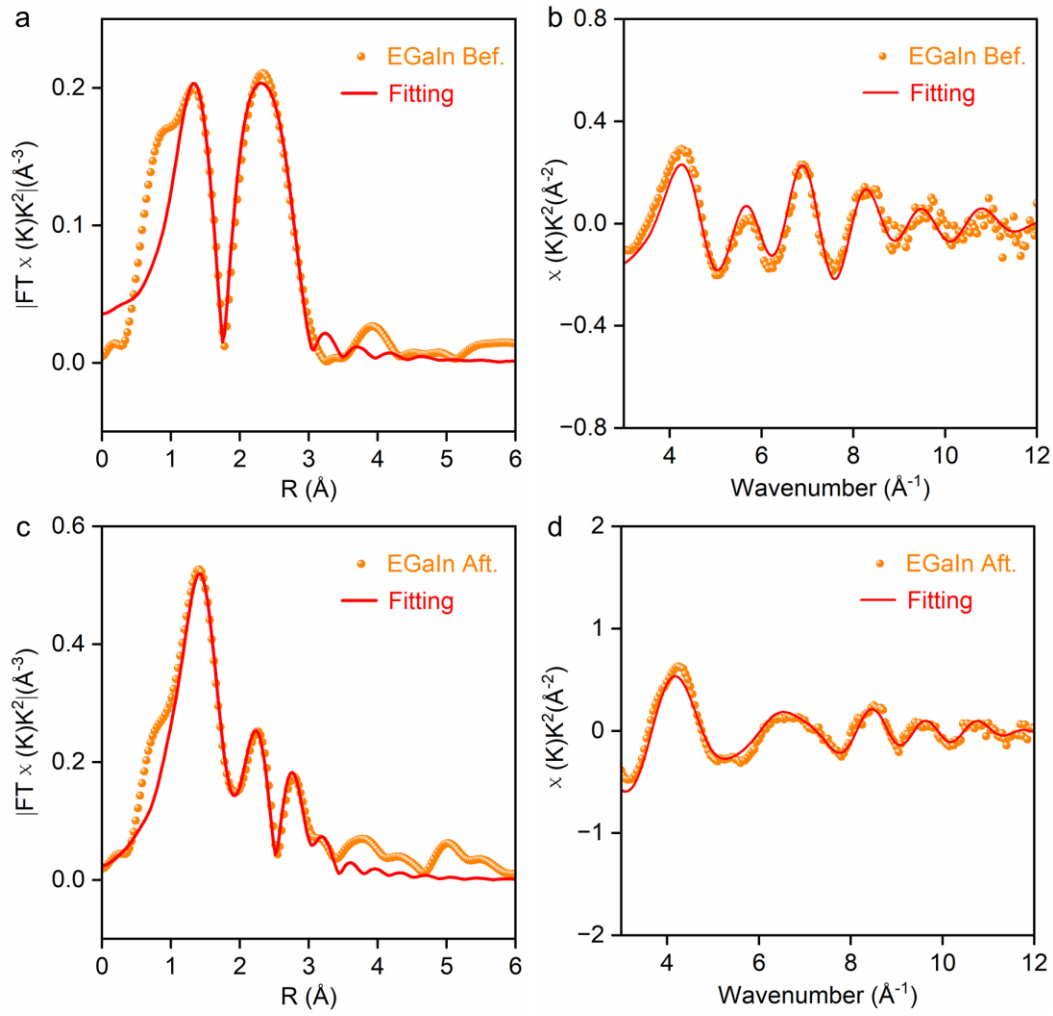

Supplementary Figure 55. EXAFS R-space and K-space fitting curves of EGaIn before and after catalyzing the plastics upcycling.

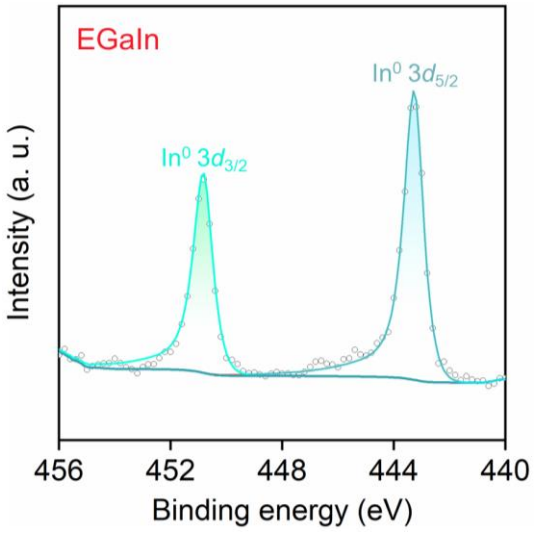

Supplementary Figure 56. XPS patterns illustrate the valence states of In within EGaIn.

Supplementary Discussion 8

Comparison of microwave-powered liquid metal depolymerization with other methods

Comparison between microwave depolymerization and electrical heating depolymerization

We initially compared the depolymerization via microwave-powered liquid metals and electrical heating methods. As presented in **Supplementary Table 10**, only 32 wt% of PP underwent depolymerization at a temperature of 450 ℃ and after 8 h of heating, resulting in an oil yield of merely 19.6 wt%. Besides, the addition of the liquid metals had no significant impact on the production and distribution of the products in the pyrolysis group. For LDPE, after being heated for 6 h, only 7.3 wt% underwent depolymerization with an oil yield of just 4 wt%. When the heating temperature was increased from 450 ℃ to 600 ℃, the conversion of LDPE and PP showed significant improvement, leading to a substantial increase in oil yield that approached that achieved by microwave-powered liquid metal depolymerization. However, despite similar oil yields, there were notable differences in the quality of the obtained oils. The carbon distribution in the oil produced through electrical heating depolymerization was erratic compared to the organized and concentrated carbon distribution observed in oils generated via microwave-powered liquid metal depolymerization (**Supplementary Figure 57**). In addition, electrical heating depolymerization consumed approximately three times more electricity than the microwave method. Overall, compared to electrical heating depolymerization, microwave-powered liquid metal depolymerization not only yielded oil products with a more concentrated carbon number distribution but also significantly reduced energy consumption.

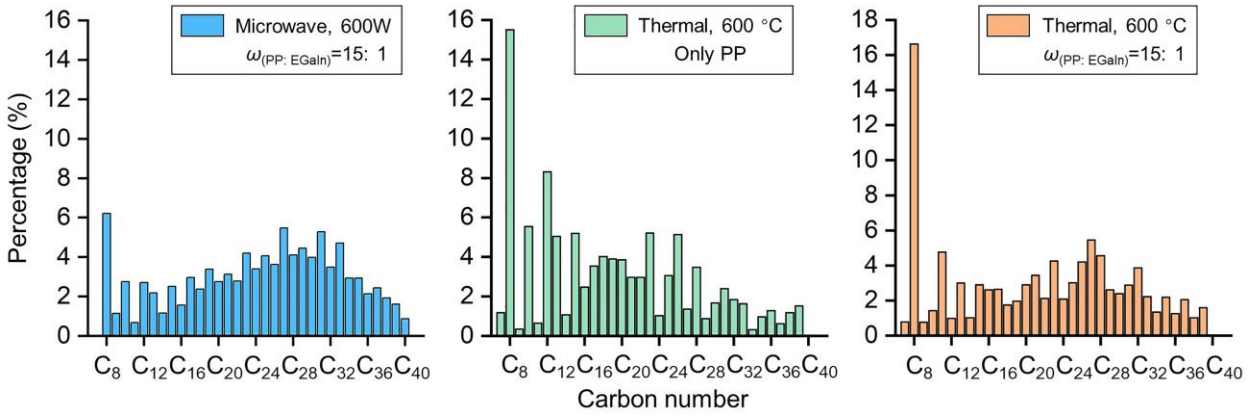

Supplementary Figure 57. Carbon number distribution of oil products obtained from different depolymerization methods.

Comparison between liquid metals and carbon-based microwave absorbents

To further demonstrate the superiority of microwave-powered liquid metal depolymerization, we selected three representative carbon-based materials with excellent microwave absorption properties (such as silicon carbide (SiC) and activated carbon (AC)), to depolymerize polyolefins under identical conditions. As shown in **Supplementary Figure 58a**, the microwave-powered liquid metals yielded more oil products (oil yield: 86.7 wt% for EGaIn and 84.5 wt% for EGaInSn), achieving a total conversion rate exceeding 99.0 wt%, while consuming the lowest amount of energy to obtain equivalent oil quality (approximately 0.033 kWh/($g_{Oil}/g_{Liquid\ metal}$)). Additionally, the liquid metals exhibited low methane (CH_4) selectivity (~3.8%, **Supplementary Figure 58b**), indicating that the gaseous products progressed fewer side reactions on the LM surface compared to carbon-based microwave absorbents. Essentially, owing to the excellent microwave absorption performance of carbon materials, the microwave energy is rapidly absorbed and converted into heat energy, subsequently transferred to the plastic, leading to nearly simultaneous fast pyrolysis. This process yields a higher proportion of solid carbon products (for example, carbon yield is 25.9 wt% for SiC and 13.1 wt% for AC), with less than half of the plastic effectively converted into oil products. However, due to the regioselectivity of plasma that is generated only in the LMs region, both the formation and location of free radical feature regioselectivity. Therefore, compared to depolymerization processes utilizing carbon materials, the depolymerization process via microwave-powered liquid metals is less violent, thereby the gaseous products progressed fewer side reactions on the LM surface, resulting in a low yield for solid carbon (the carbon yield is below 1 wt%).

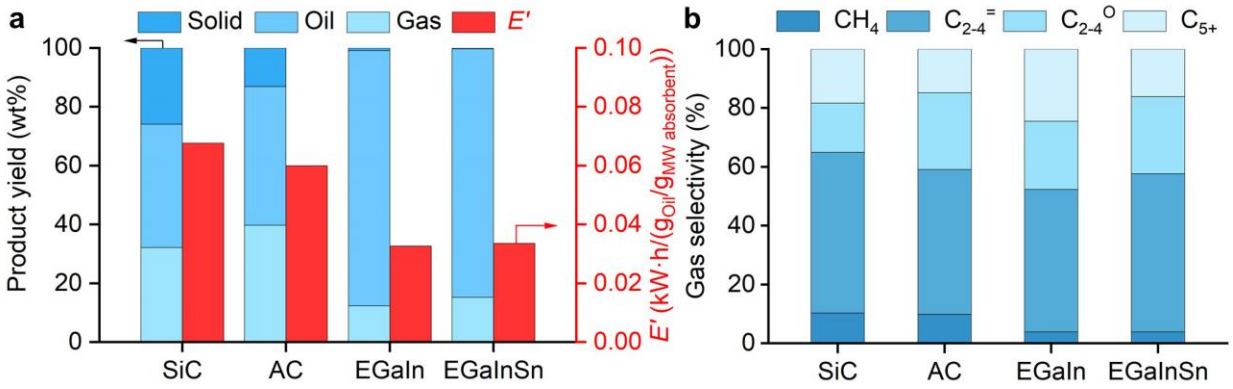

Supplementary Figure 58. Comparison between liquid metals and typical carbon materials in depolymerizing polyolefin plastics. (a) Product yield and energy consumption to obtain the same quality of oil products. (b) Gas selectivity. Plastic: LDPE-based plastic wraps; Microwave (MW) absorbent from left to right: silicon carbide (SiC), activated carbon (AC), EGaIn and EGaInSn. $\omega_{(Plastic:\ MW\ absorbent)}$=15: 1; Microwave power: P = 600 W.

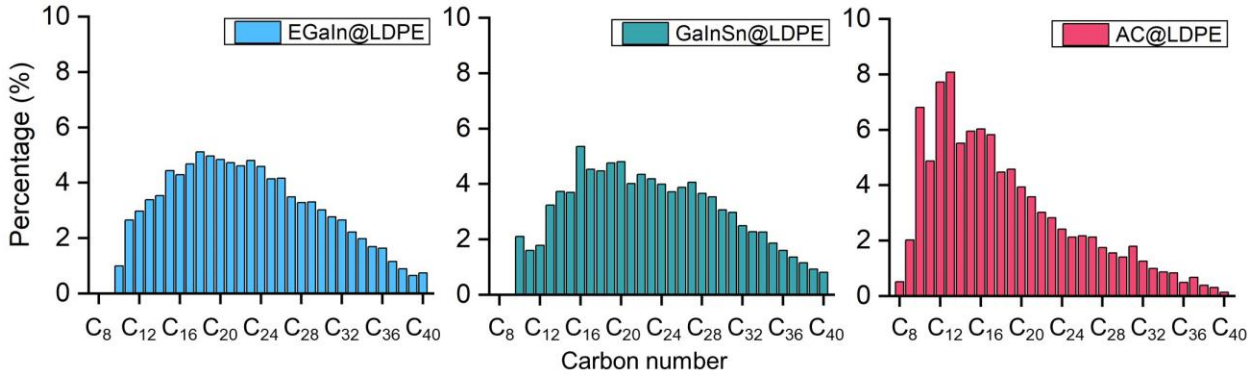

Supplementary Figure 59. Carbon number distribution of oil products obtained from depolymerization of LDPE using liquid metals and typical carbon materials.

Comparison between liquid metals and conventional metal nanocatalysts

The liquid metals, as depicted in **Supplementary Figure 60**, exhibited superior oil production capabilities compared to conventional metal nanocatalysts when subjected to the same microwave power and utilizing an equivalent mass of metals. For instance, the oil yield of liquid metal EGaIn reached 12.04 g_{Oil}/g_{EGaIn}, which was approximately 5.2 times higher than that achieved with a 50nm Fe catalyst; moreover, the oil yield of EGaInSn reached 12.63 $g_{Oil}/g_{EGaInSn}$, about 3.2 times greater than that obtained with a 50nm Co catalyst. Furthermore, gas composition analysis revealed significant dehydrogenation performance for both the 50nm Fe and 50nm Co catalysts, while it was noteworthy that liquid metals demonstrated exceptional capability in producing $C_{2\text{-}4}^{=}$ olefins. Importantly, it should be emphasized that metal nanocatalysts might undergo obvious sintering phenomena when exposed to microwave fields (**Supplementary Figure 61**); however, this phenomenon can be entirely circumvented by employing liquid metals.

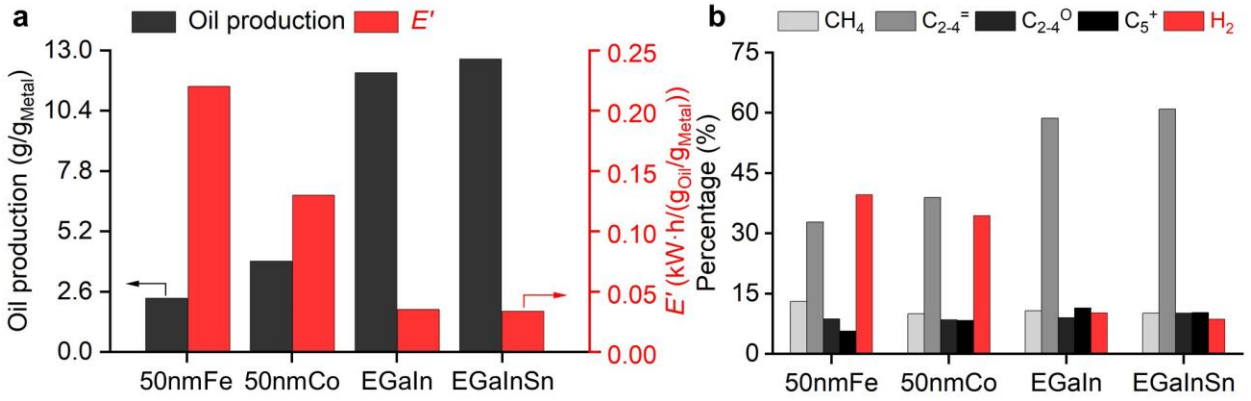

Supplementary Figure 60. Comparison between liquid metals and conventional metal nanocatalysts in depolymerizing polyolefin plastics. (a) Oil production and energy consumption to obtain the same quality of oil products. (b) Gas composition. Plastic: PP-based disposable lunch boxes; Metals from left to right: 50 nm Fe, 50 nm Co, EGaIn, and EGaInSn; Microwave power: *P* = 600 W.

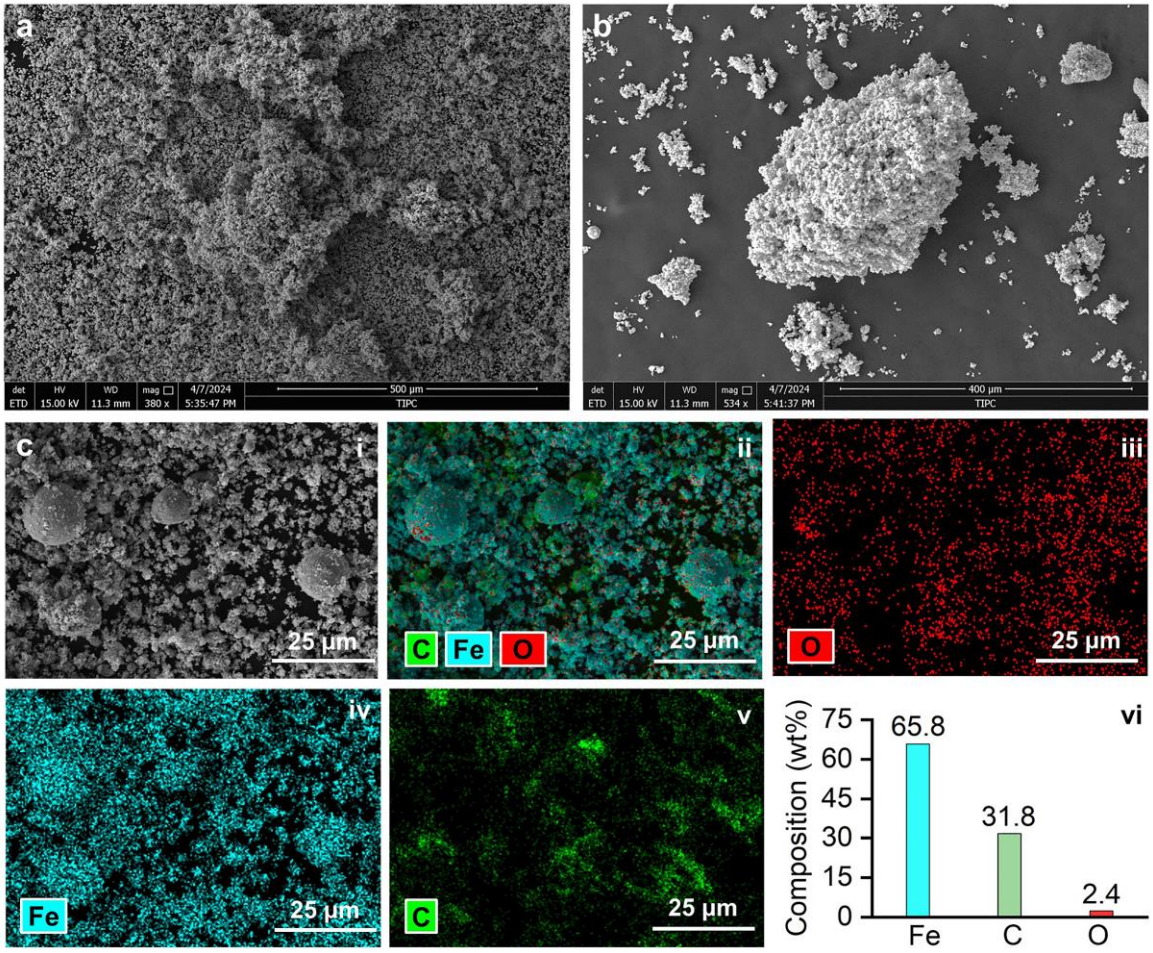

Supplementary Figure 61. Morphology and microstructure of conventional metal nanocatalysts sintered after depolymerizing polyolefins. (a-b) SEM images revealed that pure nanocatalysts underwent sintering, forming solid pieces (a) and bulk materials (b). (c) SEM image (i), EDS element mappings (ii-v), and the elemental composition (vi) analysis showed that the iron nanoparticles sintered into larger micron spheres after depolymerizing the polyolefins.

Supplementary Discussion 9

Depolymerization of HDPE and PP by liquid metal EGaIn

Depolymerization of HDPE by liquid metal EGaIn

Experimental results for ten successive depolymerization cycles of HDPE-based drug bottles via microwave-powered EGaIn were shown in **Supplementary Table 11**. GC-FID trace of the volatile products from different depolymerization cycles of HDPE-based drug bottles via microwave-powered EGaIn were shown in **Supplementary Figure 62**; GC-MS trace of the oil products were shown in **Supplementary Figure 63**; ^{1}H NMR spectrum and ^{13}C NMR spectrum of the oil products were shown in **Supplementary Figures 64** and **65**, respectively.

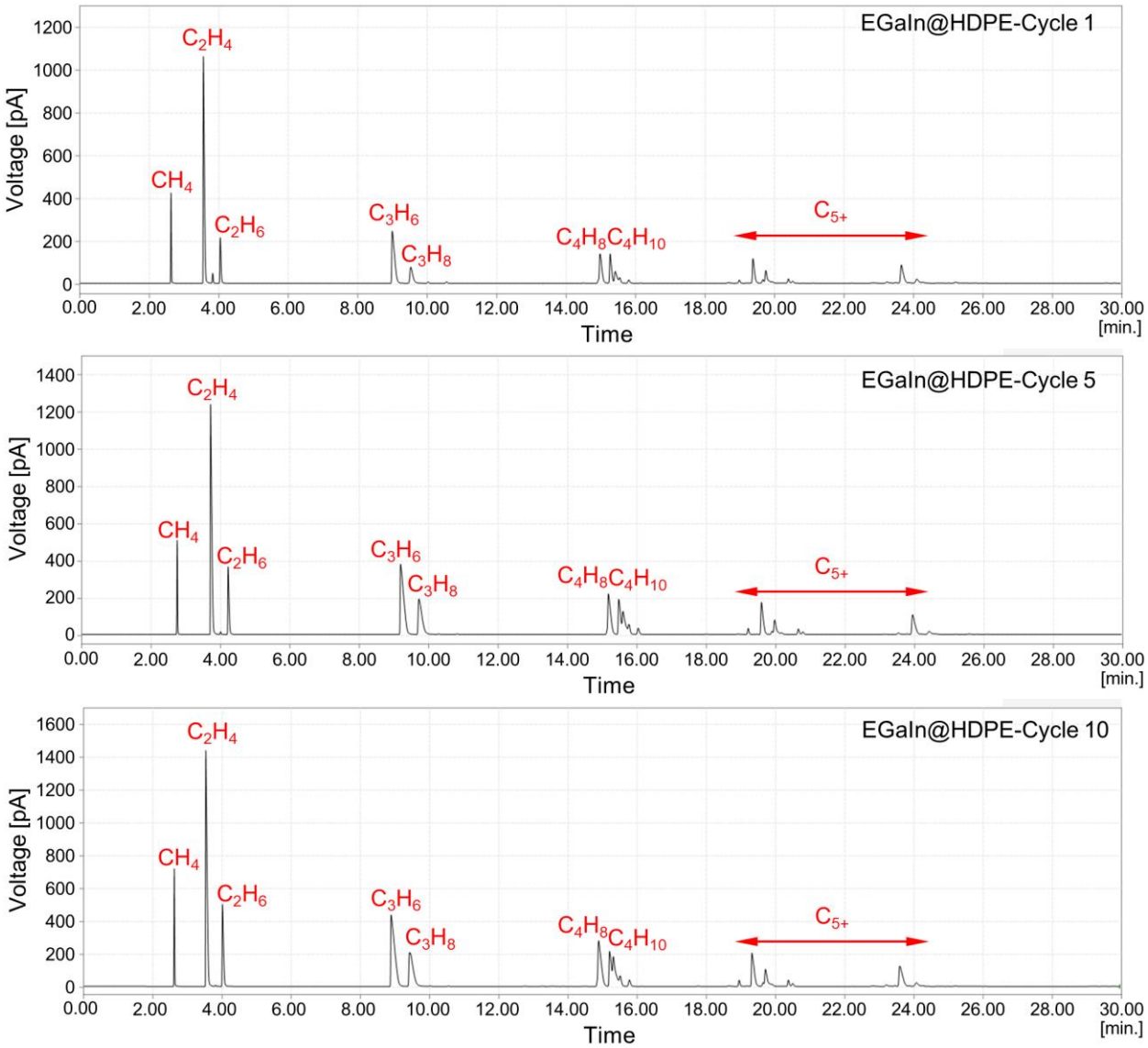

Supplementary Figure 62. GC-FID trace of the volatile products from the first, fifth and tenth depolymerization cycle of HDPE-based drug bottles via microwave-powered EGaIn.

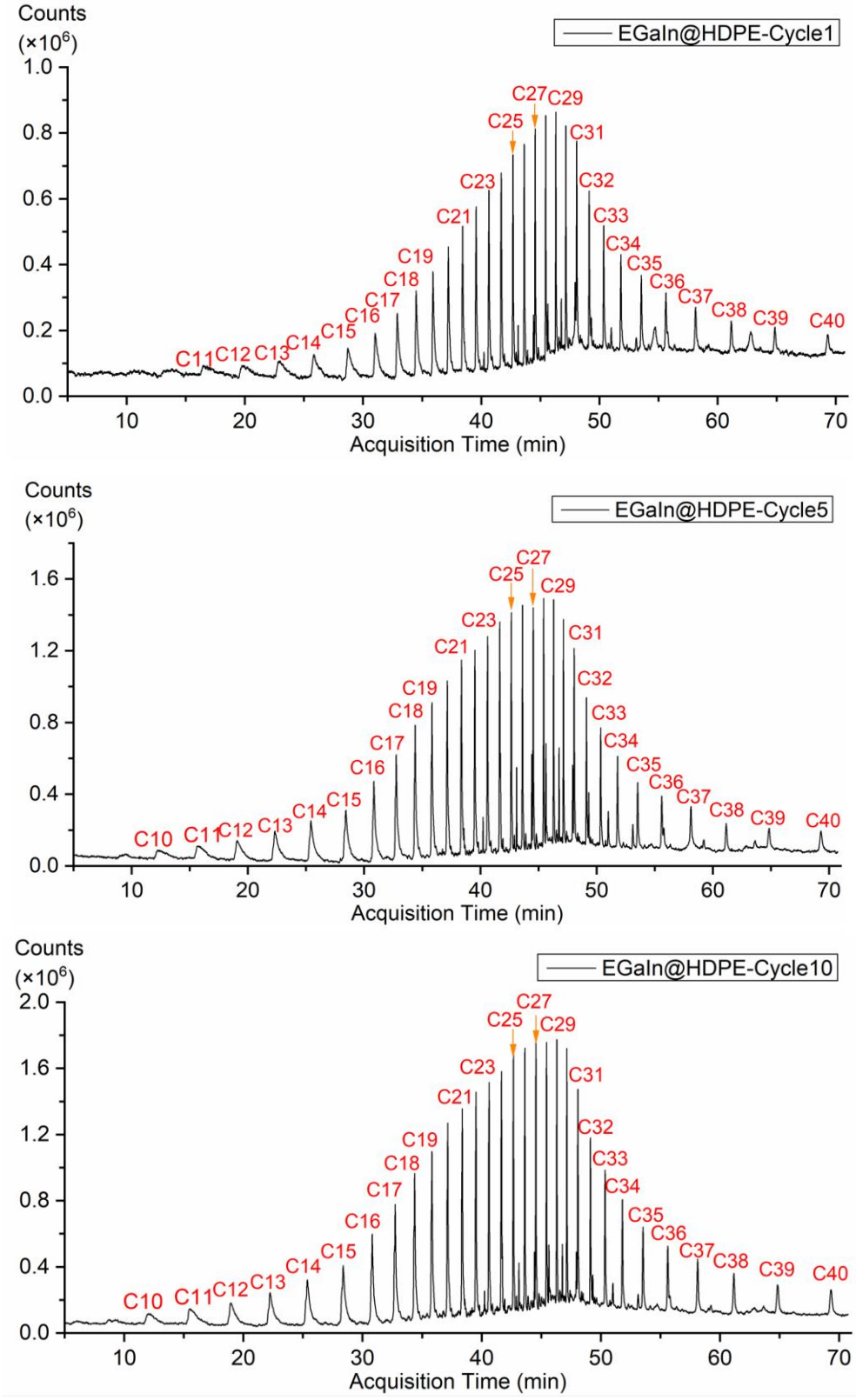

Supplementary Figure 63. GC-MS trace of the oil products from the first, fifth and tenth depolymerization cycle of HDPE-based drug bottles via microwave-powered EGaIn.

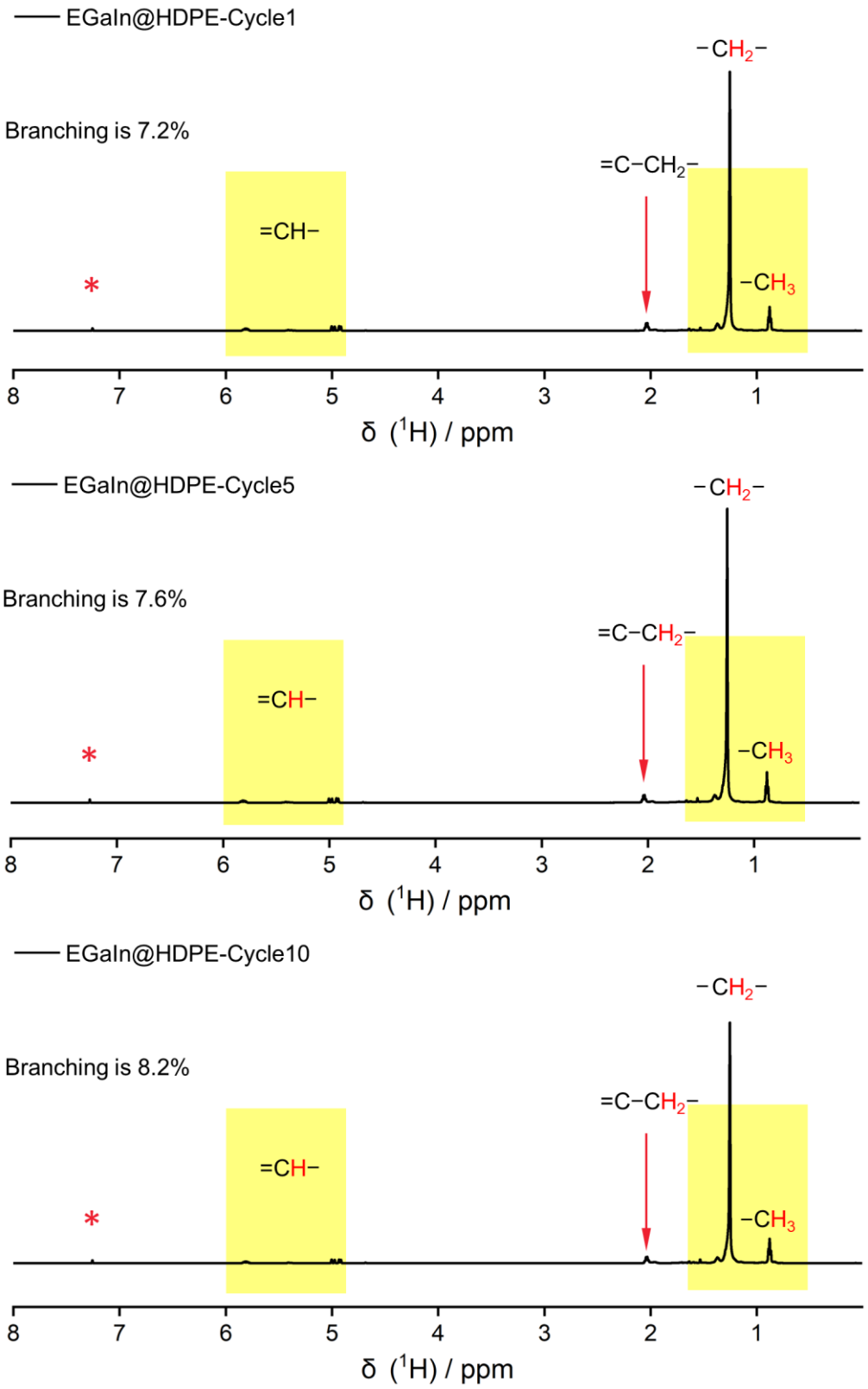

Supplementary Figure 64. ^{1}H NMR spectrum of the oil products from the first fifth and tenth depolymerization cycle of HDPE-based drug bottles via microwave-powered EGaIn.

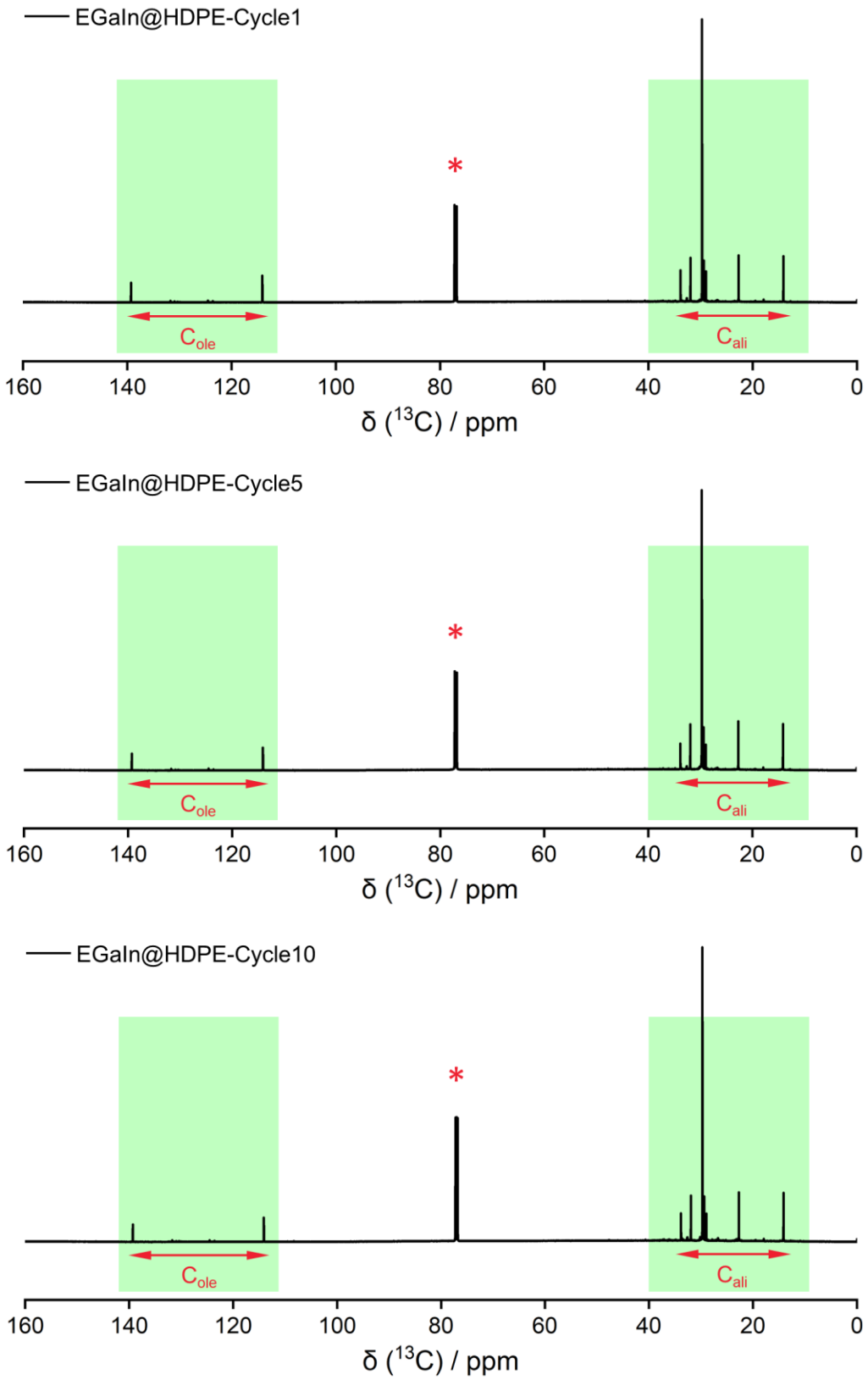

Supplementary Figure 65. ^{13}C NMR spectrum of the oil products from the first, fifth and tenth depolymerization cycle of HDPE-based drug bottles via microwave-powered EGaIn.

As shown in **Supplementary Figure 66**, the boiling points of oil products of HPDE-based plastics were mainly distributed in the range of 80-600 ℃. In addition, the boiling point distribution of oil products showed high consistency under different depolymerization cycles, suggesting the stability of microwave-powered liquid metals in depolymerizing HDPE-based plastics.

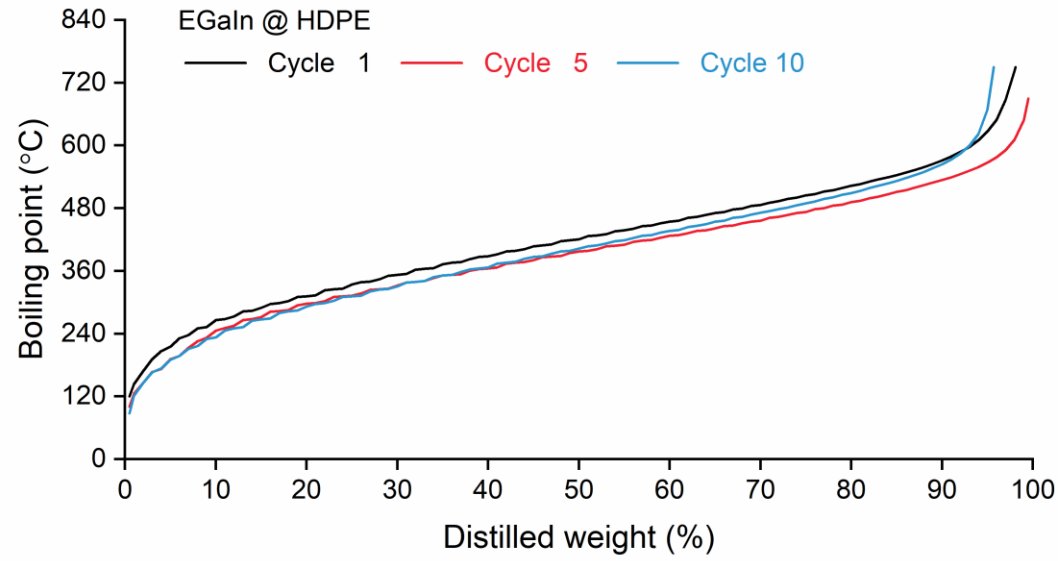

Supplementary Figure 66. Boiling point distribution of oil products after different depolymerization cycles via the simulated distillation gas chromatography. Plastic: HPDE-based medicine bottles; Liquid metal: EGaIn; P = 600 W; $\omega_{(\text{Plastic: Liquid metal})}$=15: 1.

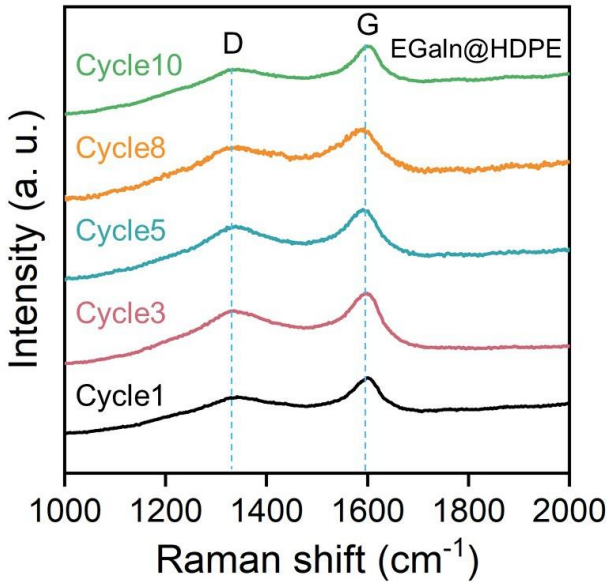

Supplementary Figure 67. Raman spectra of the residual carbon from the different depolymerization cycles of HDPE-based drug bottles via microwave-powered EGaIn.

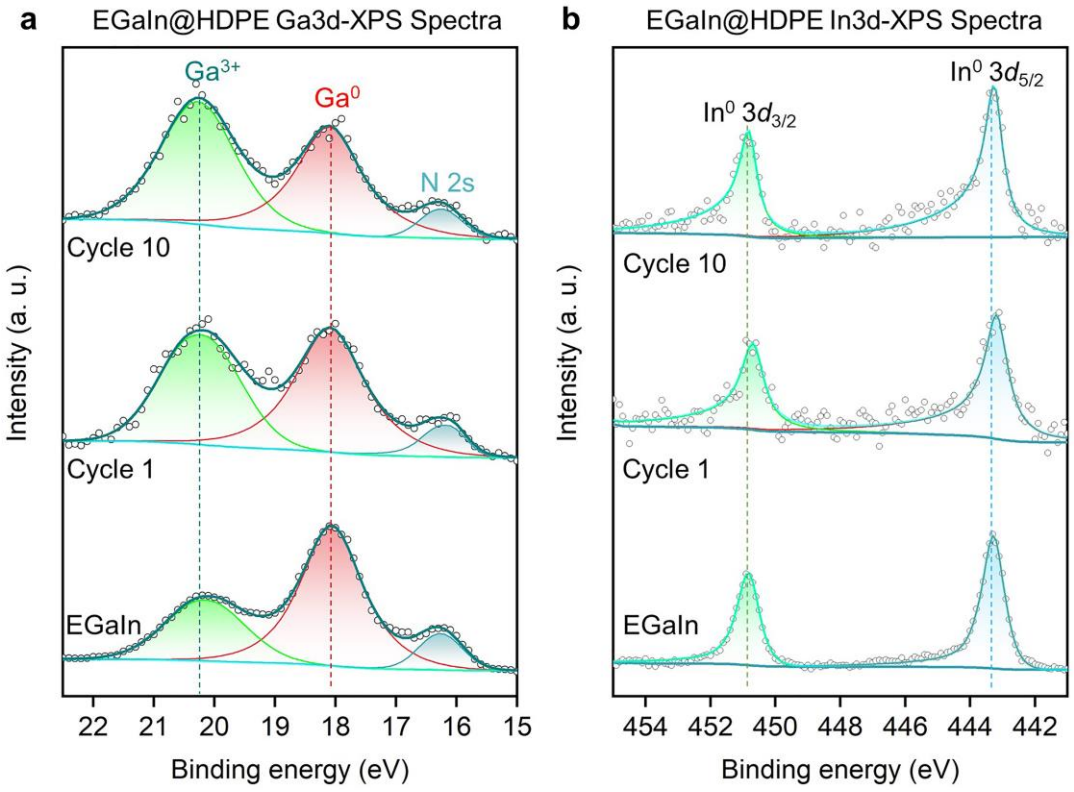

Supplementary Figure 68. XPS patterns illustrate the valence states of Ga (a) and In (b) in depolymerization residues after different depolymerization cycles. From top to bottom: EGaIn@HDPE Cycle 10, EGaIn@HDPE Cycle 1, and EGaIn, respectively.

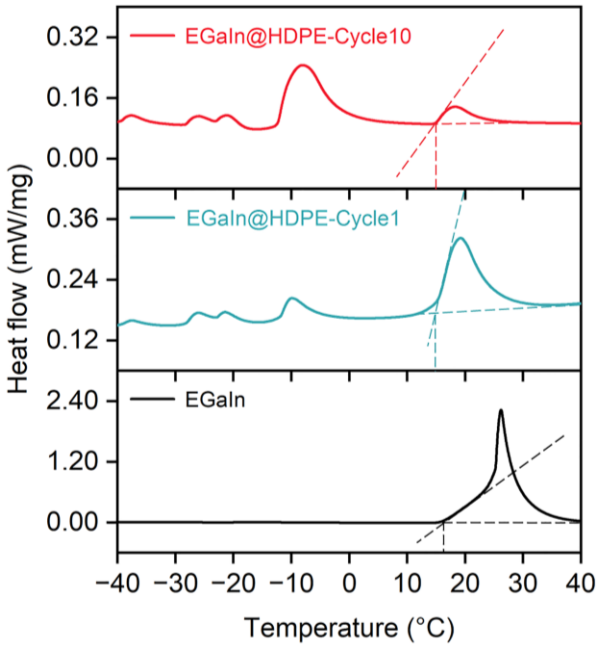

Supplementary Figure 69. DSC curves show the melting process of depolymerization residues after different depolymerization cycles. From top to bottom: EGaIn@HDPE Cycle 10, EGaIn@HDPE Cycle 1, and EGaIn, respectively. There were obvious endothermic peaks at the melting point of EGaIn after multiple cycles, which validated the presence of EGaIn.

Depolymerization of PP by liquid metal EGaIn

Experimental results for ten successive depolymerization cycles of PP-based disposable lunch boxes via microwave-powered EGaIn were shown in **Supplementary Table 12**. GC-FID trace of the volatile products from different depolymerization cycles of PP-based disposable lunch boxes via microwave-powered EGaIn were shown in **Supplementary Figure 70**; GC-MS trace of the oil products were shown in **Supplementary Figure 71**; ^{1}H NMR spectrum and ^{13}C NMR spectrum of the oil products were shown in **Supplementary Figures 72** and **73**, respectively.

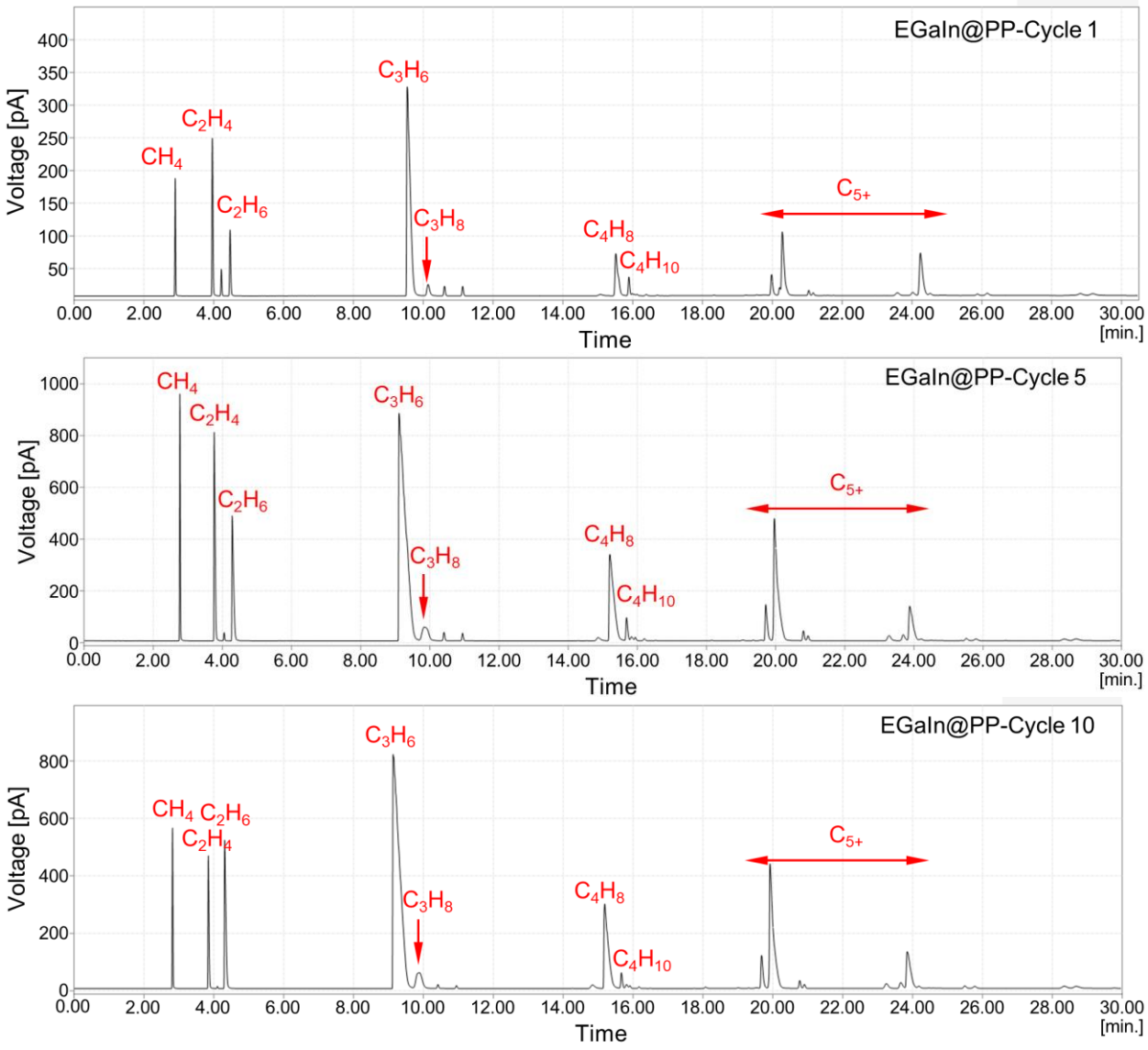

Supplementary Figure 70. GC-FID trace of the volatile products from the first fifth and tenth depolymerization cycle of PP-based disposable lunch boxes via microwave-powered EGaIn.

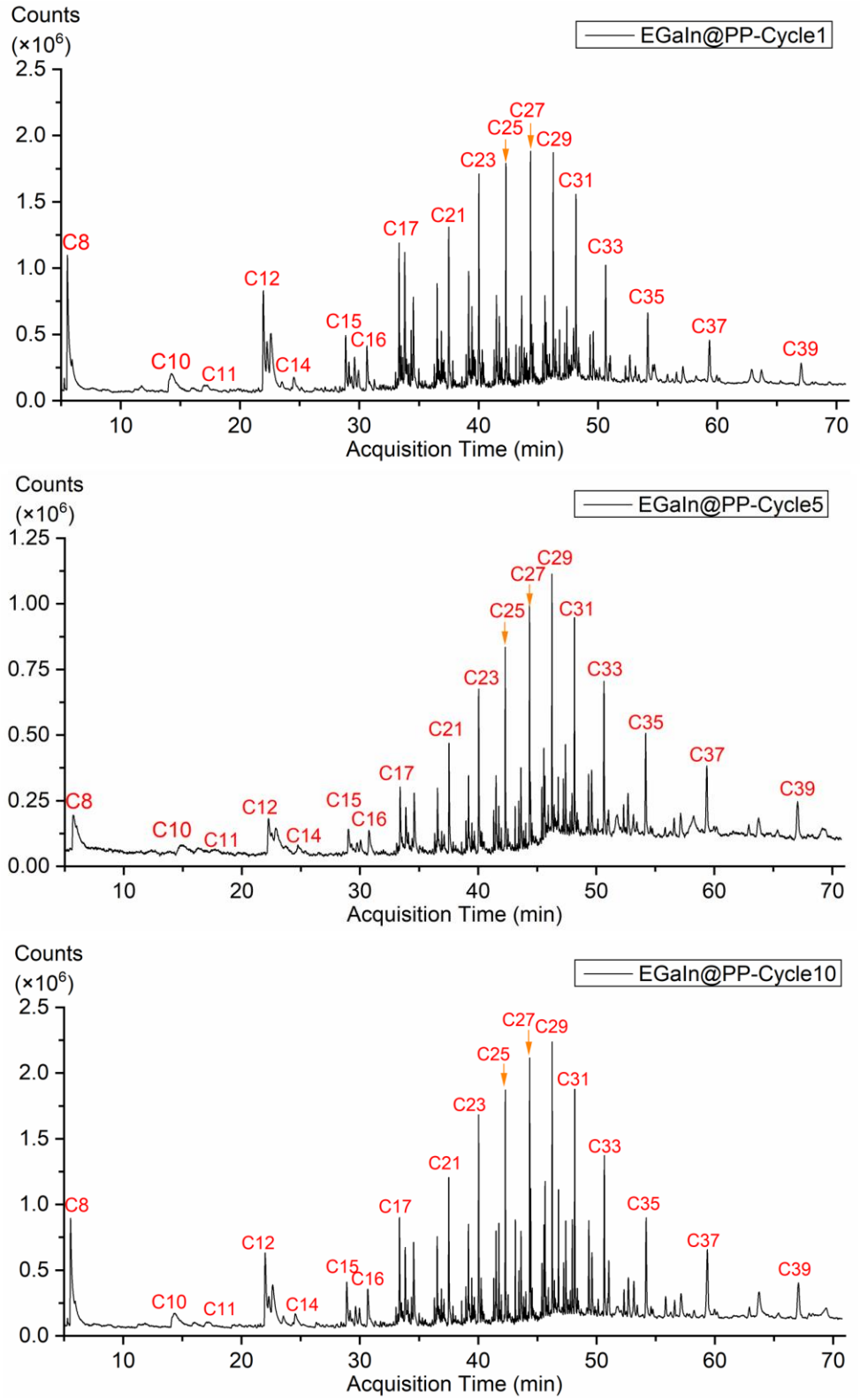

Supplementary Figure 71. GC-MS trace of the oil products from the first, fifth and tenth depolymerization cycle of PP-based disposable lunch boxes via microwave-powered EGaIn.

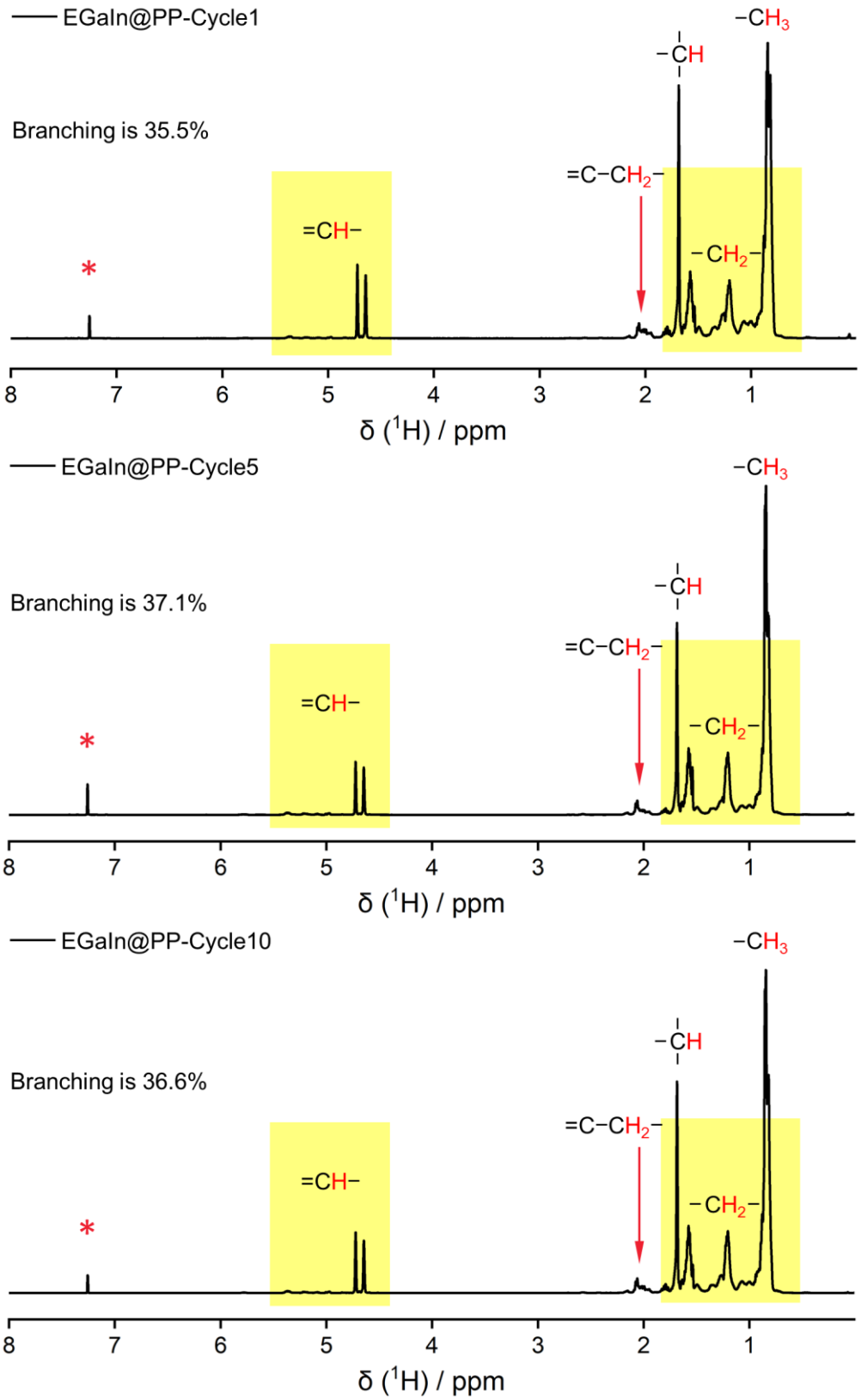

Supplementary Figure 72. ^{1}H NMR spectrum of the oil products from the first, fifth and tenth depolymerization cycle of PP-based disposable lunch boxes via microwave-powered EGaIn.

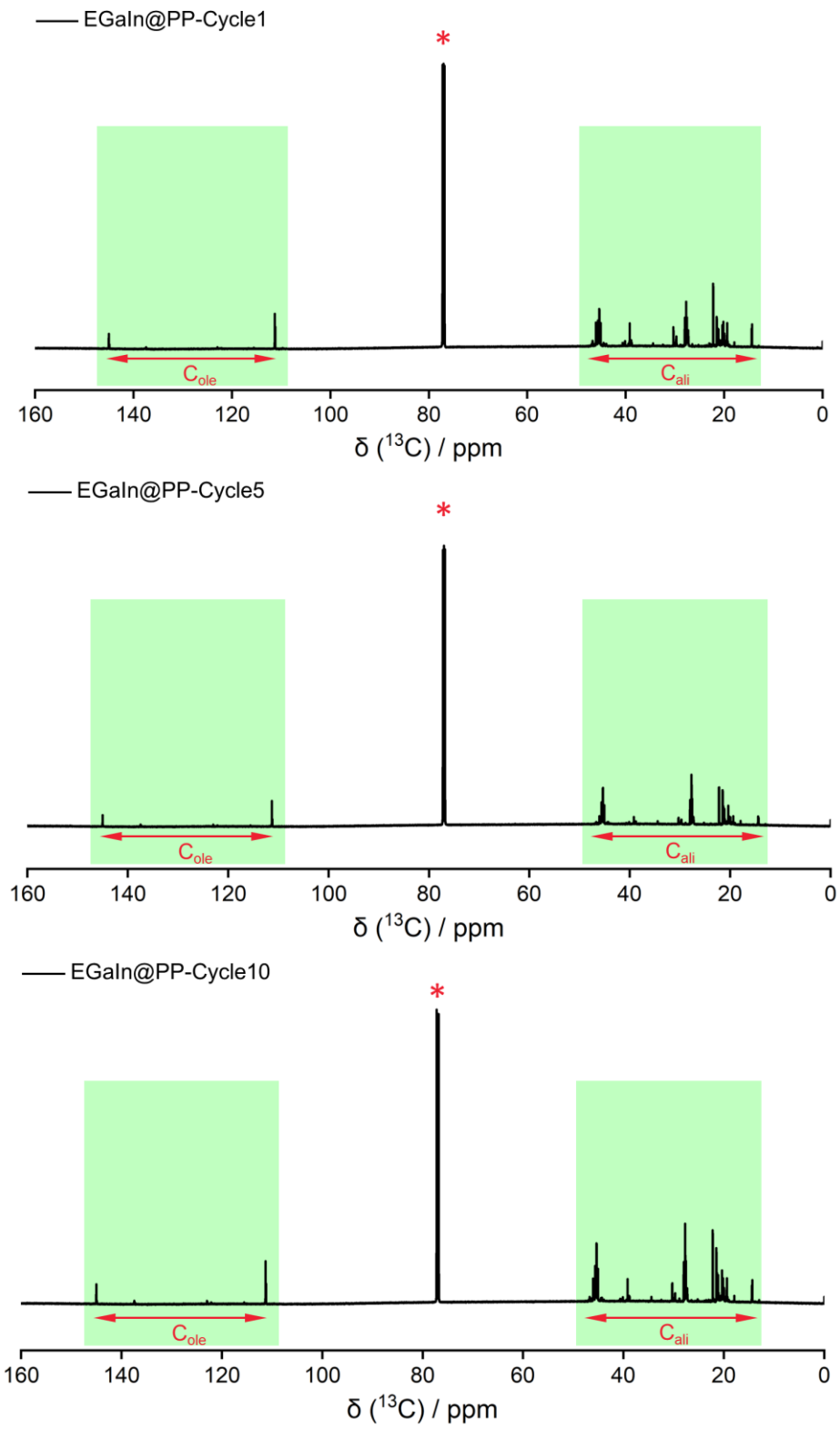

Supplementary Figure 73. ^{13}C NMR spectrum of the oil products from the first, fifth and tenth depolymerization cycle of PP-based disposable lunch boxes via microwave-powered EGaIn.

As shown in **Supplementary Figure 74**. The boiling points of oil products of PP-based plastics were similar with that of HPDE-based plastics, distributing in the range of 80-600 ℃. Besides, the boiling point distribution of oil products also showed high consistency under different depolymerization cycles, suggesting the stability of microwave-powered liquid metals in depolymerizing PP-based plastics.

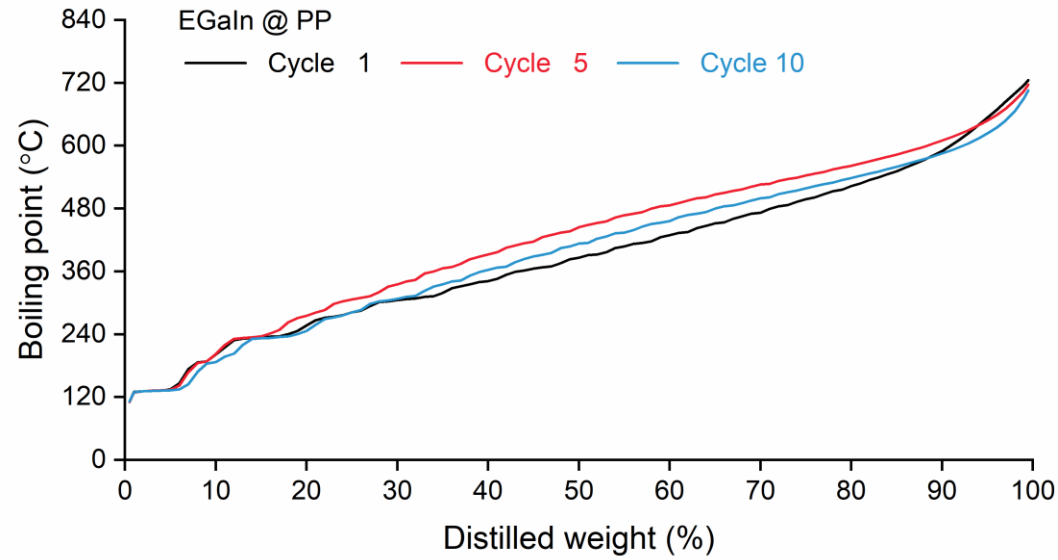

Supplementary Figure 74. Boiling point distribution of oil products after different depolymerization cycles via the simulated distillation gas chromatography. Plastic: PP-based disposable lunch boxes; Liquid metal: EGaIn; Microwave power: P = 600 W; $\omega_{(\text{Plastic: Liquid metal})}$=15: 1.

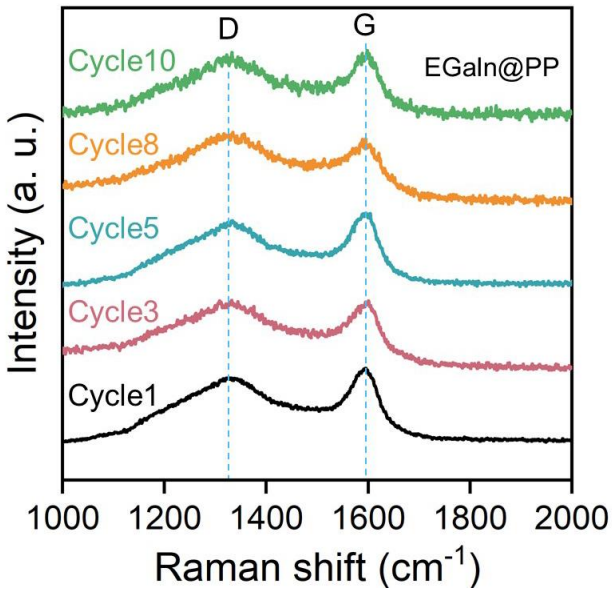

Supplementary Figure 75. Raman spectra of the residual carbon from the different depolymerization cycles of PP-based disposable lunch boxes via microwave-powered EGaIn.

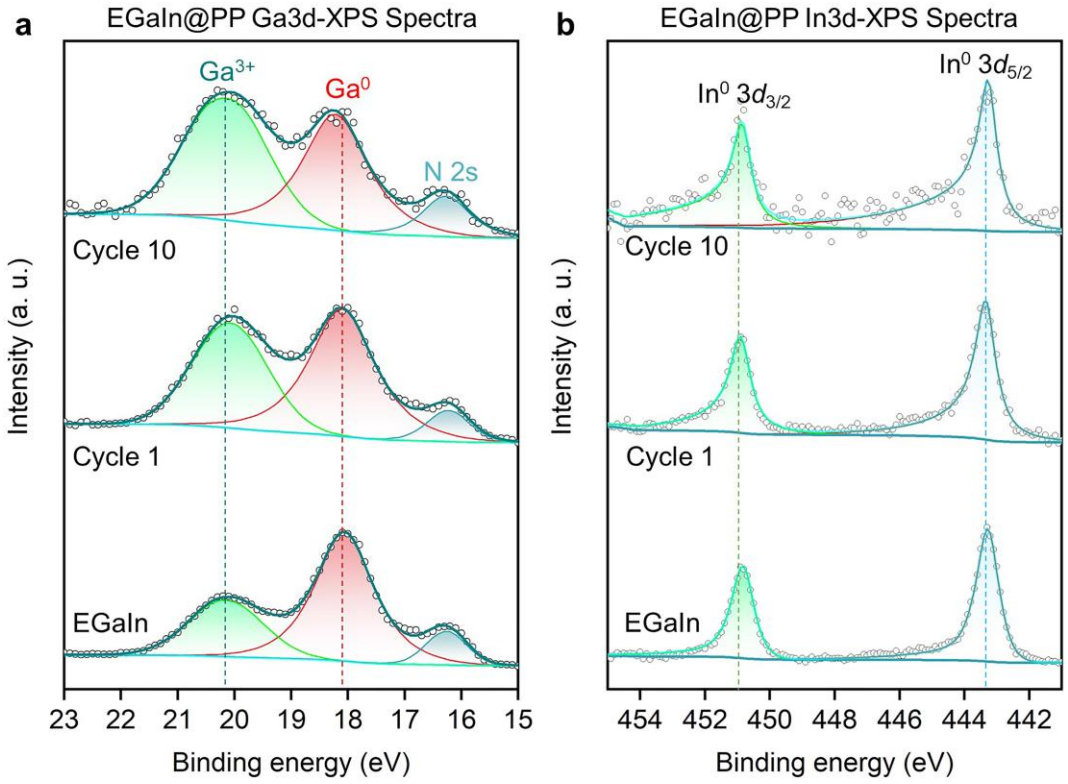

Supplementary Figure 76. XPS patterns illustrate the valence states of Ga (a) and In (b) in depolymerization residues after different depolymerization cycles. From top to bottom: EGaIn@PP Cycle 10, EGaIn@PP Cycle 1, and EGaIn, respectively.

Supplementary Discussion 10

Depolymerization of LDPE and PP by liquid metal EGaInSn

To further demonstrate the generalized purpose of microwave-powered liquid metal depolymerization, we extended the binary liquid metal systems to ternary liquid metal systems. Here, taking the ternary EGaInSn as an example, we explored its capability in depolymerizing LDPE- and PP-based plastics. During 10 consecutive depolymerization cycles, the conversions of both LDPE- and PP-based plastics have remained above 95.5 wt% (**Supplementary Figure 77a**, **Supplementary Tables 13 and 14**). Importantly, the average oil yields of LDPE- and PP-based plastics were 82.1 wt% and 83.5 wt%, and corresponding gas yields were 16.8 wt% and 15.9 wt%, respectively. Particularly, gas chromatography (GC, GC-7820, Shandong Huifen Instrument Co., Ltd., China) analysis disclosed that the gas products were dominated by olefin monomers ($C_{2\text{-}4}^{=}$), including ethylene, propylene, and butene, the average selectivities of which were 51.7% and 69.6% for LDPE- and PP- based plastics, respectively. In addition, the average selectivity of ethylene monomer (C_2H_4) via the depolymerization of LDPE-based plastics was maintained at 24.3%, while the average selectivity of propylene monomer (C_3H_6) produced by PP-based plastics depolymerization was as high as 53% (**Supplementary Figure 77b**). Besides, the oil products were characterized by gas chromatography-mass spectrometry (GC-MS, GCMS QP2010 Ulltra, Shimadzu, Japan). GC-MS analysis revealed that the carbon numbers of the oil products of LDPE-based plastics exhibited a Gaussian distribution (C_{21}-centred) in the range of C_8-C_{40} (**Supplementary Figure 77c**). And the carbon numbers of the oil products of PP-based plastics exhibited a non-Gaussian distribution, but they were still concentrated in C_{16}-C_{40}. Overall, the electromagnetic microwave-powered ternary EGaInSn also demonstrated excellent performance in depolymerizing polyolefin plastics.

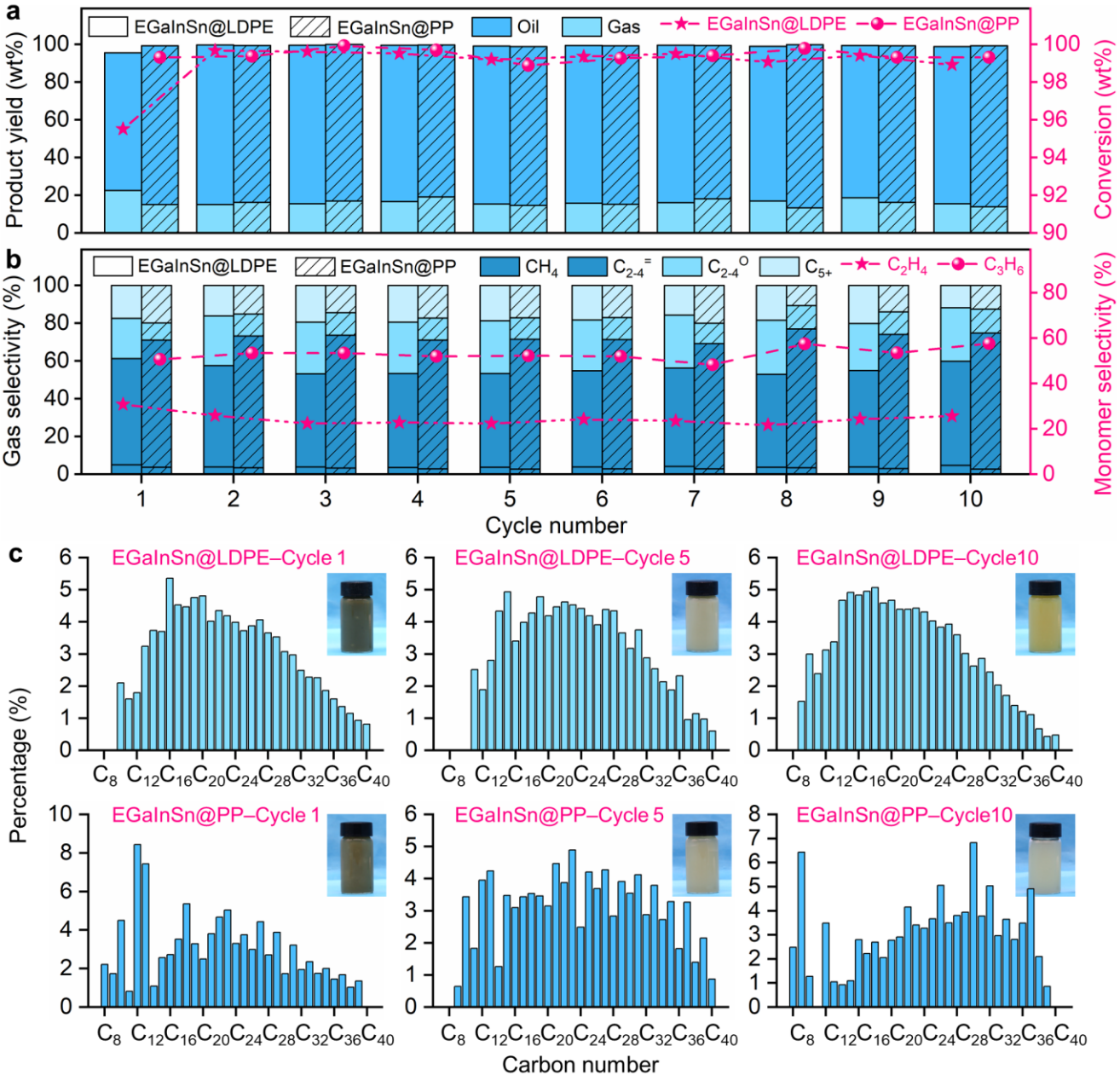

Supplementary Figure 77. Distribution of the depolymerization products of LDPE and PP using microwave-powered ternary liquid metal EGaInSn. (a-b) Product yield and conversion (a) and selectivity of gas products and constituent monomer (b). (c) Carbon number distribution of oil products of the depolymerization of LDPE and PP in cycles 1, 5, and 10. Insets show the corresponding optical image of oil products.

GC-FID trace of the volatile products and GC-MS trace of the oil products from different depolymerization cycles of LDPE-based plastic wraps via microwave-powered EGaInSn were shown in **Supplementary Figures 78** and **79**, respectively.

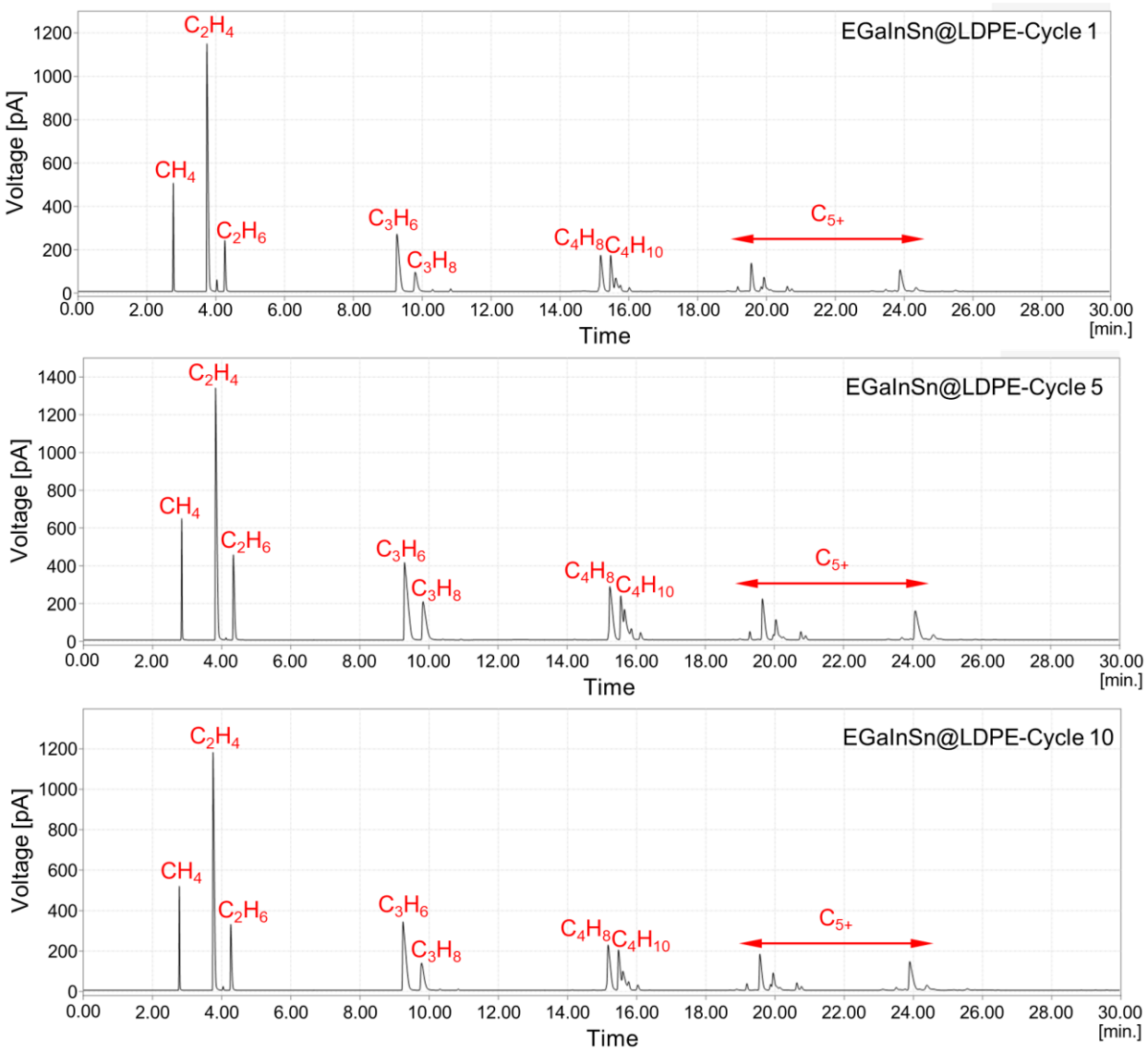

Supplementary Figure 78. GC-FID trace of the volatile products from the first fifth and tenth depolymerization cycle of LDPE-based plastic wraps via microwave-powered EGaInSn.

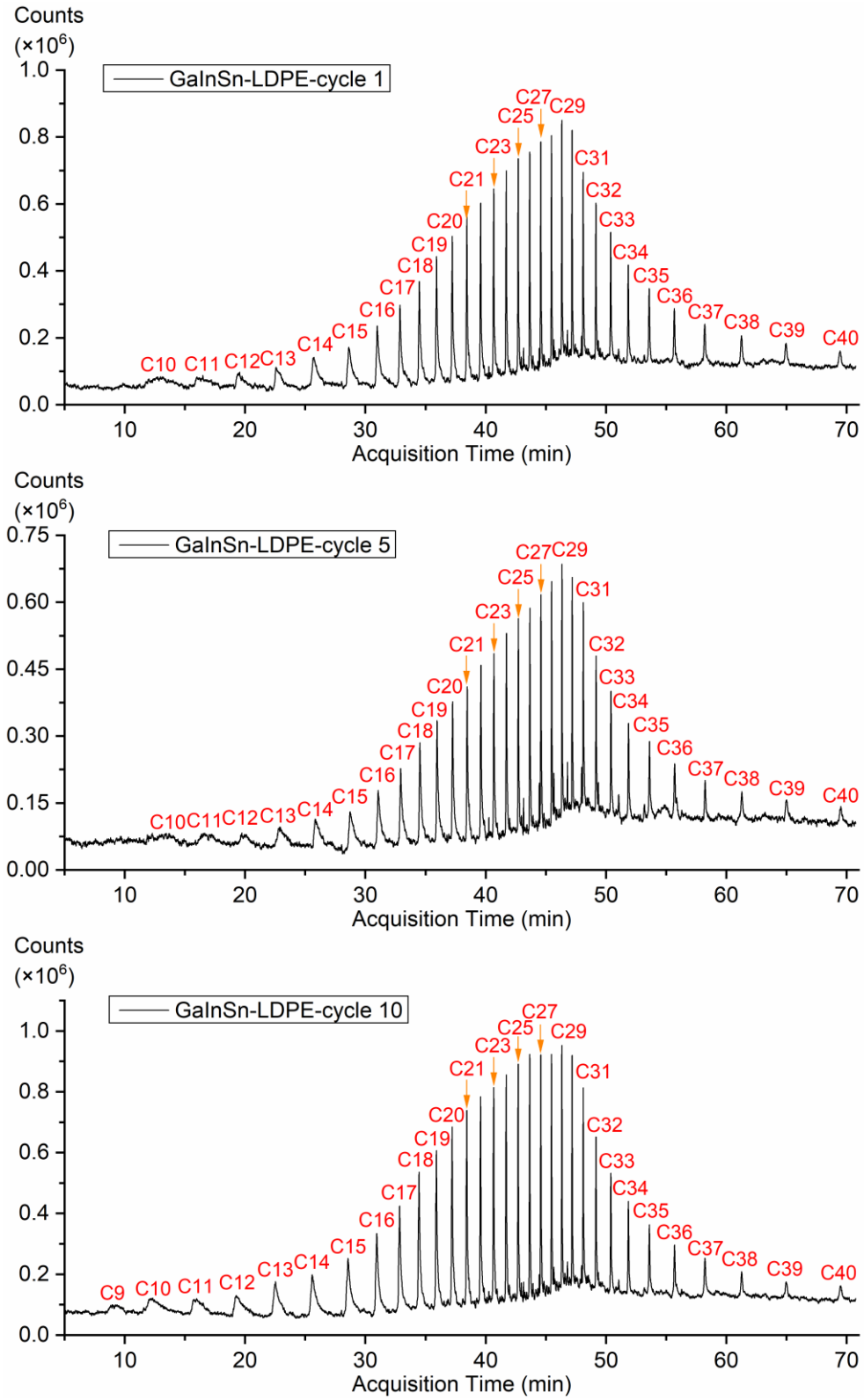

Supplementary Figure 79. GC-MS trace of the oil products from the first fifth and tenth depolymerization cycle of LDPE-based plastic wraps via microwave-powered EGaInSn.

GC-FID trace of the volatile products and GC-MS trace of the oil products from different depolymerization cycles of PP-based disposable lunch boxes via microwave-powered EGaInSn were shown in **Supplementary Figures 80** and **81**, respectively.

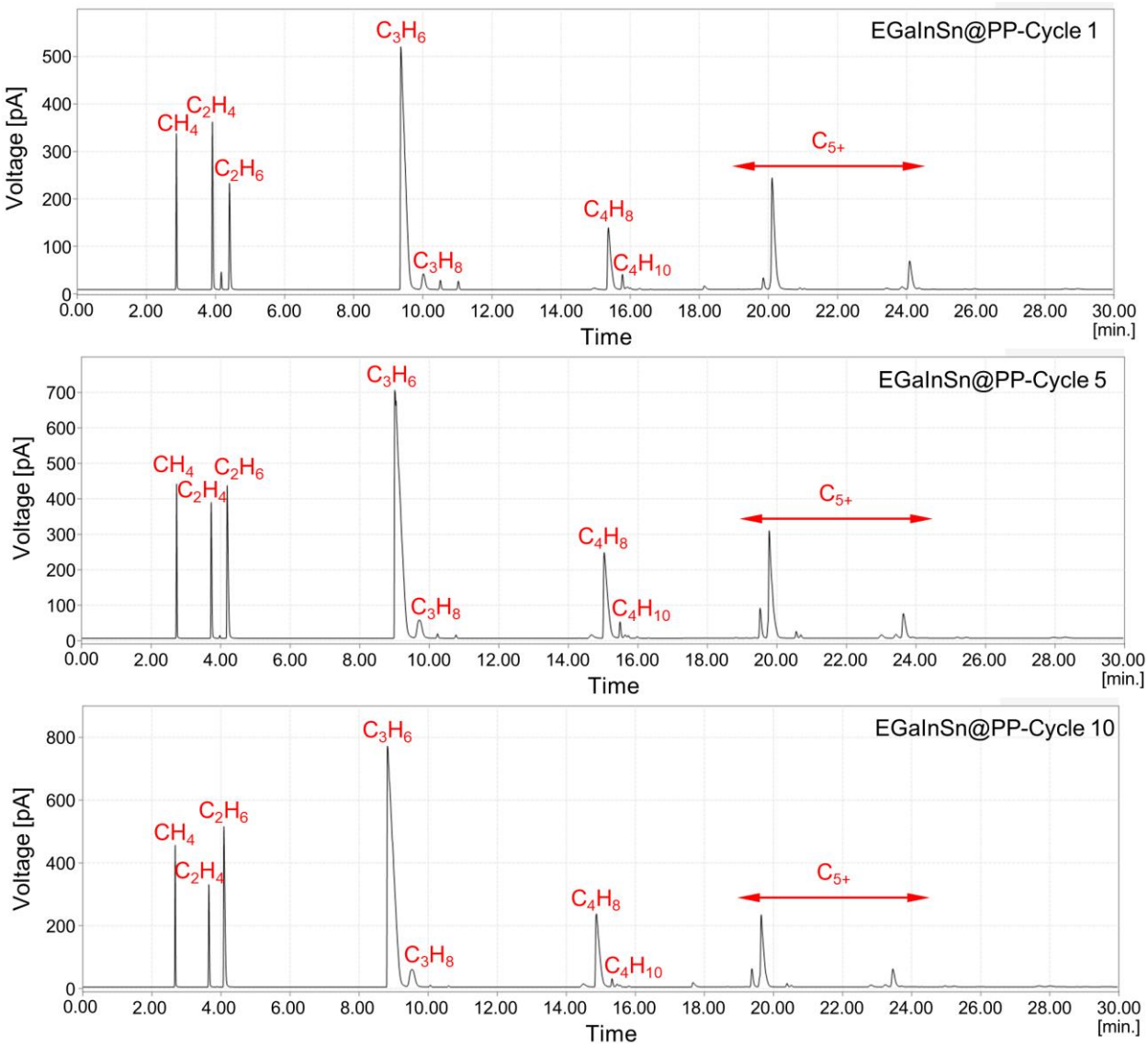

Supplementary Figure 80. GC-FID trace of the volatile products from the first fifth and tenth depolymerization cycle of PP-based disposable lunch boxes via microwave-powered EGaInSn.

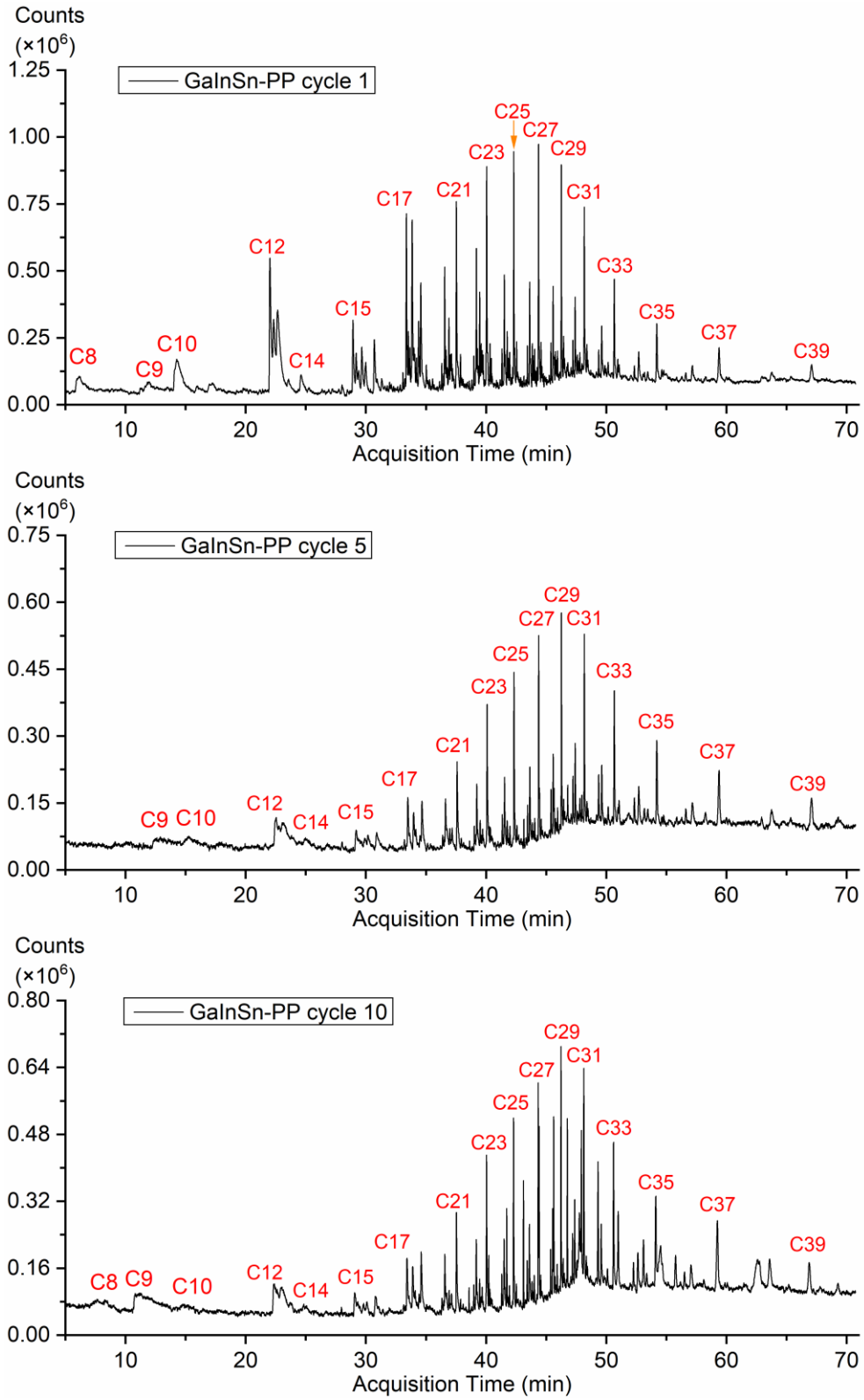

Supplementary Figure 81. GC-MS trace of the oil products from the first, fifth and tenth depolymerization cycle of PP-based disposable lunch boxes via microwave-powered EGaInSn.

References

1 Fan, L. *et al*. Ex-situ catalytic upgrading of vapors from microwave-assisted pyrolysis of low-density polyethylene with MgO. *Energ. Convers. Manage.* **149**, 432-441 (2017).

2 Ding, K. *et al*. Catalytic microwave-assisted pyrolysis of plastic waste over NiO and HY for gasoline-range hydrocarbons production. *Energy Convers. Manage.* **196**, 1316-1325 (2019).

3 Jie, X. *et al*. Microwave-initiated catalytic deconstruction of plastic waste into hydrogen and high-value carbons. *Nat. Catal.* **3**, 902-912 (2020).

4 Zhou, N. *et al*. Catalytic pyrolysis of plastic wastes in a continuous microwave assisted pyrolysis system for fuel production. *Chem. Eng. J.* **418**, 129412 (2021).

5 Jing, X. *et al*. Interaction between feedstocks, absorbers and catalysts in the microwave pyrolysis process of waste plastics. *J. Clean. Prod.* **291**, 125857 (2021).

6 Wang, Y. *et al*. Microwave-driven upcycling of single-use plastics using zeolite catalyst. *Chem. Eng. J.* **465**, 142918 (2023).

7 Tuli,V., Luo, C., Robinson, B., Hu, J. & Wang, Y. Microwave-assisted catalytic technology for sustainable production of valuable chemicals from plastic waste with enhanced catalyst reusability. *Chem. Eng. J.* **489**, 151551 (2024).

8 Tennakoon, A. *et al*. Catalytic upcycling of high-density polyethylene via a processive mechanism. *Nat. Catal.* **3**, 893-901 (2020).

9 Rorrer, J. E., Beckham, G. T. & Román-Leshkov, Y. Conversion of polyolefin waste to liquid alkanes with Ru-based catalysts under mild conditions. *JACS Au* **1**, 8-12 (2021).

10 Wang, C. *et al*. Polyethylene hydrogenolysis at mild conditions over ruthenium on tungstated zirconia. *JACS Au* **1**, 1422-1434 (2021).

11 Wu, X. *et al*. Size-controlled nanoparticles embedded in a mesoporous architecture leading to efficient and selective hydrogenolysis of polyolefins. *J. Am. Chem. Soc.* **144**, 5323-5334 (2022).

12 Chen, S. *et al*. Ultrasmall amorphous zirconia nanoparticles catalyse polyolefin hydrogenolysis. *Nat. Catal.* **6**, 161-173 (2023).

13 Du, J. *et al*. Efficient solvent- and hydrogen-free upcycling of high-density polyethylene into separable cyclic hydrocarbons. *Nat. Nanotechnol.* **18**, 772-779 (2023).

14 Cen, Z. *et al*. Upcycling of polyethylene to gasoline through a self-supplied hydrogen

strategy in a layered self-pillared zeolite. *Nat. Chem.* **16**, 871-880 (2024).

15 Zhang, F. *et al*. Polyethylene upcycling to long-chain alkylaromatics by tandem hydrogenolysis/aromatization. *Science* **370**, 437-441 (2020).

16 Xu, Z. *et al*. Chemical upcycling of polyethylene, polypropylene, and mixtures to high-value surfactants. *Science* **381**, 666-671 (2023).

17 Zhang, W. *et al*. Low-temperature upcycling of polyolefins into liquid alkanes via tandem cracking-alkylation. *Science* **379**, 807-811 (2023).

18 Varga, M. *et al.* Diamond/carbon nanotube composites: Raman, FTIR and XPS spectroscopic studies. *Carbon* **111**, 54-61 (2017).

19 Okuda, H. *et al.* Investigating nanostructures in carbon fibres using Raman spectroscopy. *Carbon* **130**, 178-184 (2018).

20 Tang, J. *et al.* Dynamic configurations of metallic atoms in the liquid state for selective propylene synthesis. *Nat. Nanotechnol.* **19**, 306-310 (2024).